Icarus **154**, 40–79 (2001)
doi:10.1006/icar.2001.6671, available online at http://www.idealibrary.com on IDEAL®

The Evolution of the Martian Hydrosphere: Implications for the Fate of a Primordial Ocean and the Current State of the Northern Plains

Stephen M. Clifford

Lunar and Planetary Institute, 3600 Bay Area Blvd., Houston, Texas 77058
E-mail: clifford@lpi.usra.edu

and

Timothy J. Parker

Jet Propulsion Laboratory, MS 183-501, 4800 Oak Grove Dr., Pasadena, California 91109

Received July 12, 1999; revised May 15, 2001

In this paper we consider the hydraulic and thermal conditions that gave rise to the elevated source regions of the Late Hesperian outflow channels and explore their implications for the evolution of the Martian hydrosphere. We find that if the outflow channel floodwaters were derived from a subpermafrost aquifer, then it implies that, throughout the planet's first billion years of evolution, as much as one third of its surface was covered by standing bodies of water and ice. Following the development of the global dichotomy, the bulk of this water would have existed as an ice-covered ocean in the northern plains. We demonstrate that the progressive crustal assimilation of this early surface reservoir of H_2O (punctuated by possible episodes of less extensive flooding) was a natural consequence of the planet's subsequent climatic and geothermal evolution—potentially cycling the equivalent of a km-deep global ocean of water through the atmosphere and subsurface every $\sim 10^9$ years. In response to the long-term decline in planetary heat flow, the progressive cold-trapping of H_2O into the growing cryosphere is expected to have significantly depleted the original inventory of groundwater—a development that could well explain the apparent decline in outflow channel activity observed during the Amazonian. Although primarily a theoretical analysis, our findings appear remarkably consistent with the geomorphic and topographic evidence that Mars once possessed a primordial ocean and that a substantial relic of that body continues to survive as massive ice deposits within the northern plains. Confirmation of the presence of such deposits, combined with the potential detection of a global-scale groundwater system, would provide persuasive support for the validity of this analysis.

Key Words: **Mars, surface; Mars, atmosphere; Mars, climate; ices; exobiology.**

1. INTRODUCTION

The possibility that a large ocean once occupied the northern plains of Mars is based largely on the work of Parker *et al.* (1987, 1989, 1993), who identified evidence of potential shorelines in Viking Orbiter images. This interpretation has recently received additional support from elevation measurements made by the Mars Orbiter Laser Altimeter (MOLA). These measurements indicate that at least one of the putative shorelines lies along a boundary of near constant elevation—a result that is most easily explained by erosion associated with a fluid in hydrostatic equilibrium (Head *et al.* 1998, 1999).

Although the geologic evidence for a former ocean appears increasingly persuasive, its genesis and timing are more poorly constrained. Until recently, the most widely held belief was that, if an ocean ever did exist, it was likely formed by the discharge of the outflow channels, suggesting a first appearance about midway through the planet's geologic history. However, Clifford and Parker (1999) have argued that the former presence of an ocean can be deduced independently by considering the hydraulic conditions required to explain the origin of the circum-Chryse outflow channels, and extrapolating them backwards in time. This analysis suggests that an ocean on Mars (as on Earth) was almost certainly an initial condition, having condensed shortly after the planet formed.

At the time of peak outflow channel activity, during the Late Hesperian (Tanaka 1986), the mean elevation of channel source regions was about −1 km, or ∼4 km above the lowest elevation in the northern plains. The abrupt emergence of these channels, from regions of collapsed and disrupted terrain, is generally attributed to the catastrophic discharge of subpermafrost groundwater (Carr 1979, 2000). If this interpretation is correct, then the maximum elevation of the outflow channel source regions places a constraint on the minimum elevation of the global water table at the time the channels formed—a conclusion that requires that some mechanism exist for maintaining a planetary-scale groundwater system in hydraulic disequilibrium with the global topography.

The global confinement of a planetary-scale groundwater system is possible during the Late Hesperian because the

0019-1035/01 $35.00

combination of mean annual surface temperature and geothermal heat flow is thought to have been low enough to have resulted in an equilibrium thickness of frozen ground as much as several kilometers deep. However, while such conditions may have prevailed during the Late Hesperian, the substantially higher geothermal heat flux of the Early Noachian would have made confinement of an elevated groundwater system impossible—suggesting the planet's lowest elevations were originally flooded with water. If the global dichotomy dates back to this era, then it implies that a primordial ocean—up to several kilometers deep and covering as much as a third of the planet—must have resided in the northern plains.

Although recent spacecraft investigations have improved our understanding of the nature and evolution of Mars, many details of its geologic and climatic history remain uncertain—a fact that clearly undermines any attempt to reconstruct the precise chronology and complexity of past events. In this analysis we have set a more modest goal, seeking to reconcile the available observational evidence with our present theoretical understanding of the planet's long-term volatile evolution in an effort to provide a geologically and hydrologically consistent first-order description of the evolution of water on Mars. To this end, our analysis is based on four key assumptions: (1) that the majority of mid- to Late Hesperian outflow channels originated from the discharge of groundwater from a confined aquifer, (2) that the large-scale hydraulic properties of the Martian crust are similar to those of the Earth, and that both the present climate (3) and global topography (4) of Mars are reasonable approximations of what has characterized the planet since the Late Noachian.

Based on these assumptions, our analysis indicates that the existence of a primordial ocean was an inevitable result of both the large size of the Martian inventory of H_2O and the hydraulic and thermal conditions that are thought to have existed throughout the planet's first billion years of geologic history. It further suggests that the subsequent assimilation of the resulting frozen ocean, the rise of the global water table, the episodic reflooding of the northern plains, and the apparent decline in outflow channel activity during the Amazonian, were natural consequences of the evolution of the post-Noachian climate and geothermal heat flow.

2. VOLATILE STRUCTURE AND THERMAL EVOLUTION OF THE MARTIAN CRUST

Plausible values of the large-scale physical, thermal, and hydraulic properties of the Martian crust have been discussed by Clifford (1993). In Appendix A, we briefly review, revise, and update several aspects of that earlier analysis in an effort to more accurately describe the potential range of these properties, the effects of crustal heterogeneity, and the new insights provided by the Mars Global Surveyor (MGS) spacecraft. We also discuss the origin of several key relationships (Eqs. 1–5)—describing the porosity, permeability, and thermal structure of the crust—that form the basis for the quantitative arguments presented later in this paper. These relationships, as well as brief descriptions of several important variables, are summarized in Table I.

Substituting the present best estimates of mean annual surface temperature (154–218 K), geothermal heat flow ($\sim$30 mW m^{-2}), and basal melting/freezing temperature (252–273 K) into Eqs. (3) and (5), we find that the present thickness of frozen ground on Mars (a region also known as the cryosphere, Appendix A.2) is likely to range from $\sim$2.3–4.7 km at the equator to $\sim$6.5–13 km at the poles (Fig. 1, Table II). However, natural variations in crustal heat flow and thermal conductivity may result in significant local departures from these predicted values.

Theoretical models suggest that the martian geothermal heat flux was substantially greater in the past (e.g., Stevenson *et al.* 1983, Schubert *et al.* 1992) (Fig. 2). Assuming the present range of mean annual surface temperatures, this implies a proportionately thinner cryosphere. In response to the subsequent decline in planetary heat flow, the freezing front at the base of the cryosphere propagated downward with time (Fig. 3)—creating a cold-trap for any H_2O present in the crust. As a result, the cryosphere is expected to be ice-rich, a belief that is supported by the geomorphic interpretation of a wide variety of surface features, many of which resemble cold-climate features found on Earth (Carr and Schaber 1977, Lucchitta 1981, Rossbacher and Judson 1981, Kuzmin 1983, Carr 1986, 1996, Squyres *et al.* 1992).

3. GEOLOGIC EVIDENCE FOR A PRIMORDIAL OCEAN IN THE NORTHERN PLAINS

3.1. Photogeologic Evidence

The geomorphic evidence for the former presence of a large, and possibly recurrent, standing body of water in the northern plains has been summarized by Parker *et al.* (1987, 1989, 1993), based on the tentative identification of paleoshorelines. These plains margins were first recognized in Viking Orbiter moderate- to high-resolution images of the west Deuteronilus and Cydonia Mensae regions. Multiple "nested" margins have also been identified in Acheron Fossae, southern Elysium, and north of Tempe Terra (Parker and Schenk 1995, Parker 1998). More recently, an additional contact has been described in the western Arabia Terra and northern Meridiani Sinus regions (Edgett and Parker 1997), based on the identification of possible water-lain sediments covering much of this area. To the south of these deposits, a sharp geomorphic contact has also been identified between the highland surface to the south, which is dissected by numerous ancient valley networks, and the Arabia surface to the north, which has a much lower network frequency and appears deficient in the number of large impact basins (see also Carr and Chuang 1997, Frey and Roark 1997). The nature of this boundary (Fig. 4) is similar to that described in Parker *et al.* (1989, 1993), involving both the erosion of a margin into the higher terrain to the south, and burial of the lower terrain to the north, characteristics that are typical of paleolake shorelines on Earth (Fig. 5).

TABLE I
Summary of Assumed Thermophysical and Hydrologic Properties of the Martian Crust (from Appendix A)[a]

Relationship/ Variable	Expression/Description		Value/Range
Porosity vs depth	$\Phi(z) = \Phi(0)\exp(-z/2.82)$, where the depth z is in km	Eq. (1)	$\Phi(0) = 0.35 \pm 0.15$
Permeability vs depth	$\log(k) = -12.65 - 3.2\log(z)$, where the permeability k is in m^2 and z is in km	Eq. (2b)	$\sim 10^{-13}$–10^{-17} m^2 over the depth interval of 1–25 km
Local thickness of cryosphere	$z = \kappa_{ave}(T_{mp} - T_{ms})/Q_g$	Eq. (3)	~2.3–4.7 km @ equator, ~6.5–13 km @ poles
Temperature-dependent thermal conductivity of ice	$\kappa_{ice}(T) = 12.52 - 6.90 \times 10^{-2}\,T + 1.15 \times 10^{-4}\,T^2$	Eq. (4)	2.25–4.62 W m^{-1} K^{-1} over the range of 273–154 K.
Equilibrium thickness of Ocean Ice	$z = [12.52(T_{mp} - T_{ms}) - 3.45 \times 10^{-2}(T_{mp} - T_{ms})^2 + 3.8310^{-5}(T_{mp} - T_{ms})^3]/Q_g$	Eq. (5)	
T_{ms}	Local mean annual surface temperature: With the exception of variations induced by the chaotic evolution of Mars' obliquity, mean annual surface temperatures are assumed to have remained close to their present values throughout geologic time. If the early climate was warmer, it would have prolonged the temporal development of the cryosphere predicted in this study; while colder temperatures would have accelerated it (see Section 4).		~218 K @ equator ~154 K @ poles
T_{mp}	Melting/freezing temperature at base of the cryosphere: Where the cryosphere and groundwater are in direct contact, the freezing temperature may be depressed below 273 K by the presence of dissolved salts. Various stability arguments suggest that the most potent freezing-point depressor on Mars is likely to be NaCl, which has a freezing point of 252 K at its eutectic (Clark and Van Hart 1981). In the absence of groundwater, the base of the cryosphere is likely to be defined by the position of the 273 K isotherm.		252–273 K
κ_{ave}	Column-averaged thermal conductivity of the cryosphere: Based on a review of the measured thermal conductivities of frozen soil and basalt, Clifford (1993) argued that the column-averaged thermal conductivity of the cryosphere is likely to vary between ~1.0–3.0 W m^{-1} K^{-1}, with a most probable mean global value ~2.0 W m^{-1} K^{-1}. The sublimation of near-surface ground ice is expected to result in generally lower values near the equator, while the strong temperature-dependent thermal conductivity of ice is expected to result in higher values near the poles.		~2.0 W m^{-1} K^{-1} estimated global mean
Q_g	Geothermal heat flux: Thermal history models of Mars indicate that the global heat flow has declined substantially with time (Fig. 2). In the present study, it is assumed that, to a first-order, this heat loss was globally symmetric—with expected regional (~107 km^2) variations of ±50% about the global mean. The potential consequences of a higher, and hemispherically asymmetric, early heat flow are discussed in Section 11.1.		~3.0×10^{-2} W m^{-2} estimated present global mean

[a] All units mKs unless specified otherwise.

The origin of these margins by other frequently cited plains-forming processes, particularly volcanism and eolian deposition, can probably be excluded. For example, when flood lavas bury the underlying terrain, they create margins that onlap the neighboring elevated topography. Thermal or mechanical erosion by flood lavas appears unlikely, as these processes are only observed in fast-moving lava channels. The other principal alternative, eolian deposition, would not be topographically confined to an equipotential upper surface, nor would the margins of eolian-modified surfaces conform to the local topography, even though they might exhibit erosional as well as depositional components.

The numerous features related to plains margins has complicated the process of identification and of establishing an appropriate nomenclature for purposes of local and regional correlation. To mitigate this problem, a mapping scheme and naming system similar to that used by terrestrial geomorphologists for shorelines in the Pleistocene Lake Bonneville basin was proposed by Parker (1998). The choice of which term to apply to these features, to keep the names as nongenetic as possible, is complicated by the fact that an individual "contact" is not necessarily a simple line separating geologic units, but can be expressed by a number of landform types.

Describing such features as "contacts" (as was originally done by Parker *et al*. 1989, 1993) implies that the geomorphic units to either side of a particular division are clearly distinct from one another. Indeed, at the regional scale, the largest features often do show clear textural differences across a contact, such as the one separating the mottled plains from the thumbprint terrain in east Acidalia Planitia (45°N, 350°W) (Franklin and Parker 1999). But for the less extensive or smaller-scale features, the differences are often gradational and less distinct. Complicating the picture still further, even the best-expressed of these features display frequent breaks in continuity within the regions covered by the available Viking Orbiter images.

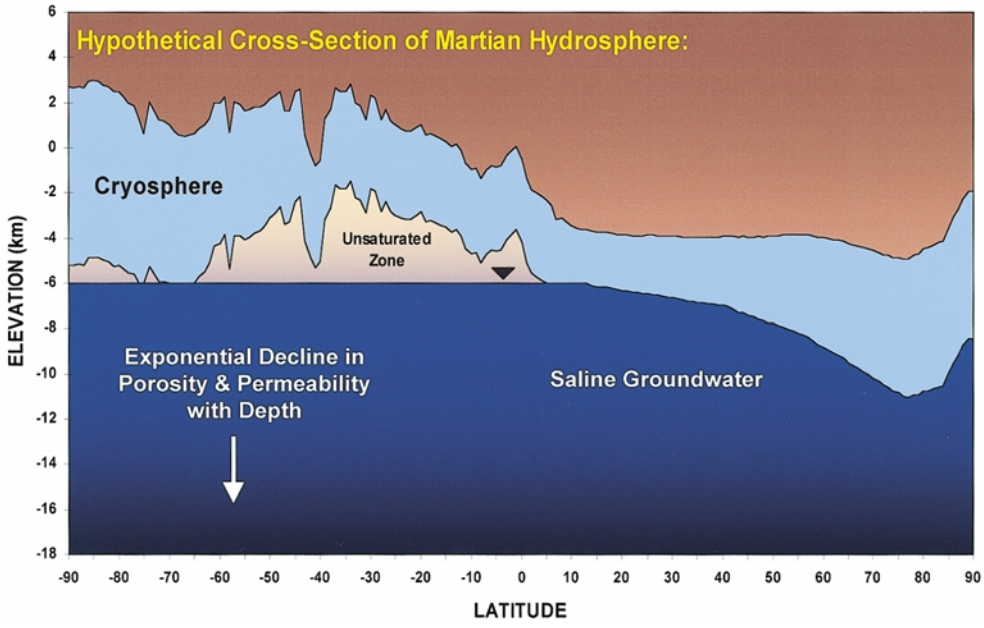

FIG. 1. Hypothetical pole-to-pole cross-section of the present-day Martian crust (along 157°W longitude), illustrating the potential relationship between surface topography, ground ice, and groundwater. Surface elevations are from the MOLA 1° × 1° Digital Terrain Model (MOLA Science Team 1999). At those locations where the base of the cryosphere is in contact with the water table, the presence of dissolved salts may reduce the thickness of frozen ground by depressing the freezing point of the groundwater to a value as low as the 252 K eutectic temperature of a saturated NaCl brine. Conversely, where the cryosphere and groundwater are not in direct contact, the leaching of soluble salts by low-temperature hydrothermal convection (e.g., Clifford 1991, 1993) should ensure that the intervening unsaturated zone is solute-free, resulting in a basal melting temperature of ~273 K. Geographic variations in surface temperature and geothermal heat flow, combined with stratigraphic variations in the thermophysical and diffusive properties of the crust, are likely to result in considerable local deviations from the idealized distributions of water and ice illustrated here. Given the instability of ice at low latitudes, this heterogeneity may result in local depths of crustal desiccation that range from centimeters to as much as a kilometer—with the potential for significant and complex variations in saturation state beneath the sublimation front (Clifford 1998). Similar variations may also occur in the unsaturated zone between the base of the cryosphere and groundwater table, where the effects of capillarity and low-temperature hydrothermal convection are likely to contribute to complex transitions in saturation state, including the development of perched aquifers (Clifford 1993).

TABLE II
Thickness of Cryosphere as a Function of Composition, Latitude, and Basal Melting Temperature (km)

			Latitude (degrees), mean annual surface temperature (K)							
			0°, 218 K T_{mp} =		30°, 211 K T_{mp} =		60°, 179 K T_{mp} =		90°, 154 K T_{mp} =	
Composition	Time (Ga)	Q_g (W m^{-2})	252 K	273 K	252 K	273 K	252 K	273 K	252 K	273 K
Frozen ground	4.5	400	0.17	0.28	0.21	0.31	0.37	0.47	0.49	0.60
	4.3	205	0.33	0.54	0.40	0.60	0.71	0.92	0.96	1.16
	4	150	0.45	0.73	0.55	0.83	0.97	1.25	1.31	1.59
	3	95	0.72	1.16	0.86	1.31	1.54	1.98	2.06	2.51
	2	65	1.05	1.69	1.26	1.91	2.25	2.89	3.02	3.66
	1	45	1.51	2.44	1.82	2.76	3.24	4.18	4.36	5.29
	0	30	2.27	3.67	2.73	4.13	4.87	6.27	6.53	7.93
Ice	4.5	400	0.23	0.35	0.28	0.40	0.55	0.68	0.82	0.94
	4.3	205	0.44	0.68	0.54	0.78	1.08	1.32	1.60	1.84
	4	150	0.60	0.93	0.74	1.07	1.48	1.80	2.18	2.51
	3	95	0.95	1.47	1.17	1.69	2.33	2.85	3.45	3.96
	2	65	1.39	2.15	1.72	2.47	3.41	4.16	5.04	5.79
	1	45	2.01	3.10	2.48	3.57	4.93	6.02	7.27	8.36
	0	30	3.02	4.65	3.72	5.35	7.39	9.02	10.91	12.54

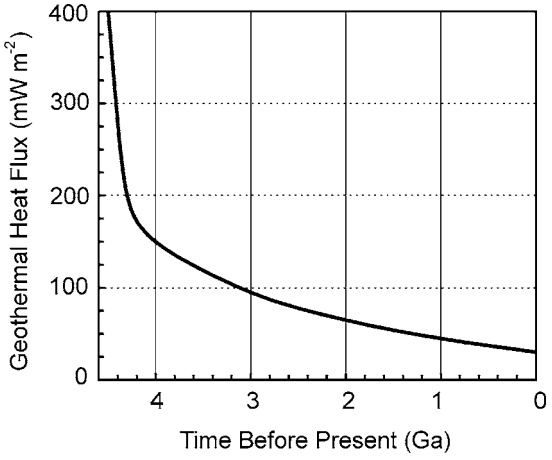

FIG. 2. Variation of Martian mantle heat flow with time (after Stevenson *et al*. 1983).

For these reasons, the unambiguous identification of a shoreline from orbiter images alone is an extraordinarily difficult task. For example, terrestrial paleolake shorelines are often expressed as nothing more than narrow terraces cut into a preexisting lithologic unit, such as an outcrop of basalt, or a geomorphic unit, such as an alluvial fan. The lithology and morphology of the preexisting surface is not necessarily changed nor obscured, although at some increased level of resolution, modification or burial of the surface during shoreline transgressions, regressions, and lacustrine sedimentation can usually be identified. On Earth, this may require submeter scale aerial photography or even field observations at ground level. But even at these scales, the identification of geomorphic indicators of former standing water can be frustrated if subsequent, unrelated processes have modified or destroyed coastal landforms. For example, the 10 Ka Bonneville Shoreline lies at approximately the same elevation as the 100–150 Ka Little Valley episode of ponding within the Bonneville Basin, but no coastal features associated with the earlier stage are positively identified, except in section, because of subsequent destruction through erosion and burial by younger, more extensive lacustrine sediments (e.g., McCoy 1987, Oviatt, 1989). At the other extreme, lacustrine materials or landforms can be recognized at regional scales, provided that the longevity and extent of the lake were great enough (or the rates of sedimentation high enough) to produce readily identifiable changes to the preexisting topography (assuming that those changes were not themselves later erased by subsequent, unrelated processes).

Objections to the shoreline interpretation have been raised by Malin and Edgett (1999), who suggest that the contacts proposed by Parker *et al*. (1989, 1993) as shorelines are only changes in slope, or albedo and texture, that are more consistent with stratigraphic exposures. On this basis, they conclude that there are no shorelines at the proposed locations. However, the features they describe are in fact common expressions of the shorelines associated with large terrestrial paleolakes, and their Fig. 1 is actually a good example of what paleoshorelines look like on Earth (e.g., as evident by comparing Figs. 4 and 5). Therefore, Malin and Edgett's conclusion that "the hypotheses that relied on specific landforms and their associations to interpret the past presence of seas or oceans on Mars have failed a critical test" is itself invalid and fails as an objective test of the shoreline hypothesis.

If the global-scale contacts identified by Parker *et al*. (1989, 1993) are indeed the erosional signature of a primordial ocean, then Malin and Edgett's (1999) failure to detect meter-scale evidence of fluvial erosion is not at all surprising—as the age of the oldest shoreline (i.e., "Contact 1" in Sect. 3.3) is at least ~4 Ga, while the age of the youngest may be as much as ~2–3 Ga. As discussed in Section 6, it appears unlikely that

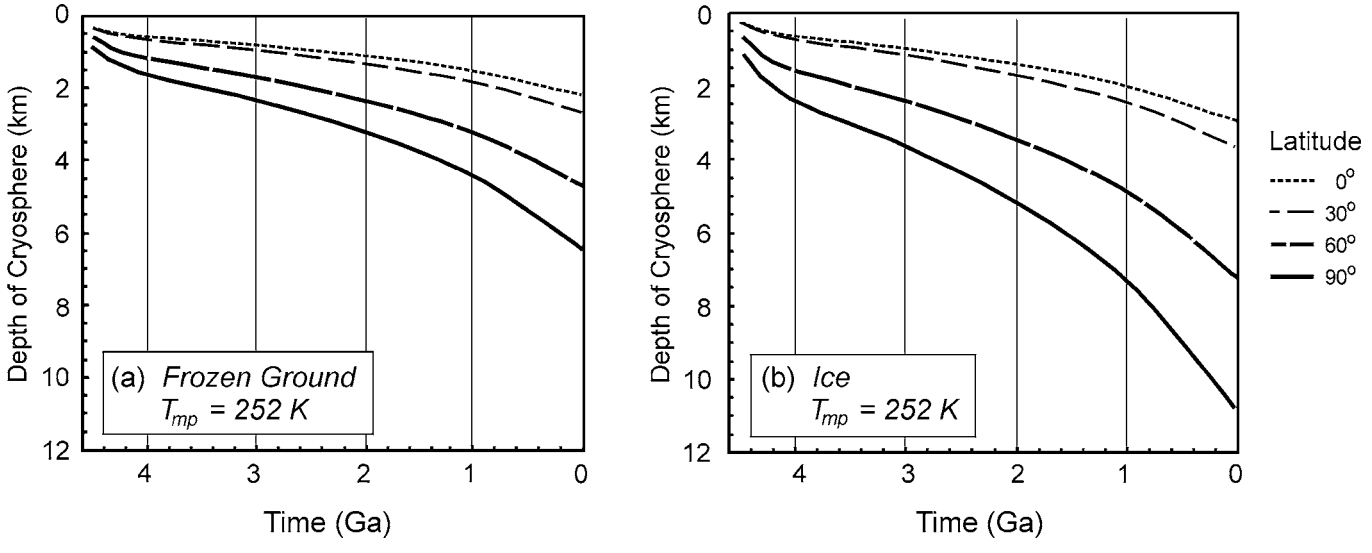

FIG. 3. Depth of cryosphere vs. time at four latitudes for (a) frozen ground and (b) ice. Graphs are based on the data in Table II and assume a groundwater freezing temperature of 252 K, a frozen ground thermal conductivity of 2.0 W m^{-1} K^{-1}, and a temperature-dependent thermal conductivity for ice given by Eq. (4).

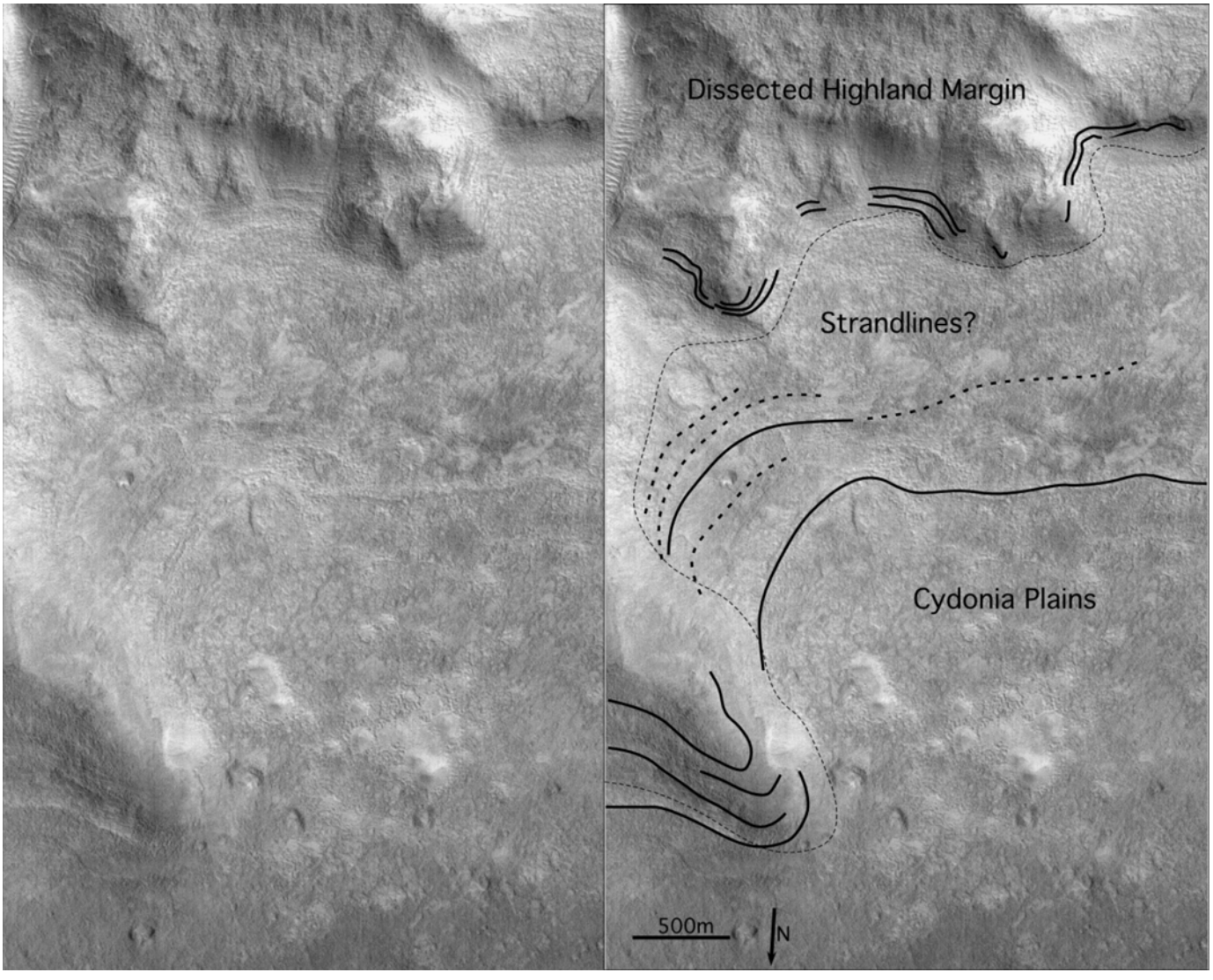

FIG. 4. Portion of a MOC 4.6m/pixel image crossing "Arabia Shoreline" at the "gradational boundary" east of Cydonia Mensae (36.45°N, 9.14°W). Numerous subtle arcuate ridges parallel the dissected margin of the highlands in this view (highlighted in the annotated image on the right). These occur both on the Cydonia plains surface and on the margin of the highlands, where they are expressed as terraces or benches in the terrain. Total relief of the highland scarp in this scene is about 600 meters. The difference in elevation from the lowest to highest "strandline" feature is about 300 meters. MOC narrow angle image M0704326 (NASA/JPL/MSSS). Topography based on MOLA profile ap124201 (NASA/GSFC/MOLA Science Team).

even the oldest of these features originated from the action of wind-driven waves. Rather, our analysis suggests that a more plausible origin is by coastal and/or other erosional processes associated with the long-standing presence of an ice-covered (or fully frozen) ocean in the northern plains.

3.2. Number and Relative Age Relationship of Shorelines

In an effort to investigate the regional consistency of the shoreline interpretation, and reduce the potential confusion originating from the evolving nomenclature, Parker (1998) presented a preliminary "interpretive map," which is reproduced in Fig. 6. For clarity, either local or regional feature names have been applied to these boundaries, which are provisionally referred to as "shorelines." Verification of the true nature of these features is likely to require the acquisition and analysis of new remote sensing data (including geophysical sounding), returned samples and drill cores, and *in situ* field investigations by future human explorers.

Regionally extensive "shorelines" were assigned classic albedo names from the type of locality where this is feasible (such as "Meridiani shoreline"), while those with only local expressions (largely because of lack of high-resolution, regional coverage) were assigned local feature names (such as "Mamers Valles level 2"). These may be changed to classic albedo names if regional extent is confirmed at a later date. This simplifies referral to these geomorphic boundaries over the previous naming systems used in Parker *et al*. (1989, 1993; see Table III

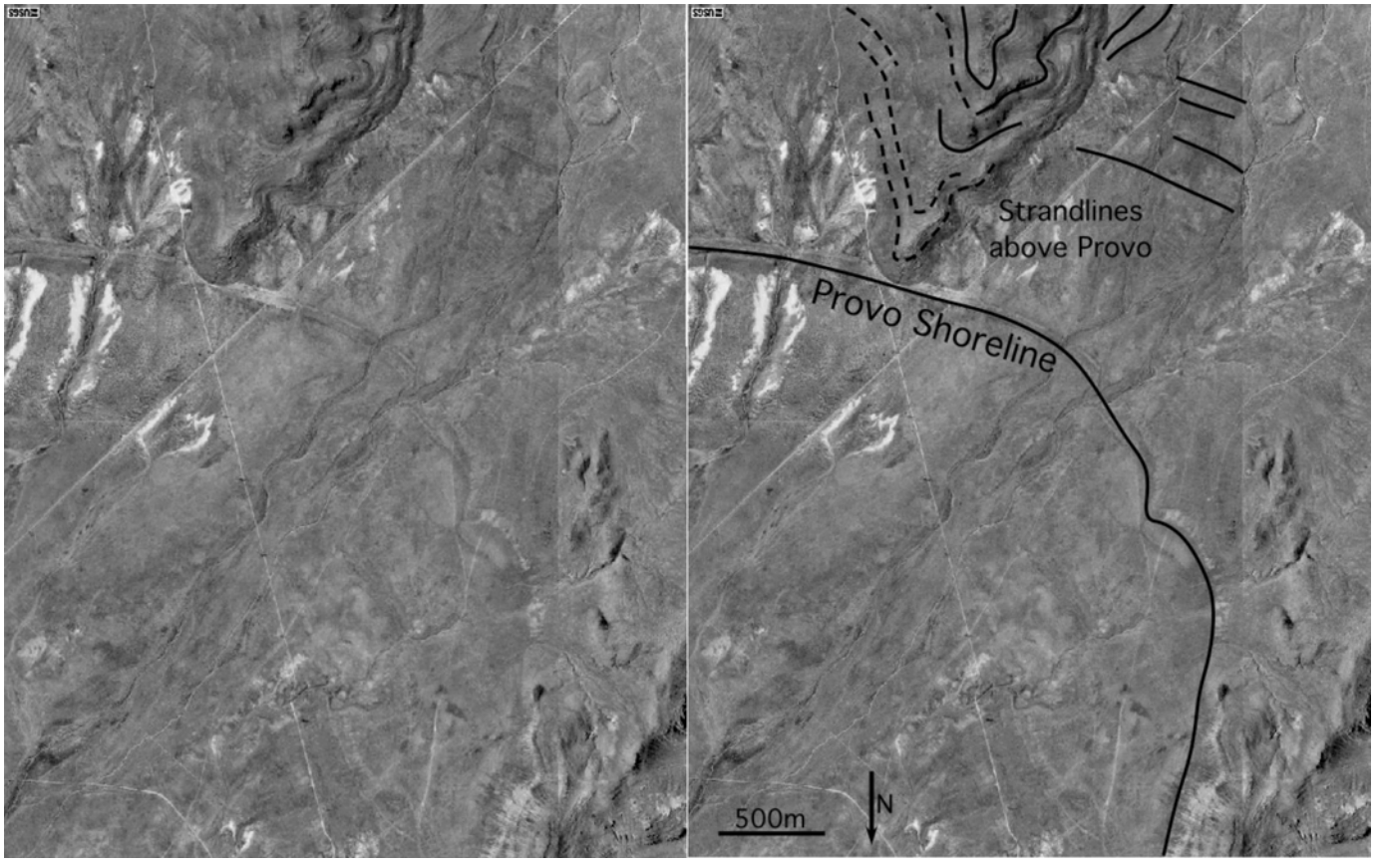

FIG. 5. An 8m/pixel aerial photomosaic of north end of Cricket Mountains, southwest Utah (courtesy of www.terraserver.homeadvisor.msn.com), showing Pleistocene Lake Bonneville shorelines. Most prominent is the Provo level, at which the lake stabilized for a time after dropping suddenly as a result of spillover at Red Rock Pass, Idaho. In this scene, the Provo shoreline consists of both erosional benches (terraces cut into bedrock promontory from the Cricket Mountains at top) and constructional barrier beach ridges (prominent arc to either side of promontory). The numerous strandlines and terraces above the Provo level are beaches that were formed during transgression to and regression from the maximum elevation of the lake at the Bonneville shoreline (out of the top of scene, to the south).

for a cross-reference) and should stand as a reasonable naming scheme for these features even in the event that they should prove to have originated by some other process.

Within the east Acidalia through Meridiani Sinus part of the highland margin (340°W to 10°W longitude), at least eight separate highstands can be identified (Franklin and Parker 1999). Similar features in Cydonia, Tempe, Utopia/Isidis, and South Elysium cannot be correlated to these, except in those instances where they are traceable globally. Thus, there is considerable uncertainty as to whether local "levels" relate directly to the features associated with the global "shorelines" in the Acidalia/Meridiani region, or whether they indicate separate erosional events. In general, a comparison of the relative preservation state of the shorelines is consistent with the interpretation of a more youthful age in the descent from the highlands to the lowlands. However, as on Earth, later transgressions may drown older shorelines without obscuring them. Currently, it is not possible to discriminate between a single early ocean whose level decayed with time, and multiple episodes of progressively less extensive flooding that may have occurred throughout the planet's history (Section 8.2).

3.3. Other Lines of Evidence

The presence of a former ocean in the northern plains is consistent with the geomorphic interpretation of a variety of landforms (e.g., Allen 1979, Rossbacher and Judson 1981, Lucchitta and Ferguson 1983, Lucchitta *et al*. 1986, Lucchitta 1984, 1993, Carr 1986, Squyres and Carr 1986, Lucchitta and Chapman, 1988, Baker *et al*. 1991, Squyres *et al*. 1992, Chapman 1994, Costard and Kargel 1995, Kargel *et al*. 1995). But perhaps the greatest support has come from the analysis of the high-resolution topographic data returned by MOLA (Head *et al*. 1998, 1999, Banerdt and Parker 1998).

In an effort to test the hypothesis that an ancient ocean once occupied the plains, Head *et al*. (1998, 1999) compared early MOLA data with the elevations of the two contacts that were first identified as possible shorelines by Parker *et al*. (1989). Contact 1 lies along the gradational and fretted boundary between the southern highlands and northern plains (i.e., the "Gradational Boundary" in Table III), while Contact 2 occurs several hundred kilometers further north, marking the division between two plains units (the "Lowland Unit A/Lowland Unit

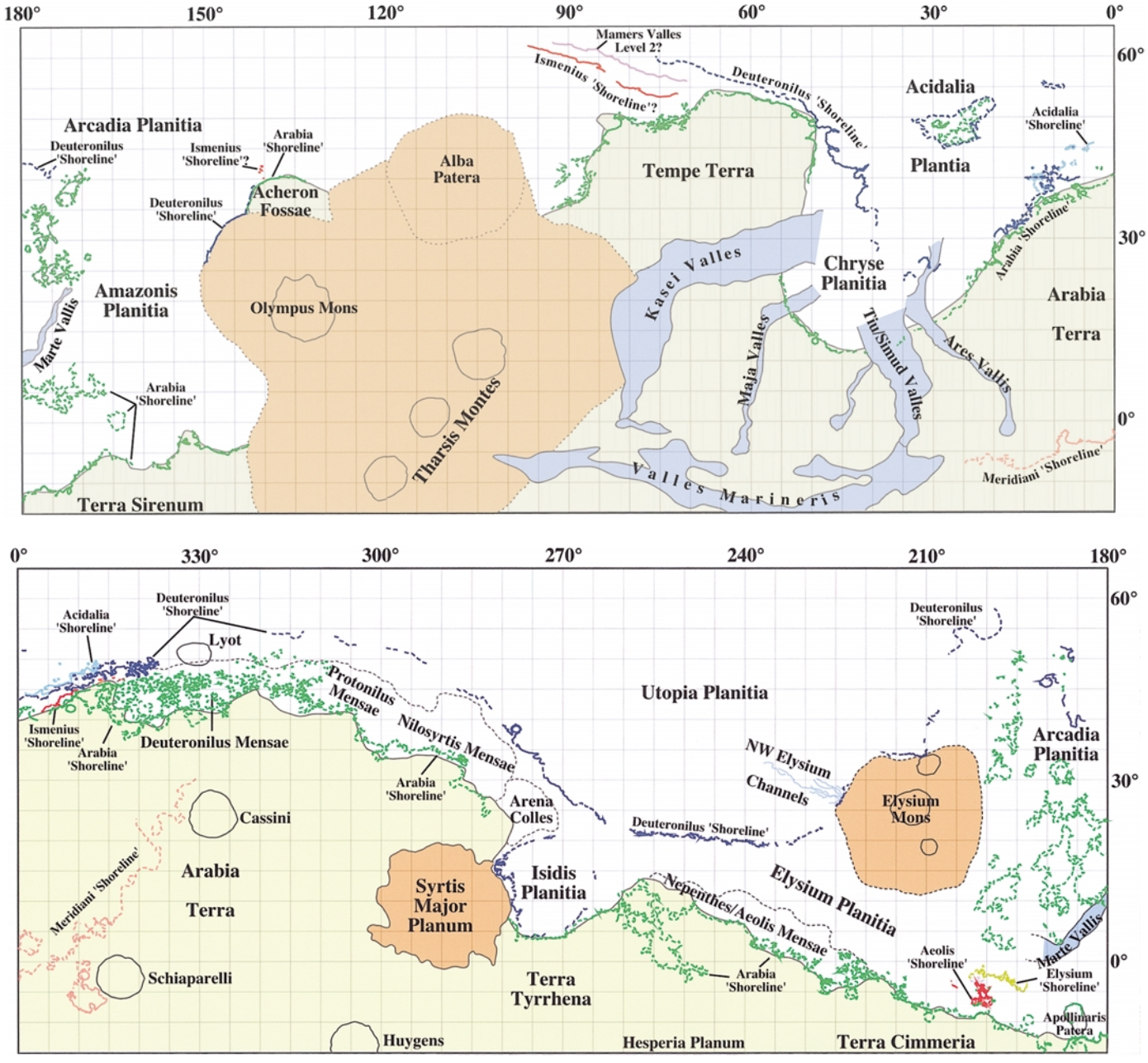

FIG. 6. A cylindrical projection of Mars, from 65°N to 15°S latitude, showing the proposed regional and global shorelines relative to major geographic features (figure from Parker 1998). From the highest elevation to the lowest (approximately oldest to youngest) these are the: Meridiani Shoreline (salmon); Arabia Shoreline (green); Ismenius and Aeolis Shorelines (red); Elysium Shoreline (yellow-brown); Mamers Valles level 2 (lavender); Deuteronilus Shoreline (blue); and Acidalia Shoreline (cyan) (Table III). The locations of these proposed shorelines are indicated by solid lines (where Viking-based image quality is good) or by dashed lines (where positive identification of features is limited by image resolution or subsequent modification).

B Contact" in Table III). Of these two boundaries, Contact 2 is the younger and better preserved, while Contact 1 encompasses the greatest area. If these contacts are shorelines, and if the gravitational figure and topography of Mars has remained the same since the contacts were formed, then their respective elevations should conform to a surface of constant geopotential—an observation that would provide persuasive evidence that they were eroded by a fluid in hydrostatic equilibrium.

Although Head *et al*. (1998, 1999) found that neither contact conforms to a constant geopotential surface, Contact 2 comes close, having an average elevation of −3.76 km (relative to the global datum) with a standard deviation of 0.56 km. They also noted that the discrepancies that do exist between the elevation of Contact 2 and an equipotential surface appear nonrandom. That is, the largest deviations are found to occur in regions such as Tharsis, Elysium, and Isidis, where vertical movement,

TABLE III
Cross-reference Chart of Representative Northern Plains Margins

Parker *et al*. (1989) Geographic region East Acidalia/ West Deuteronilus	Parker *et al*. (1993) Geographic region		New provisional name, Parker (1998) Geographic region	
	Cydonia/Tempe	Utopia/Isidis	East Acidalia & Meridiani	South Elysium
"Mottled" Plains/ "Thumbprint Terrain" contact (regional)	not discussed	not discussed	Acidalia Shoreline (regional)	should trend north of Elysium volcanic rise
Lowland Unit "A"/Lowland Unit "B" contact (global)	"Interior Plains Boundary" (global)	"Interior Plains Boundary" (global)	Deuteronilus Shoreline (global)	Deuteronilus Shoreline trends north of Elysium volcanic rise (global)
"Bench" 2 (in local high-res data only)	<----------	---------->	Mamers Valles level 2 (in local high-res data only)	<-no direct correlation South Elysium Level 1 (in local high-res data only)
"Bench" 3 (in local high-res data only)	<----------	<----------	Mamers Valles level 3 (in local high-res data only)	<-no direct correlation South Elysium Level 2 (in local high-res data only)
"Bench" 4 (regional)	<----------	---------->	Ismenius Shoreline (regional)	<-no direct correlation Elysium Shoreline (regional)
"Bench" 5 (in local high-res data only)	<----------	---------->	Mamers Valles level 5 (in local high-res data only)	<-no direct correlation South Elysium Level 4 (in local high-res data only)
not discussed	not discussed	not discussed	not discussed	Aeolis Shoreline (regional)
"Gradational Boundary" (global)	"Gradational Boundary" (global)	"Gradational Boundary" (global)	Arabia Shoreline (global)	Arabia Shoreline (global)
not discussed	not discussed	not discussed	Meridiani Shoreline (global??)	not yet identified at these longitudes

postdating the inferred time of formation of the contact, is either known or suspected. This trend is also mirrored by Contact 1 — although, with a mean elevation of −1.68 km and a standard deviation of ∼1.7 km, the amplitude of this discrepancy is substantially greater. One explanation for the larger deviation of Contact 1 may simply be its greater age, which has given tectonic forces more time to rework the global topography and allowed more recent geologic activity to bury or obliterate any evidence of the contact at many places along its circumference.

Another factor that has likely contributed to the observed discrepancies in elevation is the possibility that errors were made in the original identification of where the contacts occurred. Because the contacts identified by Parker *et al*. (1989) were often at the borderline of detectability, attempts to correlate them over distances of many thousands of kilometers (based on Viking Orbiter images that varied dramatically in quality, resolution, and coverage), invariably led to some misidentifications. This problem has been aggravated by the identification of numerous local benches that lie within topographic depressions (Hiesinger and Head 1999, 2000) or parallel the course of the global contacts (Franklin and Parker 1999). Whether these benches represent multiple nested shorelines, or are manifestations of some other phenomena, their presence clearly complicates efforts to establish individual continuity with similar features located hundreds, and sometimes thousands, of kilometers away.

An additional source of support for the former presence of a northern ocean comes from MOLA observations of regional surface slopes and roughness. These observations reveal that the northern plains are remarkably flat and smooth, topographic characteristics that Aharonson *et al*. (1998) conclude are most similar to heavily sedimented surfaces on Earth, such as the oceanic abyssal plains and continental basins filled by fluvial deposits. This interpretation is also consistent with the geomorphic characteristics of the plains, particularly those interior to Contact 2 (Rossbacher 1985, Lucchitta *et al*. 1986, Parker *et al*. 1989, 1993). While noting that neither the MOLA data, nor the geomorphic evidence, yet provides unequivocal proof, Head *et al*. (1998, 1999) conclude that they are consistent with the interpretation that the northern plains were once occupied by standing bodies of water that may have ranged in size from large seas to a hemispheric ocean.

4. HYDRAULIC CONDITIONS IMPLIED BY THE LATE HESPERIAN OUTFLOW CHANNELS

4.1. Age and Elevation of Channel Source Regions

Analysis of the relative age, elevation, and geographic distribution of large channels on Mars (summarized in Table IV) indicates that their development has spanned most of the planet's

geologic history, ranging from the Late Noachian to Late Amazonian (Carr and Clow 1981, Baker 1982, Baker *et al*. 1992, Tanaka, 1986, Tanaka *et al*. 1992, Tribe and Clifford 1993). The Late Noachian and Early Hesperian channels are few in number and exhibit no strong association with any single geographic region. However, during the mid- to Late Hesperian, there was an apparent increase in channel activity, much of it concentrated around Chryse Planitia, a distribution that was likely influenced by the concurrent development of Tharsis and Valles Marineris (Masursky *et al*. 1977, Carr 1979, Tanaka and Chapman 1990). By the Amazonian, outflow channel activity appears to have declined and become more localized around regions of probable geothermal activity (Baker *et al*. 1992, Tribe and Clifford 1993).

During the Late Hesperian, the mean elevation of channel source regions was approximately −1 km, ranging from a high of +0.65 km to a low of −3.7 km (Table IV). However, by the Amazonian, this mean fell by ∼2.1 ± 0.5 km. This range of uncertainty reflects both the small number of large channels that formed during this period and the impact of a single statistical anomaly, Olympica Fossae, whose elevation of +3.5 km substantially exceeds the −2.4-km to −4.1-km range covered by the other large Amazonian channels. This deviation may indicate that Olympica Fossae had a different mode of origin (e.g., from the local melting of ground ice, a conclusion that appears consistent with both the minimal erosion associated with this feature and its occurrence in Tharsis).

Differences in channel selection criteria, inferred age and mode of origin, and the uncertainty that exists in locating of the sources of some channels, can obviously influence the quantitative results summarized above. However, the conclusion that there was a ∼2-km decline in the mean elevation of outflow channel source regions between the Late Hesperian and Amazonian appears fairly robust. Although it is possible that this observation is a statistical artifact of the small number of large channels that occurred during the Amazonian, the concurrent shift in the geographic location of channel source regions supports the conclusion that this change was real. As discussed in Section 8.2, the decline in outflow channel elevation and activity are expected consequences of the continued growth of the cryosphere.

Although the channels listed in Table IV undoubtedly had diverse origins (Mars Channel Working Group 1983, Baker *et al*. 1992), the hydraulic conditions implied by the elevated source regions of the Late Hesperian channels appear to require a minimum groundwater table of equal or greater height (Fig. 7). Given any geologically reasonable value of large-scale crustal permeability (i.e., $\geq 10^{-15}$ m^2), virtually all of the interconnected crustal porosity lying beneath this elevation must have been saturated with either water or ice. By this reasoning, the water table of the reservoir that fed the channels reflected that of a planet-wide subpermafrost groundwater system in hydrostatic equilibrium (Clifford 1993). This conclusion has important implications for both the thickness of frozen ground necessary to ensure the groundwater system's confinement (Section 4.3) and for the ultimate fate of water discharged to the northern plains (Sections 4.4 and 8).

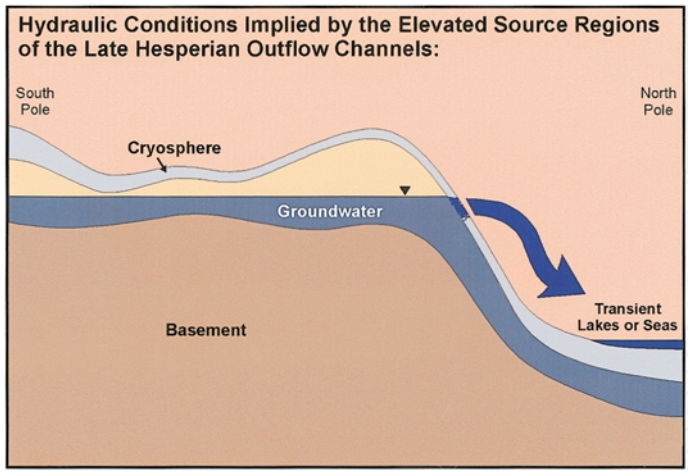

FIG. 7. An idealized illustration of the hydraulic conditions implied by the ∼+0.65 maximum elevation of outflow channel source regions during the Late Hesperian. A global water table as much as 5-km above the minimum elevation of the northern plains is permitted during the Late Hesperian by confinement beneath a 3-km thick layer of frozen ground (Sections 4.2 and 4.3).

4.2. Plausible Mechanisms of Formation

The abrupt emergence of the most outflow channels from regions of chaotic terrain is generally attributed to the widespread disruption and subsidence of the crust resulting from the catastrophic discharge of a large volume of groundwater under significant hydraulic head (Carr 1979, Baker 1982, Baker *et al*. 1992). Over the course of Martian geologic history, such discharges may have been triggered by a wide variety of potential mechanisms and local conditions. Here, we focus specifically on the origin of the outflow channels during the Late Hesperian.

The spatial and temporal association of the circum-Chryse channels with the development of Valles Marineris and Tharsis has frequently been cited as evidence of a possible genetic relationship (Masursky *et al*. 1977, Carr 1979, Tanaka and Chapman 1990). In this context, several mechanisms for initiating outflow channel activity appear viable. For example, given the existence of a global subpermafrost aquifer, any uplift of Tharsis by local mantle convection (whether continuous or episodic, e.g., see Kiefer and Kellog 1998, Kiefer 1999) would have driven the flow of groundwater to lower elevations, where the resulting increase in hydraulic pressure may have been sufficient to disrupt the confining layer of frozen ground, permitting the catastrophic discharge of groundwater to the surface (Carr 1979). Alternatively, the faulting and fracturing associated with the formation of Tharsis and Valles Marineris may have disrupted the confining layer directly, permitting the discharge of groundwater as the fractures propagated to lower elevations (Masursky *et al*. 1977, Tanaka and Chapman 1990).

It is also possible that the distribution of Late Hesperian channels around Chryse simply reflects isolated, random failures of confinement that were exacerbated by regional conditions of high artesian pressure. Carr (1979, 2000) has suggested that

TABLE IV
Elevation of Large Channel Source Regions vs. Time[a]

Age	Channel	Approximate location of initial source region[b]	Elevation (km)[c]	Nature of source region	References
Late Noachian/	Mawrth Vallis	19°N, 13.5°W	−2.8	obscure	Rotto and Tanaka (1995)
Early Hesperian	Margaritifer Valles[d]	15.5°S, 26°W	−1.7	obscure; spillway from Argyre sea?	Parker (1985); Grant (1987)
	Ladon Valles[d]	24.5°S, 30°W	0.54	obscure; spillway from Argyre sea?	Parker (1985); Scott and Tanaka (1986)
	Uzboi Vallis[d]	32°S, 35°W	0.27	obscure; spillway from Argyre sea?	Parker (1985); Scott and Tanaka (1986)
	Nirgal Vallis	27.5°S, 42.5°W	0.63	sapping	Scott and Tanaka (1986)
	Nanedi Valles	0° 49.5°W	0.54	sapping	Rotto and Tanaka (1995)
	Bahram Vallis	20.5°N, 59.5°W	−0.72	sapping	Rotto and Tanaka (1995)
	Ma'adim Vallis	28°S, 182°W	0.83	multiple & distributed	Tanaka (1986); Greeley and Guest (1987)
	Al-Qahira Vallis	20°S, 199.5°W	−0.014	multiple & distributed	Greeley and Guest (1987)
Mid- to Late Hesperian[e]	Ares Vallis	0°, 17°W	−2.8	chaos	Scott and Tanaka (1986); Rotto and Tanaka (1995)
	Channel SE of Pyrrhae Chaos	15°S, 26°W	−1.6	obscure	Scott and Tanaka (1986); Witbeck *et al*. (1991); Rotto and Tanaka (1995)
	Tiu Vallis	3.5°S, 29°W	−2.9	local chaos & Valles Marineris discharge	Scott and Tanaka (1986); Rotto and Tanaka (1995)
	Simud Vallis	3°N, 36°W	−3.1	local chaos & Valles Marineris discharge	Scott and Tanaka (1986); Rotto and Tanaka (1995)
	Ravi Vallis	1°S, 43°W	−0.2	chaos	Scott and Tanaka (1986); Witbeck *et al*. (1991); Rotto and Tanaka (1995)
	Shalbatana Vallis	3.5°S, 46.5°W	0.3	chaos	Scott and Tanaka (1986); Witbeck *et al*. (1991); Rotto and Tanaka (1995)
	Valles Marineris outflows[f]	14°S, 42.5°W	−3.7	chaos & interior lakes?	Scott and Tanaka (1986); Witbeck *et al*. (1991); Rotto and Tanaka (1995)
	Australe Planum channel	64°S, 52°W	0.65	obscure	Tanaka and Scott (1987)
	Maja Valles	1°S, 61°W	0.61	chaos	Witbeck *et al*. (1991); De Hon and Pani (1993); Rotto and Tanaka (1995); Rice and De Hon (1996)
	Kasei Valles	13.5°, 77.5°W	−0.79	chaos	Scott and Tanaka (1986); Rotto and Tanaka (1995); Chapman and Tanaka (1996)
	Mangala Valles	18.5°S, 149.5°W	0.6	graben; possible contribution from adjoining paleolake lake?	Chapman and Tanaka (1990); Tanaka and Chapman (1990); Chapman and Tanaka (1993); Craddock and Greeley (1994); Parker (1994); Zimbelman *et al*. (1994)
	Reull Valles	37°S, 248°W	0.54	obscure	Greeley and Guest (1987); Crown *et al*. (1992); Crown and Greeley (1993)
	Harmakhis Vallis	39°S, 266°W	−3.7	obscure	Greeley and Guest (1987); Crown *et al*. (1992); Crown and Greeley (1993)
	Dao Vallis	32°S, 263°W	−1.6	chaos	Greeley and Guest (1987); Crown *et al*. (1992); Crown and Greeley (1993)

such conditions may have developed in response to the growth of the cryosphere, whereby the increase in volume associated with the phase transition between water and ice placed any surviving groundwater under greater pressure, until it became sufficient to disrupt the local thickness of frozen ground (see also Section 11.1).

Other potential modes of failure include the breaching of the confined aquifer by impacts and local igneous activity, major

TABLE IV—*Continued*

Age	Channel	Approximate location of initial source region[b]	Elevation (km)[c]	Nature of source region	References
Early Amazonian	Hrad Vallis	34°N, 218.5°W	−3.9	fracture	Mouginis-Mark *et al*. (1984); Tanaka *et al*. (1992)
	Apsus Vallis	33°N, 224°W	−4.1	obscure	Tanaka *et al*. (1992)
	Tinjar Valles	28°N, 224.5°W	−3.8	obscure	Mouginis-Mark *et al*. (1984); Tanaka *et al*. (1992)
	Granicus Valles	27.5°N, 226°W	−3.9	fracture	Mouginis-Mark *et al*. (1984); Brandstrom (1986); Tanaka *et al*. (1992)
	Hebrus Valles/ Hephaestus Fossae	17.5°N, 233°W	−3.6	fracture	Mouginis-Mark *et al*. (1984); Tanaka *et al*. (1992)
Mid- to Late Amazonian	Olypica Fossae	27°N, 111°W	3.5	fracture	Mouginis-Mark (1990)
	Marte Valles	10°N, 202.5°W	−2.4	fracture	Tanaka and Scott (1986); Scott and Chapman (1995)

[a] References and elevations updated from original database compiled by Tribe and Clifford (1993). Channels listed include all deeply incised nonfretted channels larger than ∼200 km in length that have been reported in the literature. Channels are ordered by increasing West Longitude.

[b] Coordinates represent the elevation of the highest recognizable channel floor units.

[c] Elevations are based on the averages of the 1° × 1° MOLA gridded digital topography (MOLA Science Team 1999). For locations lying between two, or at the intersection of four, adjacent latitude–longitude bins the given elevation is the average of those bins. The mean elevation of outflow channel source regions during the mid- to Late Hesperian was approximately −0.7 km. During the Amazonian, it was approximately −3 km.

[d] Potential link in the "Chryse Trough" drainage system (Section 8.1.2).

[e] "Mid-Hesperian" is used here solely to convey a relative sense of timing and does not represent a formally recognized epoch.

[f] Episodic discharges from Valles Marineris occurred from multiple interior sources that included Aureum Chaos, chaotic terrain in Ganges, Capri, and Eos Chasmata, and possible lakes that may have existed deeper within canyon (see Section 10.3). The listed "source" location marks the most eastward extent of identifiable canyon channel floor deposits.

seismic events (Nummedal and Prior 1981, Leyva and Clifford 1993, Tanaka and Clifford 1993), or the decomposition of gas hydrates (Miller and Smythe 1970, Milton 1974, Baker *et al*. 1992, Fisk and Giovannoni 1999, Max and Clifford 2001). This last possibility is raised by the fact that the decomposition of 1 m^3 of gas hydrate (which can result from both pressure and thermal disturbances) yields ∼164 m^3 of gas (at STP) and 0.87 m^3 of liquid water (Kvenvolden 1993). This release is capable of generating pore gas pressures in excess of lithostatic to depths of 5 km (Max and Clifford 2001). While these pressures are clearly sufficient to disrupt a confined aquifer, it appears unlikely that the decomposition of gas hydrate was a significant contributor to the water that formed the channels. This conclusion is based on the fact that it takes considerably more energy to produce a unit volume of water from the decomposition of hydrate (with a heat of fusion of ∼73 kJ/mole; Sloan 1997) than it does from melting ground ice (∼6 kJ/mole; Peale *et al*. 1975).

But this last point does raise an important question: Could the melting of ground ice alone provide the volume of water necessary to erode the channels? This possibility was first suggested by Masursky *et al*. (1977) and has recently been raised again by McKenzei and Nimmo (1999), who argue that an episode of intense volcanic activity, centered on Tharsis, may have triggered a massive regional melting of ground ice that resulted in the hydrothermally driven and structurally controlled discharge of groundwater to the surface. While local igneous activity has almost certainly played a role in the origin of some outflow channels—such as those located to the west of Elysium Mons (Mouginis-Mark *et al*. 1984, Brandstrom 1986) and south of Hadriaca Patera (Crown and Greeley 1993, Squyres *et al*. 1987)—there are a number of serious volumetric problems with invoking this same mechanism to explain the majority of circum-Chryse channels.

For example, Carr (1987) has calculated that, if the channel flood waters carried the maximum theoretical sediment load of 40%, a minimum volume equivalent to a 50-m global ocean would have been necessary to produce the observed erosion. However, terrestrial experience indicates that the assumption of a 40% sediment load is grossly unrealistic, even for very energetic floods (Carr 1987, Baker *et al*. 1992). If more plausible values are assumed, then the minimum volume of water required to erode the channels is increased by as much as an order of magnitude.

There is also a question about the efficiency of melting and hydrothermal discharge. Depending on the size, magnitude, and location of crustal heating—as well as the nature and availability of structural pathways to the surface—it seems likely that only a small fraction (perhaps only 1–10%) of the total volume of ice melted and hydrothermally cycled by regional magmatic activity would have ever been discharged to the surface. The remainder would have either continued to convect as part of the subsurface hydrothermal system or condensed and flowed to saturate more remote and deeper regions of the crust, where it may have added

to the existing inventory of groundwater or simply been cold-trapped into the local cryosphere.

These arguments suggest that the minimum volume of ice that must have been melted in the Tharsis region to account for the water discharged by the outflow channels is equivalent to a global layer ~500-m deep. This compares with an estimated ~230–740-m total volume of H_2O that was potentially stored as ground ice in the Late Hesperian cryosphere (see Sections 6 and 8.2). Thus, if the melting of ground ice was the sole source of water for the circum-Chryse channels, it would have been necessary to melt between ~70% and 220% of the total theoretical inventory of ground ice that existed on the entire planet at this time.

The likelihood that such a large inventory of ground ice existed in the vicinity of Tharsis is exceedingly small. Given its equatorial location, and the elevated heat flow that has likely characterized this region since its early development, the inventory of ground ice in Tharsis was probably the least of any equivalent-sized area on the planet. However, even if this reasoning is wrong, and the requisite volume of ground ice was present, the extent of crustal disruption expected from its melting falls well short of that which is actually observed. These arguments suggest that while local volcanism undoubtedly contributed to the origin of some channels, the melting of ground ice alone appears incapable of producing the enormous volumes of water required to erode the majority of Late Hesperian channels.

It should be emphasized that the various mechanisms of channel genesis reviewed here are neither mutually exclusive nor do they exhaust the range of possibilities. Although there is considerable uncertainty about how individual outflow events were initiated, there is a clearer understanding of how they ceased. As discussed by Carr (1979), the catastrophic release of groundwater from a confined aquifer would have resulted in a rapid decline in local hydraulic head, reducing the local discharge to the point where the water-saturated crust was ultimately able to refreeze at the point of breakout, reestablishing both the original thickness of ground ice and the strength of the hydraulic seal.

4.3. Requirements for Hydraulic Confinement

The preceding discussion suggests that the origin of the Late Hesperian outflow channels is most consistent with the catastrophic release of groundwater from a subpermafrost aquifer, whose elevated water table was maintained in hydraulic disequilibrium with the global topography by its confinement beneath a thick layer of frozen ground (Fig. 7)—a hydraulic barrier whose presence is consistent with both the climatic and geothermal conditions that are thought to have existed at this time. Barring a mechanical or thermal disruption of the crust, the cryosphere is capable of confining groundwater under a significant hydraulic head as long as the hydrostatic pressure does not exceed the lithostatic pressure exerted by the local thickness of frozen ground, i.e.,

$$\rho_b g \Delta z > \rho_w g(\Delta h + \Delta z), \qquad (6)$$

where ρ_b is the bulk density of the cryosphere (which is assumed to be $\sim 2.7 \times 10^3$ kg m^{-3}), Δz is its thickness, ρ_w is the density of liquid water (10^3 kg m^{-3}), g is the acceleration of gravity (3.71 m s^{-2}), and Δh is the height of the global water table above the local terrain.

Clearly, the hydrostatic pressure on the cryosphere will be greatest where the surface elevation is lowest. In the northern plains, this minimum (−4.5 km) lies near the pole (Zuber *et al.* 1998a, MOLA Science Team 1999). Thus, the total elevation difference between the maximum elevation of outflow channel source regions and the minimum elevation in the north polar plains is ~5 km. Substituting this figure for Δh in Eq. (6), and solving for Δz, indicates that, at the time the channels formed, ~3 km of frozen ground would have been necessary to ensure confinement (Fig. 8). This value falls well within the ~2.1–3.7 km-thickness of the polar cryosphere estimated from theoretical models of the thermal evolution of the crust (Table II). These calculations assume a geothermal heat flux of 65–95 mW m^{-2} (appropriate for the period ~2–3 Ga; Fig. 2), a groundwater freezing temperature of 252–273 K, a mean polar surface temperature of 154 K, and an effective thermal conductivity of 2.0 W m^{-1} K^{-1}. As discussed in Section A.2, however, the column-averaged thermal conductivity of the near-polar cryosphere is probably closer to ~3.0 W m^{-1} K^{-1}. If so, then the expected thickness of frozen ground during the Late Hesperian increases to ~3.1–5.5 km, a range that comfortably exceeds the thickness required to support an elevated water table.

Note that the above calculation indicates that the ability of the polar cryosphere to support an elevated water table occurred fairly late in the planet's geologic history. In Sections 5 and

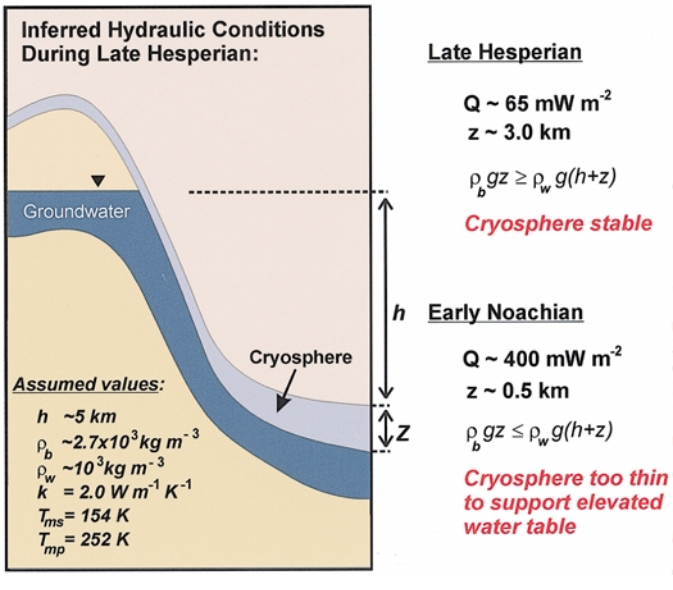

FIG. 8. Comparison of the ability of the Late Hesperian and Early Noachian polar cryosphere to confine a global groundwater table implied by the elevation of the Late Hesperian outflow channel source regions.

6 we explore the implications of this result for the hydraulic conditions that existed during the Noachian and Early Hesperian.

4.4. Fate of Water Discharged to Northern Plains

Speculation regarding the possible fate of the floodwater that was discharged to the northern plains by the channels has included local ponding and infiltration into the crust (Masursky *et al*. 1977, Baker *et al*. 1991, Head *et al*. 1999), freezing, sublimation, and eventual cold-trapping at higher latitudes (Clifford 1993); and the *in situ* survival of the resulting frozen lakes and seas to the present day, aided by their burial beneath a protective cover of eolian sediments and volcanics (Carr 1990). As discussed later in this paper, the formation of frozen lakes and seas, followed by the sublimation and cold-trapping of ice at higher latitudes, appears to have been an inevitable result of the planet's thermal and volatile evolution. However, the possibility of any significant local infiltration is effectively precluded by the physical, thermal, and hydraulic conditions that must have existed within the plains to explain the elevated Late Hesperian water table (Fig. 7).

In support of this conclusion, note that a necessary prerequisite for the widespread occurrence of groundwater is that the thermodynamic sink represented by the cryosphere must first be saturated with ice. That is, wherever a continuity of pore space exists between an unsaturated region of the cryosphere and a deeper reservoir of H_2O, the local geothermal gradient will drive the transfer of vapor from the warmer (higher vapor pressure) depths, to the colder (lower vapor pressure) near surface. This process will continue until either the cryosphere is saturated with ice or the deeper reservoir of H_2O is exhausted (Clifford 1991, 1993). By the Late Hesperian, this implies the presence of a self-sealing and effectively impermeable barrier of frozen ground $\sim$2–3 km-thick in the northern plains that would have prevented the local infiltration of water discharged by catastrophic floods. Note that the potential for infiltration is not significantly improved even if the local cryosphere is initially dry, for as water attempts to soak into the cold, dry crust, it will quickly freeze, creating a seal that prevents any further infiltration from the ponded water above.

Infiltration is also precluded by hydraulic considerations. As discussed in Section 5 (and by Clifford 1993), a global groundwater system that is released from an initial state of disequilibrium will rapidly ($<10^8$ years) reach equilibrium in response to the flow induced by the declining gradient in relative hydraulic head. Thus, any pore space that is in hydraulic communication with the rest of the crust, and that lies at an absolute elevation lower than that of the global water table, will generally be saturated with either water or ice. As a result, even if an unobstructed conduit existed between the ponded floodwaters in the plains and the global aquifer confined beneath, it would not have led to the inflow of the floodwater back into the crust, but rather the expulsion of additional groundwater onto the surface. This flow would have continued until either the floodwater in the plains and groundwater table in the highlands had reached equilibrium, or the decrease in local hydraulic head had reduced the artesian discharge sufficiently for the crust to refreeze and reestablish its hydraulic seal.

5. IMPLICATIONS FOR THE EARLY NOACHIAN

Although the thickness of the Late Hesperian cryosphere was evidently sufficient to support an elevated water table, various arguments suggest that the thickness of the earlier Noachian cryosphere was not. For example, if the valley networks are indeed evidence of an early greenhouse climate, where rainfall and surface runoff occurred over much of the planet (Masursky *et al*. 1977, Pollack *et al*. 1987, Craddock and Maxwell 1993, Carr 1999), then the distribution of networks at latitudes as high as 65°S (Baker *et al*. 1992) indicates that the early climate was too warm, and the cryosphere too thin, to support even a minimally elevated global water table.

This conclusion remains valid, even if the early climate was cold. Assuming the present range of mean annual surface temperatures, the resulting thickness of frozen ground would still have been too thin to support an elevated water table equivalent to that which existed during the Late Hesperian—a consequence of the Early Noachian's 4–6x greater global heat flux (Figs. 2 and 8, Table II). Another consequence of this high early heat flow is that a much larger fraction of the planet's total inventory of H_2O would have been present as a liquid (Section 6)—further diminishing any potential for widespread confinement.

In the absence of a sufficient confining layer, the martian hydrosphere would have been in effective hydrostatic equilibrium—responding to local perturbations caused by evaporation and precipitation, as well as seismic and thermal disturbances, by flowing from regions of elevated hydraulic head to saturate the regions of lowest geopotential. Given a planetary inventory of water equivalent to that required to explain the elevated water table of the Late Hesperian (Fig. 7), an inevitable consequence of the lack of an adequate confining layer during the Noachian would have been the formation of a primordial ocean in the northern plains (Fig. 9) and standing bodies of water in other low-lying regions such as Hellas and Argyre. As discussed in Sections 3 and 10, the former existence of such bodies is consistent with the tentative identification of ancient shorelines (Parker *et al*. 1989, 1993) as well as other lines of geomorphic evidence (e.g., Allen 1979, Chapman 1994, Kargel *et al*. 1995), which suggest that, after these reservoirs of liquid water froze, they may have persisted on the surface as massive ice deposits throughout much of the Hesperian.

An estimate of the minimum extent of Noachian flooding can be made by calculating the size of the subsurface inventory of H_2O necessary to explain the origin of the Late Hesperian outflow channels and then determining what fraction of the planet's surface would have been inundated by that volume of water if it was allowed to come into equilibrium with the present global topography. This calculation assumes that: (1) the statistical distribution of elevations has remained roughly constant

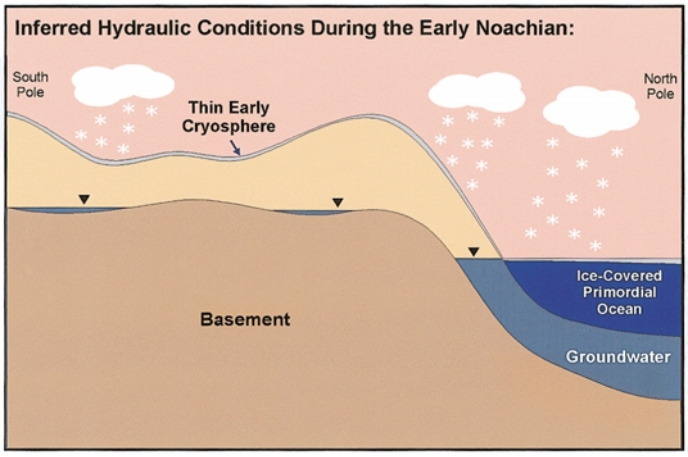

FIG. 9. An idealized illustration of the hydraulic conditions thought to have characterized the Early Noachian, assuming a cold early climate. Note that if the Noachian was warm, the argument for an unconfined groundwater system, and primordial ocean, is made even stronger.

with time, (2) the physical and thermal properties of the crust are reasonably described by the quantities and relations discussed in Appendix A (and summarized in Table I), (3) the Late Hesperian outflow channels originated under the hydraulic conditions illustrated in Fig. 7, and (4) no significant bodies of water or ice were present on the surface at the time the channels formed.

The Late Hesperian inventory of subsurface H_2O consisted of two principal reservoirs: (1) the ice necessary to saturate the pore volume of the cryosphere and (2) the groundwater required to saturate the underlying crust up to the +0.65 km maximum elevation of the outflow channel source regions. The volume of ice stored in the cryosphere is readily calculated by integrating the pore volume of the crust (i.e., Eq. (1)) between the planet's surface and the depth to the base of the cryosphere given by Eq. (3). For surface porosities of 20–50%, we find that the Late Hesperian cryosphere could have stored the equivalent of a global ocean ∼230–740-m deep as ground ice—a calculation that assumes the present latitudinal range of mean annual surface temperatures, a heat flow of 65 mW m^{-2}, and a basal melting temperature of 252–273 K (Fig. 2 and Table II). In a similar way, we can calculate the amount of groundwater necessary to saturate the crust (beneath the cryosphere) up to the +0.65 km maximum elevation of the outflow channel source regions. This volume is equivalent to a global ocean ∼320–640-m deep. Taken together, these storage figures imply a minimum planetary inventory of ∼550–1400 m of H_2O. Note that this is a highly conservative estimate, for it assumes that no other significant reservoirs of H_2O (such as the polar caps or ice-covered lakes or seas) existed on the surface at the time of peak channel activity.

Clearly, if the Early Noachian was warm, then virtually all of the planetary inventory of water would have been available to inundate the lowest elevations and saturate the lowermost porous regions of the crust. However, if the early climate was cold (i.e., resembling that of today), then some fraction of this inventory must have been cold-trapped in the Noachian cryosphere. Assuming the present range of mean annual surface temperatures and an early geothermal heat flux of 400 mW m^{-2} (Fig. 2), we find that the cryosphere could have stored the equivalent of ∼85–170 m of H_2O as ground ice. Subtracting this quantity from the estimated planetary inventory of ∼550–1400 m of H_2O suggests that, even if the early climate of Mars was cold, ∼470–1200 m of liquid water was present either on, or beneath, the surface during the Noachian. Assuming that this amount saturated the crust and ponded on the surface in hydrostatic equilibrium, then ∼26–32% of the planet's surface must have been covered by standing bodies of water and ice, assuming, once again, that the statistical distribution of surface elevations at that time was similar to that of present-day Mars (Fig. 10).

Of course, if sizable surface reservoirs of H_2O existed at the poles, in the northern plains, and elsewhere during the Late Hesperian, then the planetary inventory of water may have been as much as a factor of two greater than the ∼550–1400 m figure calculated above. Although this volume significantly exceeds the estimated maximum storage capacity of the Martian crust (equivalent to a ∼1.4 km-deep global ocean, Clifford 1993), it is readily accommodated as long as the excess is stored on the surface. The absence of such a massive surface reservoir on Mars today is consistent with either a smaller initial inventory (i.e., <1.4 km), the existence of some efficient loss process, or an excess that now resides as massive ice deposits beneath the northern plains (Section 9).

6. EARLY THERMAL AND HYDRAULIC EVOLUTION OF THE HYDROSPHERE

If Mars did possess an early ocean, then it raises two obvious questions: Where did the ocean go? And how did the planet's hydrosphere evolve from an initial state of hydraulic equilibrium with the global topography in the Noachian (Fig. 9), to a state of extreme disequilibrium by the Late Hesperian (Fig. 7)? The answers to these questions appear related, in that the progressive assimilation of a primordial ocean likely charged the crust with the water required for the later development of the outflow channels. As discussed by Clifford and Parker (1999), the process by which this assimilation occurred appears to have been a natural consequence of the evolution of the post-Noachian climate and heat flow.

If the early Noachian did start out warm, theoretical models of atmospheric evolution suggest that such conditions did not persist much beyond the end of heavy bombardment (Haberle *et al.* 1994, Carr 1999). With the transition to a colder climate, and the rapid decline in crustal heat flow, several important changes would have occurred. In the plains, the primordial ocean would have begun to freeze, developing an ice cover that thickened with both time and increasing latitude (Fig. 3, Table II). Similarly, in the south, a freezing front would have developed in the highland crust, creating a growing cold-trap for subsurface H_2O.

The increasing thickness of frozen ground in the highlands would have had three important effects. First, as ice condensed within the near-surface pores, it would have sealed off the water

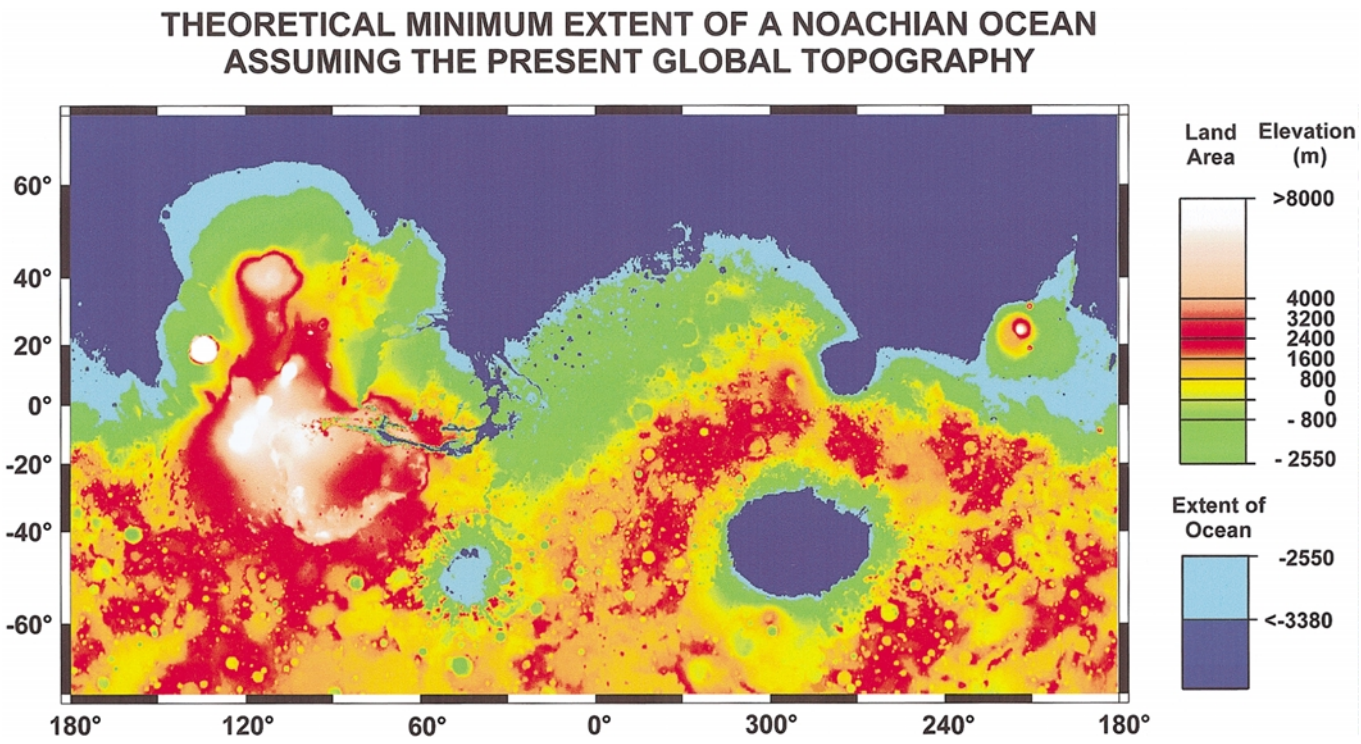

FIG. 10. A cylindrical projection of Mars, from 70°N to 70°S latitude, illustrating the theoretical distribution of surface water during the Noachian, based on the analysis presented in Section 5. Assuming that the statistical distribution of Noachian elevations resembled that of today, a minimum of ~26–32% of the planet's surface would have been covered with water and ice.

in the deeper crust from any further communication with the atmosphere (Clifford 1993). Assuming an effective crustal permeability of $\sim 10^{-15}$ m^2, the elimination of atmospheric recharge would have led to the decay of any precipitation-induced influence on the shape of the global water table in $\lesssim 10^8$ years—causing an initial increase in ocean sea-level as the former precipitation-induced groundwater table and ice-covered ocean came into effective hydrostatic equilibrium.

Second, as the cryosphere deepened with time, the condensation of ice behind the advancing freezing-front would have created a growing sink for the planet's inventory of groundwater. Where the cryosphere and water table were in direct contact, the transition from groundwater to ground ice was straightforward. However, in many locations throughout the highlands, the vertical distances separating the base of the cryosphere from the water table may have been measured in kilometers. Under such conditions, the depletion of groundwater is expected to have occurred via the geothermally induced diffusion of vapor from the warmer depths to the colder pores behind the advancing freezing-front (Clifford 1991, 1993).

By combining the crustal porosity profile given by Eq. (1), the thickness of frozen ground calculated from Eq. (3), and the decline in geothermal heat flux given by Fig. 2, the volume of H_2O lost from the groundwater inventory and assimilated by the growing cryosphere can be estimated as a function of time. The results of this calculation are presented in Fig. 11, where the growing pore volume of the cryosphere is plotted for several combinations of surface porosity and basal melting temperature. For simplicity, the calculations assume a spherically symmetric Mars (i.e., no surface topography). While this is a reasonable "back of the envelope" approach, in reality the problem is substantially more complicated. The inevitable

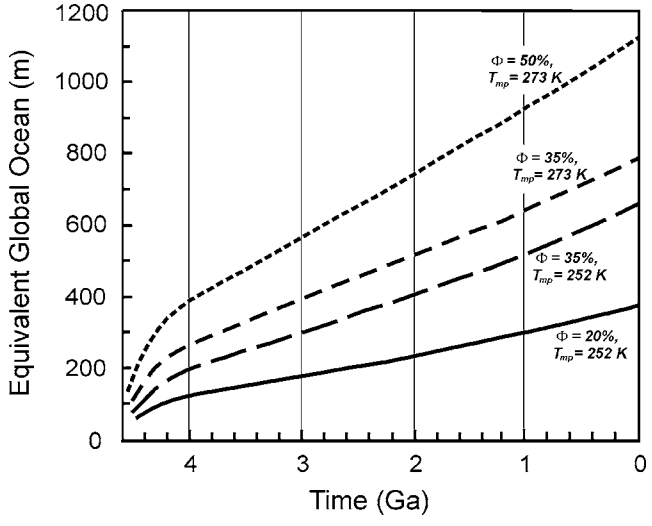

FIG. 11. The volume of H_2O (expressed as an equivalent global ocean) assimilated as ice by the cryosphere versus time. These calculations assume an effective thermal conductivity for frozen ground of 2.0 W m^{-1} K^{-1} and a temporal decline in geothermal heat flux given by Fig. 2.

flooding of low-lying elevations during the Noachian means that a considerable fraction of the planet's inventory of liquid water would have resided on the surface. Under these conditions, the volume of water assimilated per unit area into the thickening ocean ice cover would have considerably exceeded that which condensed in the expanding region of frozen ground that was developing concurrently in the highlands. This is due to both the higher thermal conductivity of the ocean ice and the 100% volumetric contribution of H_2O to the ice cover (vs. the significantly smaller volume fraction stored as ice in the pores of frozen ground). For this reason, the total amount of water potentially stored as ice during the Noachian probably fell within the higher range of values plotted in Fig. 11. A probable upper limit is represented by the top curve, which corresponds to a surface porosity of 50% and a basal melting temperature of 273 K. This combination yields a figure for the storage capacity of the Early Noachian cryosphere ($\sim$4.4 Ga) equivalent to a global ocean $\sim$200 m deep. Over the next 400 million years, the estimated volume of H_2O assimilated by the cryosphere likely doubled in response to the decline in crustal heat flow—thereafter increasing by an additional $\sim$175 m every billion years. As discussed in Section 8.2, the corresponding reduction in the planet's inventory of groundwater would have significantly limited the potential for later episodes of flooding and could well explain the apparent decline in outflow channel activity observed during the Amazonian.

Note that the calculated thickness of ocean ice presented in Table II and Fig. 3 assumes thermal equilibrium between the local mean annual surface temperature and geothermal heat flux. Although we believe that this is a reasonable approximation of the thermal state that existed over much of the ocean, there are plausible conditions under which this assumption is no longer valid, such as when an appreciable fraction of the incident sunlight penetrates the ice cover, or where there is significant sublimation from the surface of the ice (McKay *et al*. 1985). On Mars, the role of absorbed sunlight was probably minimized by the precipitation and entrainment of atmospheric dust following the decay of local and global dust storms. However, if the early climate resembled that of the present, then the potential for sublimation, especially at low latitudes, was substantial.

Under the current latitudinal range of mean annual surface temperature and atmospheric partial pressure of H_2O, ground ice is unstable at latitudes equatorward of $\sim 40^\circ$ (Section A.2). If these conditions also existed during the Noachian, then $\sim 10^{-5}$–10^{-1} m of ice may have sublimed from the low-latitude ocean ice cover each year (depending on the local surface temperature, relative humidity, average wind speed, and thickness of any overlying mantle of sediment). However, because the martian obliquity is chaotic, and may reach peak values as high as $\sim 60^\circ$ (Touma and Wisdom 1993, Laskar and Robutel 1993), there is also a significant potential for episodic sublimation at high latitudes—although a number of uncertainties make its magnitude difficult to estimate (Section 11.2).

If the sublimation rate from the early ocean was high, then a dynamic equilibrium would have eventually been reached between the ice lost from the surface and the freezing of new ice at the ice cover's base. This freezing would have occurred in response to the energy deficit between the large amount of heat lost by conduction through the ice and the small amount supplied from below by the planet's geothermal heat flow. The heat required to make up this deficit would have come from the latent heat released by freezing. Assuming that the water lost by sublimation and freezing was replenished by the ocean's communication with the rest of the subpermafrost hydrosphere, the net effect of these processes would have been to reduce the thickness of the ice cover and prolong the time required for the ocean to freeze to its base. More extensive discussions of the thermal evolution of ice-covered lakes and oceans on Mars include those by Nedell *et al*. (1987), Squyres (1989), Carr (1990), McKay and Davis (1991), Kargel *et al*. (1995), and Moore *et al*. (1995). Although differing in detail, these models yield qualitatively similar results.

As the thickness of the cryosphere increased with time, so too did its ability to confine a groundwater system under significant hydraulic head. However, this fact alone does not explain how the elevated water table of the Late Hesperian came into being, unless a corresponding mechanism can be identified for charging the subsurface with groundwater.

7. POLAR CAP FORMATION AND THE ONSET OF BASAL MELTING

The mechanism we propose for the crustal assimilation of a primordial ocean is similar to that originally advanced by Clifford (1987) to explain the removal and subsurface storage of an ancient Martian ice sheet. The process is initiated when the instability of ice at low-latitudes leads to its sublimation and eventual cold-trapping at the poles (Fig. 12, T0). In response to this added layer of insulation, the melting isotherm at the base of the cryosphere rises until thermal equilibrium is reestablished. As deposition continues, the melting isotherm eventually rises to the actual base of the polar deposits (Fig. 12, T1), where the deposition of any additional ice is offset by the melting of an equivalent layer at the base of the cap. The drainage of the resulting meltwater into the underlying global aquifer will then cause the local water table to rise in response, creating a gradient in hydraulic head that drives the flow of groundwater away from the poles (Clifford 1993). By this process, the H_2O associated with a primordial ocean may have been slowly introduced into the subsurface at both poles, ultimately raising the position of the global water table, confined by the thickening cryosphere, to the level required to explain the elevated source regions of the Late Hesperian outflow channels. While this scenario outlines the basic process of how a frozen ocean may have been assimilated into the crust, there are some important details that are unaddressed by this simple picture—the most notable being the effect of the differing elevations of the north and south polar regions on the depositional and hydraulic evolution of their respective caps.

In the south, the deposition of H_2O, derived from the sublimation of ice at lower latitudes, should have led to the early

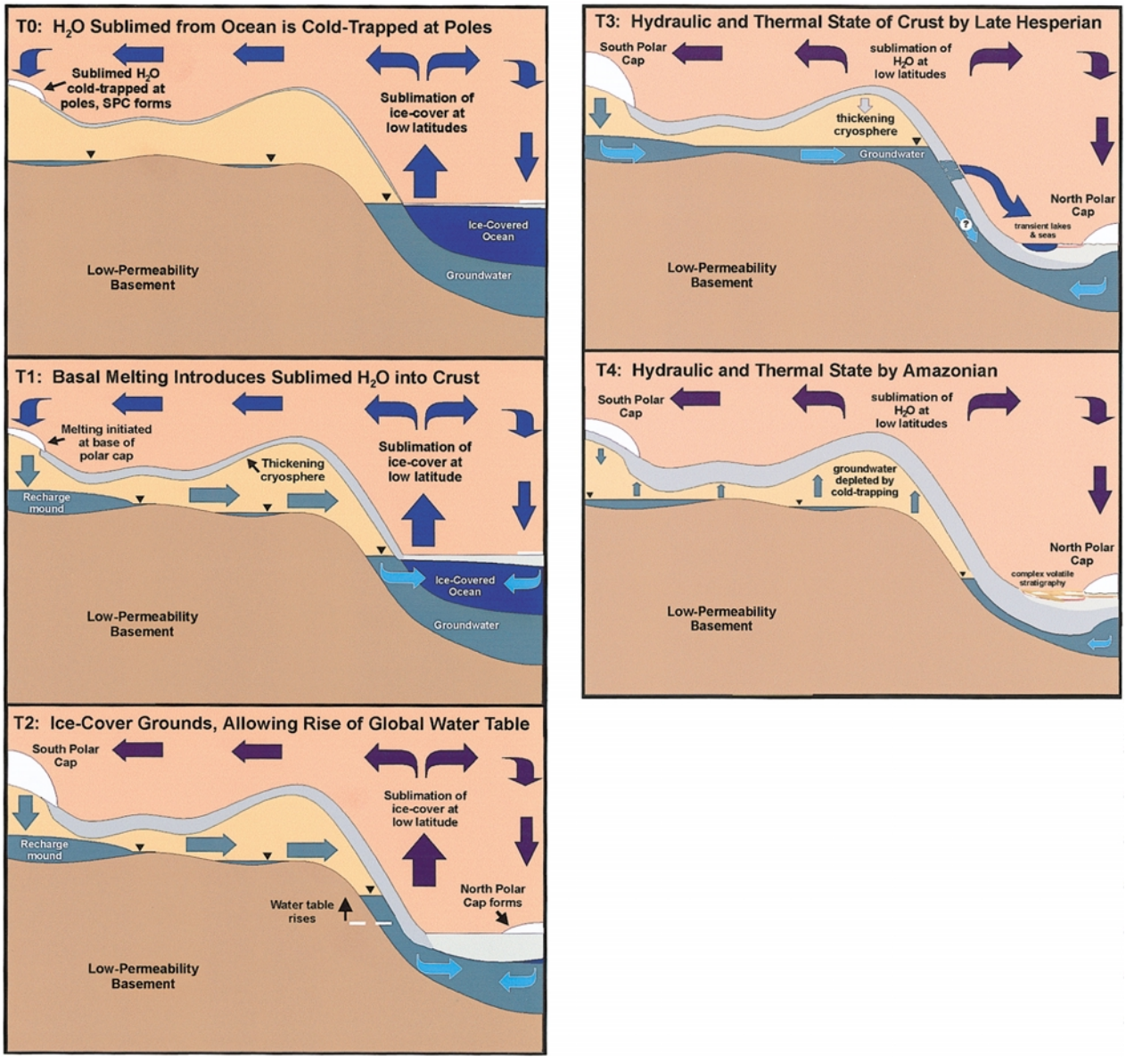

FIG. 12. An idealized illustration of the potential evolution of the Martian water table between the Late Noachian (T0) and Early Amazonian (T4). T0 illustrates the conditions expected during the early evolution of the ice-covered ocean where subliming ice at low latitudes is cold-trapped at the poles. As the process of sublimation and polar cold-trapping continues, the south polar deposits become sufficiently thick that they begin to undergo melting at their base—introducing the resulting meltwater into the global aquifer (T1). In contrast, the presence of an ocean in the northern plains would have delayed the construction of the north polar cap until the Early to mid-Hesperian, when the ocean would have finally frozen to its base. The continued growth of the cryosphere, combined with the introduction of water into the subsurface via basal melting, ultimately allowed the water table to begin its slow rise away from equilibrium (T2). By the Late Hesperian the global water table reached its peak (T3)—a maximum that reflects a turning point in the evolution of the hydrosphere where the amount of water assimilated into the cryosphere finally began to exceed the amount introduced into the subsurface via basal melting. By the Early Amazonian, the continuation of this process would have resulted in a significant reduction in the size of the planet's groundwater inventory and the elevation of the global water table (T4). This prediction appears consistent with the observed decline in outflow channel activity and source region elevation that occurred during this epoch (Table IV).

development of a perennial ice cap and the recharge of the global water table by basal melting. However, in the north, the presence of an ice-covered ocean at the pole would have caused its cap to evolve in a much different manner.

For an ocean ice cover in thermal equilibrium, the deposition of ice on the surface will necessarily result in the melting of an equivalent layer at the ice cover's base (Fig. 12, T1). If the rate of deposition exceeds the rate at which the basal ice can be geothermally melted, it might seem reasonable to expect that the thickness of the ice cover would grow in excess of the equilibrium values presented in Table II. However, when deposition occurs on a floating ice cover, the underlying liquid water is incapable of supporting the basal shear stress associated with the build-up of a cap. As a result, the expected high rate of early

deposition should have induced a radial spreading of the polar ice that redistributed the excess mass to lower latitudes, where, because of lower rates of local deposition, an equilibrium thickness could be maintained by basal melting alone. For this reason, the development of a perennial ice cap in the north must have been delayed until the primordial ocean was frozen throughout; a process that, depending on the initial depth of the ocean and local evolution of crustal heat flow, may have taken as long as $\sim 10^9$ years.

When the geothermal heat flux had declined enough for the north polar ice cover to ground, the continued propagation of the freezing front into the underlying crust finally provided an anchor that was sufficient to support the further growth of the cap. It also contributed to a significant increase in the cryosphere's confinement potential, for, although the thermal conductivities of ice and rock are nearly the same, their bulk densities are not. Therefore, as the cryosphere deepened and encompassed more rock beneath the frozen northern ocean, its ability to confine a groundwater system under significant hydraulic head also increased, permitting the global water table to rise as the H_2O from the subliming primordial ocean was introduced into the crust via basal melting. It was this critical development that we believe finally enabled the hydrosphere to begin its slow evolution away from hydraulic equilibrium with the global topography (Fig. 12, T3).

8. RISE OF THE GLOBAL WATER TABLE AND THE POTENTIAL FOR EPISODIC RE-FLOODING OF THE NORTHERN PLAINS

With the rise of the global water table in the highlands, the stability of the cryosphere, and the global aquifer confined beneath it, depended on the strength of the hydraulic seal at low elevation. For this reason, the potential for reflooding the northern plains (and any other region of low elevation) was greatest when the cryosphere was thinnest, during its early development.

Breaches of the global aquifer were undoubtedly frequent, arising from impacts, earthquakes, local volcanic activity, and the thermal disturbances caused by the ponded floodwater discharged by these events. These mechanical and thermal disruptions were likely supplemented by two other sources of instability: (1) the planet-wide increase in artesian pressure caused by the rise of the global water table, and (2) the more localized increase in hydraulic head associated with the occurrence of basal melting at the poles.

In the north, the low density of the polar ice cap, combined with its low elevation within the plains, made it highly susceptible to hydraulic disruption. For this reason, if the global water table rose too quickly, the increase in artesian pressure would have destabilized the cap, permitting the underlying aquifer to discharge to the plains. This discharge would have continued until the local hydraulic head had fallen sufficiently for the cryosphere to refreeze and reestablish its hydraulic seal. In this way, the growth of the polar cryosphere may have been the limiting factor that determined how rapidly the global water table was able to rise with time.

Alternatively, the water table may have risen slowly enough that the confinement potential of the thickening cryosphere was never seriously threatened. Such slow growth may have resulted from either low rates of polar deposition and basal melting, or by the presence of enough local leaks in the cryosphere's hydraulic seal that destabilizing hydraulic pressures may simply have never developed. However, the possibility of limited polar deposition and basal melting is at odds with expectations. Indeed, given both the susceptibility of the exposed ocean ice cover to sublimation, and the substantially higher ($\sim$3–5 $\times$ present) geothermal heat flux of the Early and mid-Hesperian, the rate of polar deposition and basal melting at this time was likely near its maximum (Section 8.1.1). If so, then it suggests that either local leaks in the global aquifer were common, or that the hydraulic pressure at low elevation was near (and may have frequently exceeded) the confinement potential of the cryosphere.

8.1. Hydraulic Head Development in Response to Polar Basal Melting

In an unconfined aquifer, the influx of water derived from basal melting will result in the rise of the local water table in the form of a groundwater mound (Fig. 13a; see also Clifford 1993). The resulting gradient in hydraulic head will then drive the flow of groundwater away from the pole, where it may eventually replenish the H_2O lost at lower latitudes by artesian discharges to the surface and by the sublimation of ice from the regolith and ocean ice cover (Fig. 12).

The development of a groundwater mound in response to polar basal melting was investigated by Clifford (1993) based on the previous work of Hantush (1967), who considered the analogous terrestrial problem of the artificial recharge of an aquifer beneath a circular spreading basin. Subject to the simplifying assumptions discussed by Clifford (1993), the maximum height h_m of a groundwater mound following the onset of basal melting is given by

$$h_m = \left[\frac{Q_r \nu}{2\pi k g} \left(W(u_o) + \frac{1 - e^{-u_o}}{u_o} \right) + h_i^2 \right]^{1/2}, \qquad (6)$$

where Q_r is the recharge volume ($=\pi a^2 w$, where a is the radius of the region at the base of the cap undergoing basal melting and w is the recharge rate per unit area), $u_o = a^2 \nu \varepsilon / 4 k g \bar{h}\, t$ (where ν is the kinematic viscosity of water, ε and k are the effective porosity and permeability of the aquifer, g is the acceleration of gravity, $\bar{h}$ is a constant of linearization ($=0.5(h + h_i)$, and t is the elapsed time), and $W(u_o)$ is the well function for a nonleaky aquifer given by

$$W(u_o) = \int_{u_o}^{0} \frac{e^{-u_o}}{u_o} du_o$$

$$= -0.5772 - \log_e u_o + \sum_{i=1}^{n} (-1)^{1+n} \frac{u_o^n}{n \cdot n!}. \qquad (7)$$

As noted by Hantush (1967) the solution given by Eq. (6) is

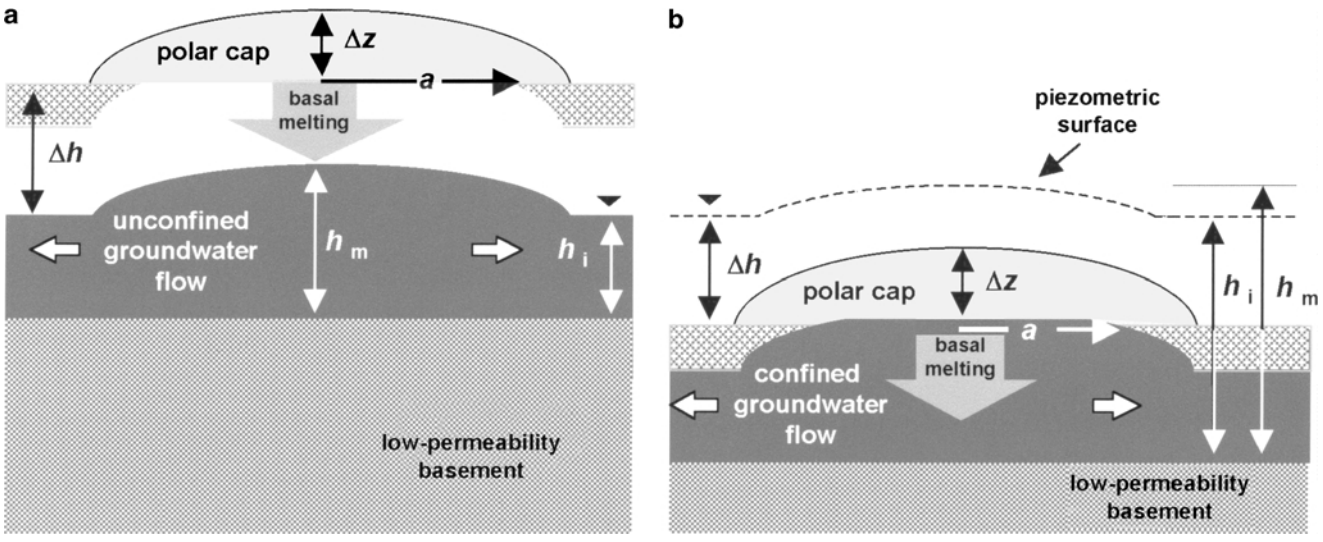

FIG. 13. (a) The development of a groundwater mound beneath the south polar cap resulting from basal melting. The illustrated hydraulic relationships assume that the global aquifer is locally unconfined. (b) Hydraulic head development beneath the north polar cap in response to basal melting. Note that the elevation of the global water table above the local terrain does not preclude the introduction and flow of groundwater away from the pole. The necessary criteria for such flow is that the lithostatic pressure exerted by the cap must exceed the artesian pressure associated with the elevated water table, as well as any additional increase in local hydraulic head due to basal melting (Eq. 8b).

valid for groundwater mound heights ($h_m - h_i$) up to 50% of the initial depth of saturation (h_i).

The hydraulic conditions illustrated in Fig. 13(a) might well describe those that once existed (and may episodically still occur) beneath the south polar cap, whose ∼2 km absolute elevation (Smith *et al*. 1999) is both 6 km higher than the north polar cap and ∼1.4 km above the maximum elevation of Late Hesperian outflow channel source regions. These topographic relationships strongly suggest that the global aquifer beneath the south polar cap was initially unconfined (e.g., Fig. 12).

The corresponding hydraulic conditions expected beneath the north polar cap are illustrated in Figs. 12 and 13(b). Under these confined conditions, the development of a groundwater mound, in the form depicted in Fig. 13(a) and described by Eq. (6), is no longer possible. However, the introduction of basal meltwater into a confined aquifer will result in a similar evolution in local hydraulic head—an expectation that can be verified, for radial distances $r \geq a$, by a comparison with the conceptually similar (but technically poorer) analog of the confined recharge well equation (e.g., see Fetter 1980).

Development times for polar groundwater mounds 1.0–2.5 km in height are presented for various permutations of aquifer hydraulic properties, saturated thickness, recharge volume, and basal melting area, in Table V and Fig. 14. These examples were chosen to represent the effective properties of aquifers of equivalent thickness beneath the cryosphere (note that the assumption of column-averaged properties in these calculations is a necessary simplification to obtain an analytical result).

For a fixed recharge volume Q_r, groundwater mound development times are lengthened by an increase in aquifer depth, porosity, permeability, or recharge area. For the combination of conditions considered in Table V, development times for a groundwater mound 2.5 km high range from $\sim 10^4$–10^5 yrs. These results indicate that, at the south pole, a groundwater

TABLE V
Increase in Polar Hydraulic Head vs Time as a Result of Polar Basal Melting

Radius of basal melting area a, km	Aquifer thickness, h_i or b, km	Porosity, %	Permeability k, m^2	Recharge volume Q, km^3 yr^{-1}	Hydraulic Head = $h_m - h_i$, km	Time (yrs) 1.0	1.5	2.0	2.5
500	5	5.0	1E-13	5.00		8.49E + 03	1.18E + 04	1.57E + 04	1.98E + 04
	10	1.0	1E-14	0.50		1.57E + 04	2.37E + 04	3.23E + 04	4.15E + 04
	20	0.1	1E-15	0.05		1.61E + 04	2.53E + 04	3.65E + 04	5.00E + 04
750	5	5.0	1E-13	10.00		1.92E + 04	2.65E + 04	3.55E + 04	4.46E + 04
	10	1.0	1E-14	1.00		3.54E + 04	5.35E + 04	7.25E + 04	9.37E + 04
	20	0.1	1E-15	0.10		3.65E + 04	5.70E + 04	8.19E + 04	1.13E + 05

Note. A permeability of 1 darcy = 1×10^{-12} m^2.

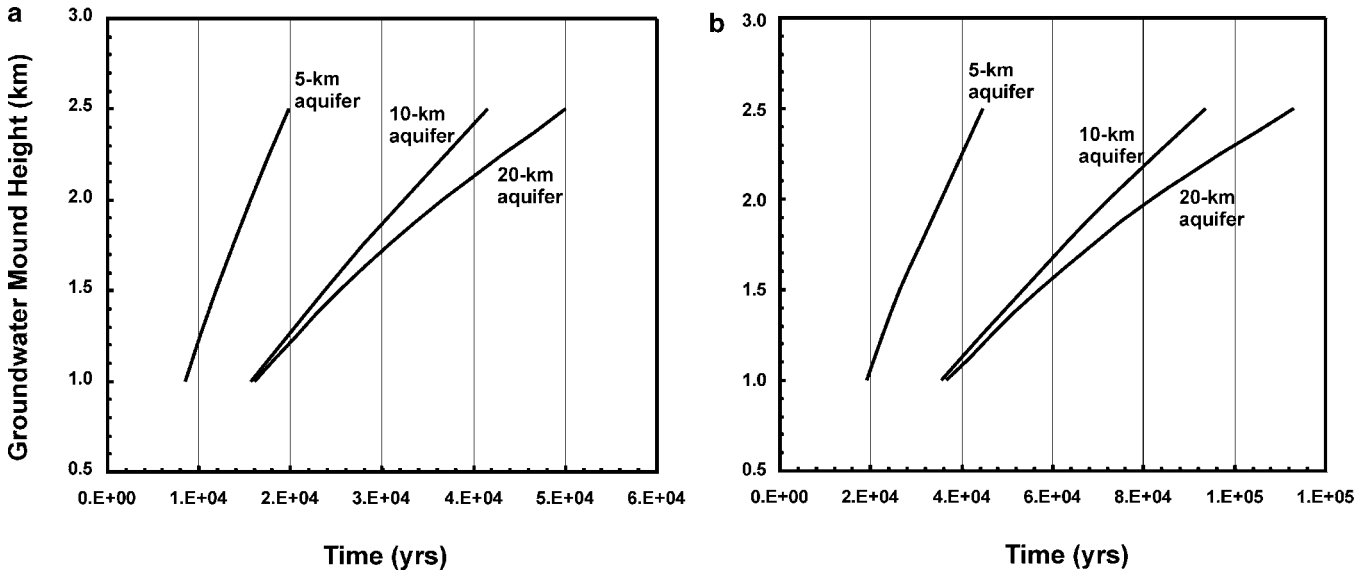

FIG. 14. Ground water mound development times for basal melting areas with radii of (a) 500 km and (b) 750 km, for the aquifer characteristics and recharge volumes given in Table V.

mound in an initially unconfined aquifer could quickly evolve to the point of contact with the base of the cap. In that event, a continued increase in local hydraulic head is permitted as long as it does not exceed the lithostatic pressure exerted by the cap, i.e.,

$$\rho_{\rm pd} g \Delta z > \rho_{\rm w} g[(h_{\rm m} - h_{\rm i})\Delta h], \tag{8a}$$

where $\rho_{\rm pd}$ is the density of the polar deposits, Δz is their total thickness, $\rho_{\rm w}$ is the density of water, Δh is the difference in elevation between the global water table and base of the polar cap, and $(h_{\rm m} - h_{\rm i})$ is the pressure head induced by basal melting. A similar stability criterion applies in the north, although here the introduction of meltwater under artesian conditions (Fig. 13(b)) makes the condition for confinement more demanding, i.e.,

$$\rho_{\rm pd} g \Delta z > \rho_{\rm w} g[\Delta h + (h_{\rm m} - h_{\rm i})]. \tag{8b}$$

Given the hydraulic relationships described by Eqs. (6) and (8), the potential range and heterogeneity of crustal properties, local cryosphere thickness, and the expected temporal variations in polar deposition and basal melting, a variety of possible scenarios can be envisioned for the evolutionary development of the polar caps and local groundwater system.

8.1.1. Implications for the evolution of the global aquifer at the south pole. At the south pole, the development of a polar cap and the onset of basal melting probably began during the Noachian, well before the northern ocean had frozen throughout. At that time, large deposition rates (resulting from the sublimation of the ocean ice-cover at low-latitudes), combined with the planet's high early heat flow, could have easily resulted in the introduction of $\geq$10 km^3 of basal meltwater (per 10^6 km^2 of polar deposits) into the global aquifer each year (Fig. 15). However, until the northern ocean had frozen to its base, this recharge would have had little effect on the elevation of the global water table—although it would have had a considerable impact on the development of a groundwater mound beneath the southern cap. Depending on the rate of basal melting in relation to the permeability of the underlying crust, the hydraulic evolution of the south polar aquifer may have proceeded in one of several different ways.

If the basal melting rate exceeded the rate at which the resulting meltwater was able to infiltrate the underlying crust, then it would have led to the build-up of a subglacial reservoir whose growth would have eventually destabilized the cap and resulted in a major discharge to the surrounding plains. Alternatively, the permeability of the crust may have been sufficient to accommodate the initial infiltration of basal meltwater, but low enough

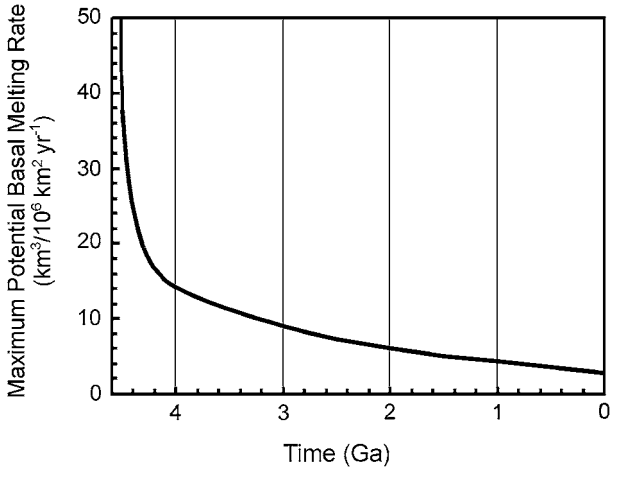

FIG. 15. Maximum theoretical polar basal melting rate vs. time. Volume of meltwater is per 10^6 km^2 of polar deposits undergoing basal melting. Assumed geothermal heat flow is that given by Fig. 2.

that it led to the rapid growth of a groundwater mound and a quick transition to confined conditions. If so, then the continued increase in local hydraulic head would have again led to the generation of destabilizing pressures and the eventual discharge of meltwater to the surface.

Possible evidence of Hesperian-age basal melting is found in Dorsa Argentea (78°S, 40°W), a region that is located just beyond the periphery of the present-day south polar layered deposits. The evidence consists of an extensive network of sinuous and braided ridges that resemble terrestrial eskers, features that result from the deposition of fluvial sediments in subglacial rivers and streams (Howard 1981, Kargel and Strom 1992, Metzger 1992, Head and Fishbaugh 2000, Head and Pratt 2001). While other modes of origin are also possible (e.g., Howard 1981, Metzger 1992, Ruff 1994), the existence of esker-like features beyond the periphery of the present south polar deposits is consistent with the theoretical expectation and other geomorphic evidence that the cap was once more extensive and produced a considerable volume of basal meltwater (Kargel and Strom 1992, Tanaka 2000, Head and Fishbaugh 2000, Head and Pratt 2001).

If this tentative identification of eskers is accurate, it suggests that, in some areas, the relative permeability of the polar crust was too low to permit significant infiltration. Elsewhere, however, the permeability may have been high enough that, even during the most intense periods of deposition and basal melting, the bulk of the meltwater was able to reach the aquifer, causing only a modest rise in the local water table. If so, it is interesting to consider how much water may have been cycled through the global groundwater system given the assumption of steady-state conditions. After Clifford (1993), this flux can be estimated by an application of the steady unconfined well flow equation, whose solution is given by

$$h_m^2 - h_i^2 = \frac{Q_r \nu}{\pi k g} \ln(R/a), \tag{9}$$

which, when solved for the recharge volume, Q_r, yields

$$Q_r = \frac{\pi k g \left(h_m^2 - h_i^2\right)}{\nu \ln(R/a)}, \tag{10}$$

where R, the radius of influence, represents the distance at which the local hydraulic head remains unchanged by the constant recharge (Todd 1959).

Assuming a groundwater mound height of 2.5 km, a value of R equivalent to the planetary radius (~3400 km), a basal melting radius of 750 km, and the hydraulic characteristics of the shallowest and deepest aquifers described in Table V, we find that $\sim 10^7 - 5 \times 10^8$ km^3 of H_2O could have been cycled through the crust every billion years by the south polar cap alone. This is an enormous volume of water, equivalent to a global ocean ~0.1–3.5 km deep. However, it is probably also a conservative estimate of the total flux, for it ignores the considerable geomorphic evidence that the south polar cap was once much larger (Kargel and Strom 1992, Tanaka 2000, Head and Fishbaugh 2000, Head and Pratt 2001), as well as the contribution of the north polar cap. Although the assumption of steady-state conditions overlooks a number of obvious complexities (such as the long-term decline in planetary heat flow and the potential for large obliquity-driven variations in polar mass balance), it clearly demonstrates the considerable role that basal melting and groundwater transport may have had in the long-term cycling of water on Mars.

Of the water introduced into the subsurface by basal melting, the bulk is expected to have flowed back to the ice-covered ocean in the northern plains. However, along the way, some fraction was undoubtedly lost by local discharges to the surface and by cold-trapping into the thickening cryosphere (Fig. 12, T1). A lack of constraints makes the volume of water discharged by local leaks impossible to estimate. However, because these leaks could only have occurred where the elevation of the global water table exceeded the local topography, we can at least identify the most probable locations of the largest discharges—in Hellas, Argyre, and Valles Marineris (Sections 10.2 and 10.3).

While the volume of groundwater lost by local discharges is unknown, the rate of loss because of cold-trapping by the cryosphere appears to have been small. This conclusion is based on a comparison of the maximum potential rate at which water was assimilated by the growth of the cryosphere (Fig. 11) versus the rate at which it was introduced into the subsurface by basal melting (Fig. 15). This comparison indicates that, after the Noachian, the cryosphere may have assimilated as much as ~175 m of H_2O every 10^9 years—a rate that falls ~1–2 orders-of-magnitude short of that potentially supplied by basal melting.

8.1.2. Overland flow and the development of the Chryse Trough drainage system. The preceding analysis suggests that, at the south polar cap, basal melting may have introduced and cycled an enormous volume of groundwater through the crust. But what became of the basal meltwater that was discharged to the surface?

Various lines of geomorphic and topographic evidence suggest that this water drained initially into Argyre and ultimately into the northern plains (Fig. 16; Pieri 1979, Parker 1985, 1989, 1994, Parker *et al.* 2000, Head 2000, Head and Fishbaugh 2000, Head and Pratt 2001). Although the exact course of this drainage has been obscured in places by impacts and other processes, its total length, from its origin near the periphery of the south polar deposits to its ultimate terminus in the northern plains, is over 8000 km, making it the longest known fluvial system on either the Earth or Mars (Parker 1989).

The case for a fluvial connection between the south polar deposits and Argyre is supported by the presence of three large valley networks—Surius Valles, Dzígai Valles, and Palacopas Valles—that flow from the periphery of the deposits and through the mountains that form Argyre's southern rim (Parker 1989, 1994). After filling Argyre, the water from the south polar cap would have flowed into the "Chryse Trough" (Saunders 1979), a long and extremely broad topographic depression that dips gently northward all the way to Chryse Planitia. The first part of

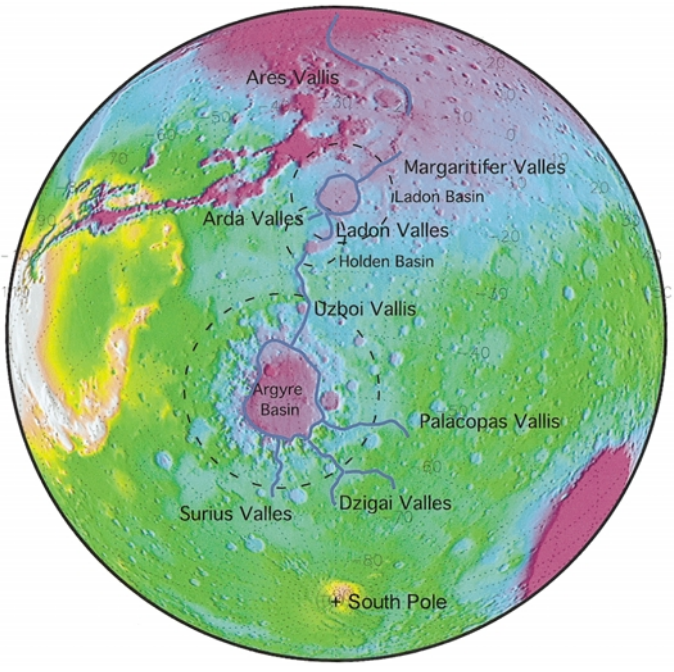

FIG. 16. Hemispheric view of the South Polar-Argyre-Chryse Trough drainage system based on MOLA gridded topography (from Parker *et al.* 2000).

this journey would have occurred via Uzboi Vallis, a relatively large Noachian outflow channel that cuts the northern rim of Argyre and drains northward into Holden Basin (Schultz *et al.* 1982). From the northeast rim of Holden, Parker (1985) identified a broad topographic "ramp" where Ladon and Arda Valles converge and drain into the interior of Ladon Basin. Although geomorphic evidence of channeling disappears just inside the inner rim of Ladon, it resumes on the basin's northeast side, at Margaritifer Valles (Grant 1987).

Margaritifer Valles branches into a large, complex distributary system at about 13°S, 24°W, where it broadens to about 300 km in width and eventually fades into the highland terrain around 8°S, 23°W. Individual branches of Margaritifer Valles exhibit two distinct preservation states—one that appears sharply defined and another that is quite subdued with channel walls that are often "gullied." Uzboi and Ladon Valles exhibit similar morphologic characteristics, suggesting that there were at least two distinct episodes of catastrophic flooding that originated from Argyre (Parker 1985). The termination of Margaritifer Valles coincides with the location of the proposed "Meridiani Shoreline" (Table III and Fig. 6), an association that suggests that the distributary nature of Margaritifer's distal end may represent a delta that formed when the overland flow from Argyre finally reached the primordial ocean that occupied the northern plains.

8.1.3. Implications for the evolution of the global aquifer at the north pole. Although the presence of a primordial ocean over the north pole would have prevented the early construction of a cap, it is likely that the rates of deposition and basal melting experienced by the local ice cover were similar to what was occurring in the south (Section 6). For this reason, once the northern ocean froze, and a true cap began to develop, the local increase in hydraulic head resulting from basal melting is likely to have made it extremely unstable, causing frequent ruptures and discharges to the surrounding plains. Alternatively, it is also possible that the existence of numerous leaks in the cryosphere's hydraulic seal may have reduced the local increase in hydraulic head sufficiently that the cap's stability was rarely threatened. Whatever its early state, the stability of the cap should have improved with time as the declining global heat flow increased the thickness of the polar deposits required for basal melting. Indeed, by the Late Hesperian/Early Amazonian, the lithostatic pressure exerted by the deposits may have grown sufficiently large that the hydraulic influence of the north polar cap may have finally begun to rival that of its southern counterpart (Fig. 12, T3).

The ability of the northern cap to generate an increase in local hydraulic head through basal melting may appear questionable given the fact that any basal meltwater will necessarily occupy less volume than the basal ice from which it was derived. For this reason, if the polar ice were suspended in a rigid porous matrix (e.g., filling the vesicles and fractures of a thick volcanic flow), its melting would actually result in a reduction in local hydraulic head. However, the sedimentary nature of the polar layered deposits (and the high volume fraction of ice that they appear to contain), suggests that any reduction in the volume of H_2O resulting from basal melting will be compensated for by the consolidation of thawed sediments at the base of the cap. In this way, basal meltwater can be introduced into the subsurface and driven to lower latitudes, even against the hydrostatic head associated with an elevated global water table, as long as the lithostatic pressure exerted by the cap exceeds the total hydraulic head (i.e., Eq. (8b)). This suggests that the hydraulic role of the north polar cap may have evolved from being little more than a pressure release valve that regulated the rise of the global water table during the Early and mid-Hesperian, to becoming an active and full component of the planet's long-term hydrologic cycle by the end of that epoch.

8.2. Flooding of the Northern Plains: Initiation Mechanisms, Maximum Potential Extent, and the Elevation of the Global Water Table vs. Time

The circum-Chryse outflow channels are the greatest recognized examples of fluvial discharge on Mars (e.g., Baker *et al.* 1992). Yet, consideration of the potential hydraulic conditions that existed beneath the Late Hesperian cryosphere (Fig. 12, T3) suggests that the most probable location for the very largest and most frequent discharges was where the hydraulic pressure was greatest—at the lowest elevations within the northern plains (Section 4.3). That no visible trace of these outbursts survives, could well be due to the relative location of their source regions to the standing bodies of water that they (and later outbursts) would have produced. By this reasoning, the geologic evidence has survived for discharges that originated above the

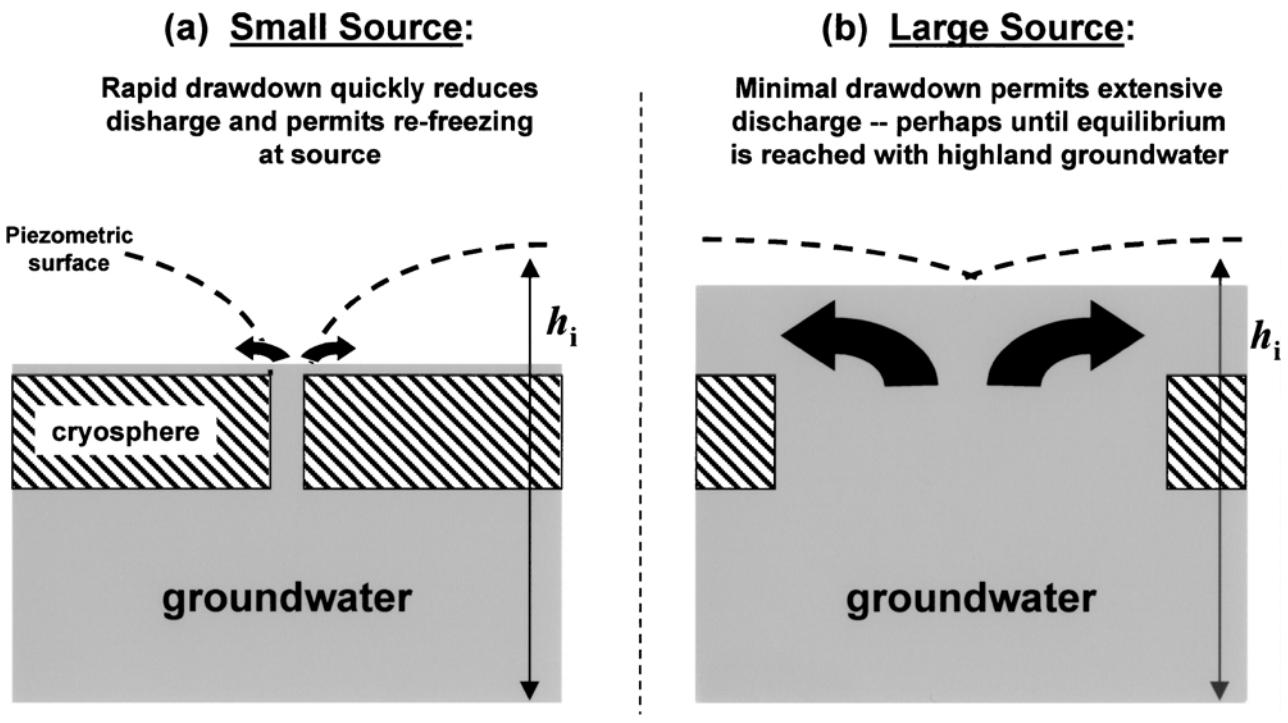

FIG. 17. The effect of rupture source area on drawdown and discharge from a confined aquifer. Note that small ruptures, such as might result from faults and impacts, will result in a rapid local drawdown that reduces the discharge and permits the rupture to refreeze. Larger disturbances, such as those that might result from basal melting, are likely to yield larger discharges that increase the potential areal extent of reflooding in the northern plains.

floodwater catchment area, but has been resurfaced where the discharges occurred at lower elevation. If true, then a signature of these events may be preserved in the stratigraphy and subsurface structure of the northern plains—evidence that may well be detectable by geophysical investigations of the near-surface crust (Section 11.3).

All else being equal, the magnitude of an artesian discharge is related to the size of the hole through which it occurs (Fig. 17). However, this relationship is not a simple one, being proportional to $1/\ln(R/a)$, where a is the radius of the hole and R is the "radius of influence" defined in Section 8.1.1. (Todd 1959, Carr 1979). Given the hydraulic conditions that we believe existed beneath the northern plains during the Hesperian (Fig. 7), local disruptions of the confined aquifer (e.g., from impacts, earthquakes, etc.) must have been common, resulting in repeated episodes of local- and regional-scale flooding. But what processes were capable of making the biggest hole?

One possibility is that major seismic events could have caused transient increases in aquifer pore pressure that disrupted extensive areas of the northern plains by both hydraulic fracturing and liquefaction (Nummendal and Pryor 1981, Leyva and Clifford 1993, Tanaka and Clifford 1993). This potential would have been greatly enhanced by the elevated hydraulic head expected at low elevation.

Another possibility is that the widespread disruption of the cryosphere occurred in response to thermal disturbances caused by the ponding of floodwater from smaller discharge events. For example, where the discharge from an outflow channel accumulated in a topographic depression (as an ice-covered lake or sea), the insulation provided by its long-term presence would have resulted in a thinning of the local cryosphere through the process of basal melting (Clifford 1987, 1993). If this lake or sea were deep enough, the local thickness of frozen ground may have been reduced to the point where it was no longer capable of confining the groundwater beneath it, resulting in a massive artesian discharge. The frequency and magnitude of such events is difficult to estimate, but the low relative relief of the northern plains (Aharonson *et al.* 1998) suggests that, with the potential exception of the interior of Utopia (Hiesinger and Head 2000), the potential for developing kilometer-deep standing bodies of water from an initial local discharge was probably rare. However, once such an event occurred, the resulting thermal disruption of the cryosphere may have led to a scale of flooding orders of magnitude greater than that of the initiating event.

But the mechanism that appears to have had the greatest potential for reflooding the northern plains is the destabilization of the north polar cap by basal melting (Section 8.1). This conclusion is based on three factors: (1) the north polar cap lies within the region of lowest elevation (and greatest artesian pressure) in the northern plains; (2) the confining potential of the polar ice is substantially less than that of frozen ground (because of its similar thermal conductivity but lower density); and (3) the potential area affected by basal melting ($\sim 10^6$ km^2) is as much as several orders of magnitude larger than that potentially disrupted by other processes (maximizing the size of the resulting hole).

Aside from the dimensions of the discharging source, two other factors—the elevation of the global water table and the size of the planet's remaining inventory of liquid water—would have influenced the likelihood and maximum potential extent of flooding in the northern plains. This reasoning suggests that the greatest extent of inundation occurred during the Noachian, when the global groundwater system was unconfined and a high early heat flow meant that little of the planetary inventory of H_2O had yet been cold-trapped into the cryosphere. Although the subsequent growth of the cryosphere allowed the water table to begin its slow rise away from equilibrium with the global topography, it also consumed a larger fraction of the surviving inventory of liquid water (Fig. 11), reducing the amount available to reflood the northern plains. Thus, while the potential for artesian discharges increased as the global water table rose, the maximum potential extent of flooding from these events should have declined with time. This expectation is consistent with the apparent relative ages of the nested shorelines identified by Parker and Schenk (1995), Parker (1998), Franklin and Parker (1999), and Hiesinger and Head (2000) which appear to decline with decreasing elevation. This observation may reflect multiple episodes of progressively less extensive flooding, stagnation points in the assimilation of a surface reservoir from a single flooding event, or may be attributable to a combination of these and other processes.

As suggested by the significantly lower mean elevation of Amazonian outflow channel source regions (Table IV), the elevation of the global water table appears to have reached its peak during the Late Hesperian (Fig. 12, T3). If so, its later decline suggests that the introduction of basal meltwater at the poles was unable to keep pace with the amount of groundwater that was being cold-trapped into the thickening cryosphere. The combination of the increased thickness of the cryosphere and the reduction in artesian pressure because of the declining water table (Fig. 12, T4), could then explain the significant reduction in outflow channel activity observed during the Amazonian. Whether a reservoir of groundwater still survives at some depth on Mars, or has now been completely assimilated by the cryosphere, is unclear—but may well be resolved by the geophysical investigations discussed in Section 11.3.

8.3. The Current Potential for Basal Melting and Catastrophic Floods

Estimates of the present thickness of the north and south polar caps fall in the range of 3–4 km, assuming that the visible deposits are isostatically compensated by a root up to 1 km-deep (Zuber *et al*. 1998a, Smith *et al*. 1999, Johnson *et al*. 2000). This thickness appears too thin to support melting at the actual base of the deposits under current climatic and inferred geothermal conditions (Table II), suggesting that the present position of the melting isotherm lies at least several kilometers beneath the base of both caps. Given this condition, it might be argued that any active role that the polar caps have played in the planet's hydrologic evolution has long since passed. It is unclear, however, whether the current period of apparent quiescence is necessarily a representative or terminal state.

As the Martian geothermal heat flux has declined with time, the polar deposit thickness required for basal melting has increased (Fig. 3b). Should the decline in heat flow occur faster than can be compensated for by the deposition of new material at the poles, then the position of the melting isotherm will retreat deeper into the crust. However, changes in the temperature and depositional environment at the poles, arising from obliquity-driven variations in insolation, or from major geologic events (such as volcanic eruptions, large impacts, or out-flow channel activity), can slow, halt, or even reverse the melting isotherm's descent. Depending on the magnitude of these events, the potential for basal melting can vary significantly over geologically short timescales, even during the present epoch.

An example of this potential short-term variability is illustrated in Fig. 18 where, starting from an initial condition similar to that which may now exist at the north pole (Fig. 18, T0), we consider the consequences of a sudden episode of rapid deposition (Fig. 18, T1). Under such conditions (which might arise from a renewed period of outflow channel activity), the growth of the cap could exceed the rate of thermal reequilibration at its base. Because the rheology of ice is strongly temperature dependent, this could allow the total thickness of the cap to grow quite large before its base became warm enough to significantly deform (Fig. 18, T2). However, once deformation began, the resulting deformational and frictional heating could contribute to a substantial reduction in the thickness required for basal melting. For example, a basal sliding velocity of 10 m yr^{-1}, under a basal shear stress of 100 kPa, produces sufficient frictional heat ($\sim$30 mW m^{-2}) to halve the equilibrium thickness necessary for basal melting during the present epoch (Clifford 1987, 1993). In this way, a thick cap that accumulated rapidly could undergo a rapid collapse—thinning to a fraction of the thickness required to sustain basal melting under equilibrium conditions (Fig. 18, T3).

Depending on the current hydraulic head beneath the north polar cap, the evolutionary scenario described above could end in one of two ways. If the hydraulic head is low (or nonexistent, in the case of a fully cold-trapped groundwater inventory), then the rapid thinning of the cap will simply be followed by the resumption of the downward propagation of the melting isotherm until thermal equilibrium is reestablished (Fig. 18, T4a). However, if the hydraulic head is high, then the cap's rapid expansion and thinning could violate the hydraulic stability requirement given by Eq. (8b), resulting in the disruption of the cap and a catastrophic re-flooding of the northern plains (Fig. 18, T4b).

Changes in polar insolation resulting from the chaotic evolution of the martian obliquity could also result in a rapid thinning of the cap, solely by sublimation (Jakosky *et al*. 1995). The possible permutations of such complex evolutionary scenarios appear limitless, particularly during the planet's early history—a time when the geothermal heat flow was higher, the inventory of groundwater larger, and standing bodies of water and ice may have been present in abundance.

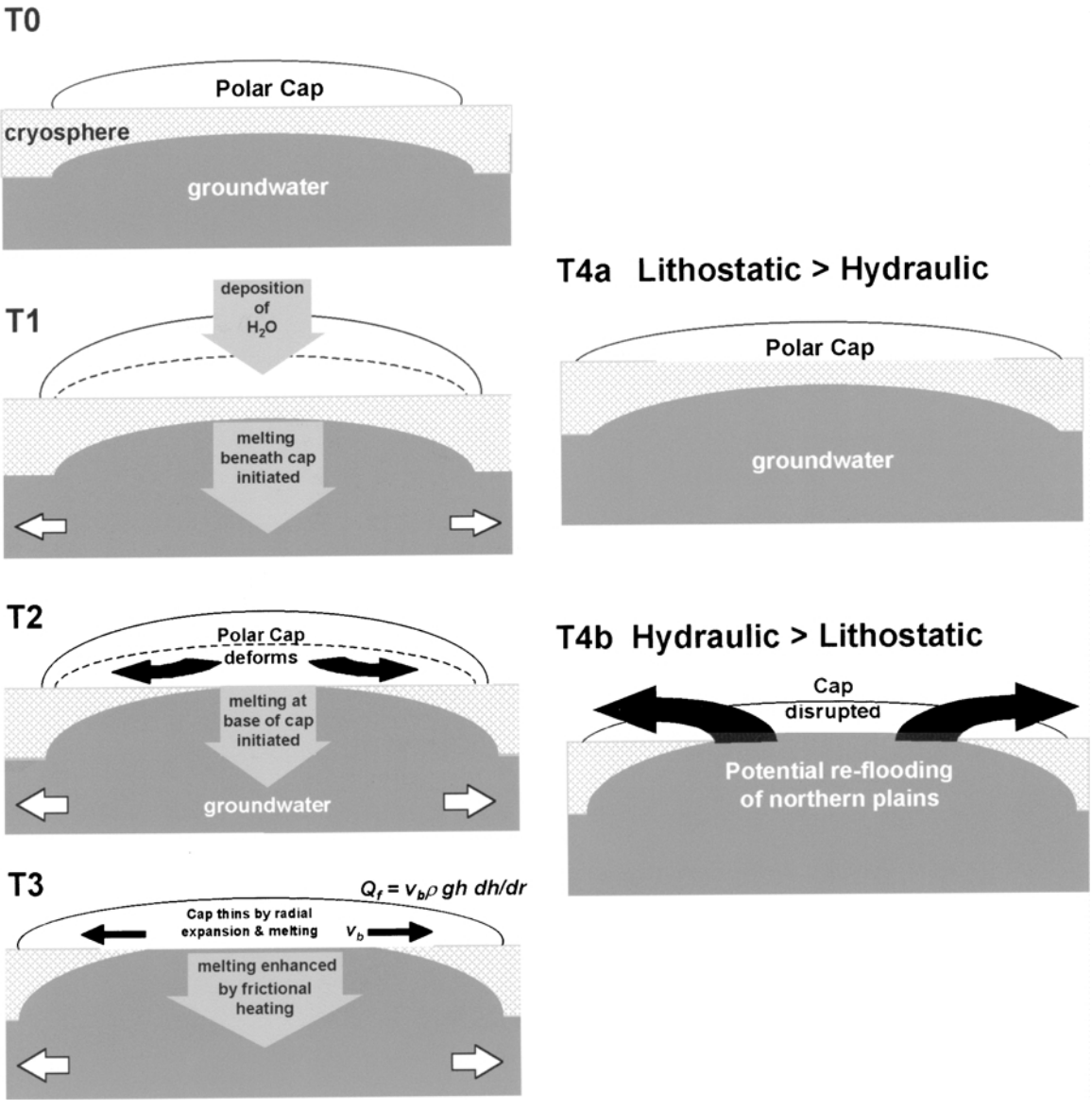

FIG. 18. Potential response of the present-day north polar cap to an episode of sudden deposition.

9. IMPLICATIONS FOR THE CURRENT STATE OF THE NORTHERN PLAINS

Thermal and diffusive stability considerations suggest that substantial remnants of the floodwaters that once inundated the northern plains could still survive beneath thin mantles of dust and volcanics that have accumulated since the water froze (Carr 1990, 1996). Indeed, given the initial presence of a Noachian ocean and the potential for extensive and repeated flooding, the volatile stratigraphy of the plains is likely to be quite complex—having been built up through multiple episodes of flooding, freezing, sublimation, and burial. This complexity has undoubtedly been compounded by local differences in hydraulic and geologic evolution arising from impacts, volcanism, tectonism, and a variety of other processes. The resulting structure of the crust is expected to exhibit considerable heterogeneity; however, in many areas the stratigraphy and bulk properties of the uppermost ~0.1–1.0 km are likely to be dominated by multiple, overlapping deposits of water ice—with individual flows ranging from meters to many hundreds of meters thick (Fig. 19).

The presence of massive ice deposits beneath the northern plains is consistent with the conclusions of many previous investigators based on the geomorphic interpretation of a variety of landforms (e.g., Rossbacher and Judson 1981, Lucchitta and Ferguson 1983, Lucchitta *et al.* 1986, Lucchitta 1984, 1993, Carr 1986, Squyres and Carr 1986, Lucchitta and Chapman, 1988, Squyres *et al.* 1992, Chapman 1994, Costard and Kargel 1995, Kargel *et al.* 1995). But perhaps the most intriguing evidence has been provided by MOLA.

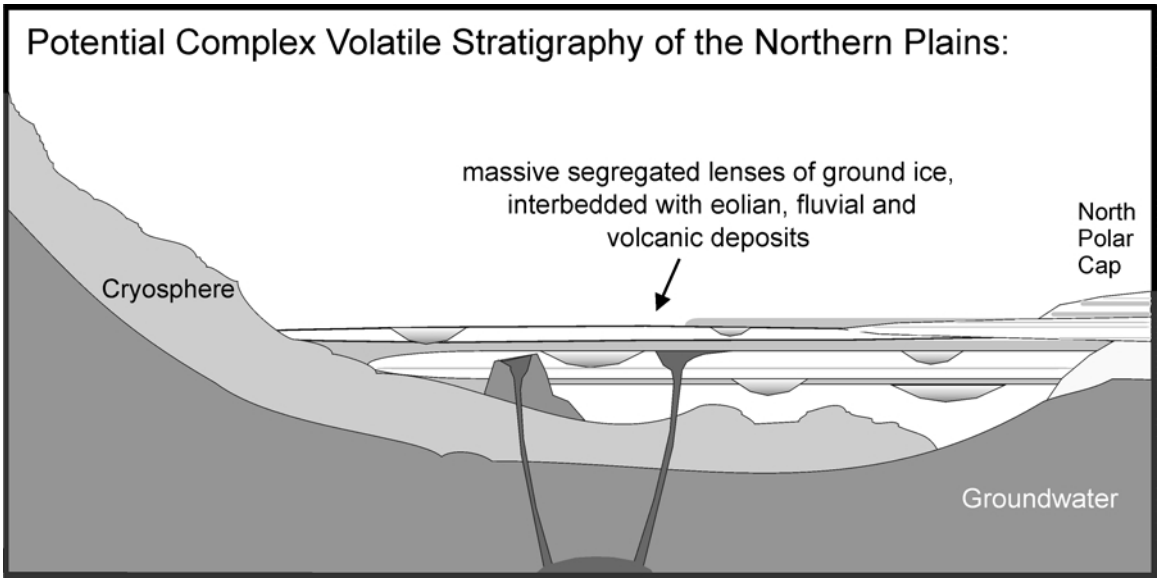

FIG. 19. Potential volatile stratigraphy of the northern plains. Given the potential for the long-term preservation of ice under a thin mantle of debris, massive segregated deposits of ground ice may be present throughout the northern plains—an expectation based on the possible former existence of a Noachian ocean, and the geomorphic evidence for extensive and repeated flooding by Hesperian-age outflow channel activity. As a result, the volatile stratigraphy of the northern plains is likely to be quite complex, having been built up through multiple episodes of flooding, freezing, sublimation, and burial (Sections 9 and 11.2). This complexity has undoubtedly been compounded by local differences in geologic evolution and by climatic fluctuations associated with the chaotic evolution of the planet's obliquity. While the resulting fine-scale structure of the crust is expected to exhibit considerable heterogeneity, in many areas the bulk properties of the uppermost ~0.1–1.0 km may be dominated by multiple, overlapping deposits of ice—with individual flows ranging from meters to many hundreds of meters thick. This possibility is consistent with the anomalous smoothness and low relief of the plains—characteristics that may be explained by a combination of multiple flooding events (that filled in the most significant topographic lows) and by the large-scale viscous relaxation of the resulting ice-rich topography.

As discussed earlier, the Martian northern plains are one of the smoothest and flattest planetary surfaces found anywhere in the solar system (Aharonson *et al*. 1998, Zuber *et al*. 1998b, Head *et al*. 1998, 1999). The deep oceanic plains of Earth are frequently cited as its closest terrestrial analog—an observation that is consistent with, but does not prove, an origin by marine deposition. Although the presence of a thick accumulation of marine sediments cannot be ruled out (e.g., Lucchitta *et al*. 1986), our analysis suggests that two other processes may have contributed to the anomalous smoothness of the plains.

Perhaps the most obvious explanation for the unusually low relief of the plains is that repeated flooding has simply filled in the deepest depressions, a process that began with the formation of the original primordial ocean, whose sea-level would have conformed to an equipotential surface. However, after the ocean froze, a variety of climatic and geologic processes would have acted to evolve the landscape away from this initial condition. For example, within the first $\sim 10^8$ years, sublimation and cold-trapping alone may have redistributed the equivalent of 100s of meters of ice across the northern plains. The efficiency of this process was undoubtedly modified by geographic variations in climate, and by local differences in the thermal and diffusive properties of any overlying mantle of dust, volcanic ash, or other debris, that may have accumulated on the surface. Impacts, volcanism, and tectonic activity would have also contributed to substantial changes in vertical relief. In many instances, these changes were erased or modified by later floods that, depending on their location and volume, may have resurfaced individual areas ranging up to $\sim 10^7$ km^2. As discussed in Section 8.2, the magnitude and extent of the largest of these events would have diminished with time in response to the progressive assimilation of the groundwater inventory by the thickening cryosphere.

The potential presence of massive ice deposits beneath the plains also suggests that any changes in local or regional topography may be moderated by the deformation of the landscape itself (e.g., Squyres and Carr 1986, Squyres 1989). This deformation is an expected consequence of the effect of any topographically induced shear stress on an ice-rich crust—a rheologic response that can occur at both short- and long-wavelengths, but which is enhanced by the higher temperatures and pressures present at depth. Although the topographic signature of regional tectonics, and other geologic processes, is still clearly present, the combined effects of repeated flooding and viscous relaxation may well explain the extraordinary smoothness and low relief of the northern plains.

10. THE TOPOGRAPHIC EVOLUTION OF EARLY MARS AND ITS IMPLICATIONS FOR THE LOCATIONS OF FORMER OCEANS, LAKES, AND SEAS

Throughout the preceding discussion it has been assumed that the topography of Mars underwent little change since the

Noachian. But there is considerable evidence that, during its first billion years, the planet's surface underwent dramatic changes in its physical evolution and vertical relief. This evidence suggests that the locations of the earliest "oceans" or "seas" may have been significantly different from those inferred from the present-day topography.

10.1. Global Dichotomy

The single greatest event in the topographic evolution of Mars was the development of the global dichotomy. The age of the degraded terrain at the boundary between the northern plains and southern highlands suggests an origin that dates back at least as far as the Late Noachian/Early Hesperian and perhaps even earlier (McGill and Squyres 1991). Hypotheses for the origin of the dichotomy include either subcrustal erosion (or thinning) resulting from mantle convection (Wise *et al*. 1979, McGill and Dimitriou 1990) or, less plausibly, excavation by one or more large impacts (Whilhelms and Squyres 1984, Frey and Schultz 1988). Whatever the cause of the dichotomy, there is little debate that the resulting ∼5 km difference in hemispheric elevation had a dramatic influence on the planet's subsequent geologic and hydrologic evolution—an evolution that resurfaced the northern third of the planet as recently as the Late Hesperian/Early Amazonian (Tanaka *et al*. 1992, Baker *et al*. 1992, Smith *et al*. 1999). Whether the predichotomy distribution of surface water on Mars occurred in numerous lakes and seas or was concentrated in a few large bodies is unknown; however, our analysis indicates that the postdichotomy distribution was dominated by the existence of a primordial ocean in the northern plains.

10.2. Impact Basins

Perhaps the greatest agents of early topographic change on Mars were large impacts (Schultz *et al*. 1982, Schultz and Frey 1990). Of the readily identifiable impact basins, the three largest—Hellas (∼2300 km in diameter), Argyre (∼1500 km), and Isidis (∼1100 km)—all date back to the Noachian (Tanaka *et al*. 1992). McGill (1989) has presented evidence of another Hellas-size impact in Utopia. Although the basin is buried by younger (Late Hesperian) material, MOLA topographic data has confirmed the presence of an ∼2100 km diameter impact basin centered at approximately 45°N, 248°W (Frey *et al*. 1999, Thompson and Head 1999, Smith *et al*. 1999). Because of their size and the limited confinement capability of the early cryosphere, it is likely that all four of these basins (as well as many others whose record has been erased or only partly preserved) hosted interior ice-covered lakes or seas during the Noachian that may have lasted into the Hesperian (Fig. 10).

In Utopia and Isidis, resurfacing by Late Hesperian plains material has eliminated any interpretable record of a previous lucustrine environment. Despite this fact, consideration of the initial depth of these basins, and their location in the northern plains, argues for an initially flooded condition. Various lines of geomorphic evidence indicate that this state may have persisted through, or episodically reoccurred during, the Late Hesperian and Early Amazonian—a probable consequence of the concurrent activity of the circum-Chryse and Elysium out-flow channels (Lucchitta *et al*. 1986, McGill 1986, 1992, Grizzaffi and Schultz 1989, Scott *et al*. 1992, Parker *et al*. 1993, Chapman 1994, Costard and Kargel 1995, Hiesinger and Head 1999, 2000). Any attempt to estimate the original volumes of Isidis and Utopia is complicated by the extensive topographic degradation and infilling both basins have experienced. Assuming an original depth-diameter ratio comparable to Argyre and Hellas, the original volumes were $\sim 10^6$ km^3 for Isidis and $\sim 10^7$ km^3 for Utopia. The latter figure is roughly an order-of-magnitude greater then the present volume of Utopia determined from the MOLA topography (Thompson and Head 1999). If our interpretation of the evolution and current state of the northern plains is correct (i.e., Section 9 and Fig. 19), then much of this volume difference may be attributable to subsequent episodes of flooding that are now preserved as thick deposits of massive ice.

In light of the potential for significant flooding during the Noachian, and the geomorphic and topographic evidence that massive ice deposits may still survive beneath the northern plains, it seems reasonable to expect that some frozen remnant of this early water might also survive in the low-lying interiors of Hellas and Argyre. However, as this is written, no evidence for the presence of massive ice deposits in these locations has yet been found. This result may reflect either the absence of such deposits or the masking of their geomorphic and topographic expression by later processes and events.

The apparent absence of ice in Hellas and Argyre may be attributable to their origin by large impacts. Based on the crater-diameter scaling relationships of Grieve and Cintala (1992), Clifford (1993) has estimated that the formation of a $\sim 1.5 \times 10^3$ km diameter impact basin will produce $\sim 10^7$ km^3 of impact melt, the majority of which is expected to have pooled in the basin's interior. In addition, the intense fracturing of the underlying crust is likely to have focused considerable postimpact igneous activity in these locations (Schultz and Glicken 1979, Wichman and Schultz 1989, Tanaka and Leonard 1995). As a result, the lithology of the basin floors, as well as much of the surrounding terrain, may well be dominated by a combination of coherent igneous rock and rewelded breccias.

Given the size and expected longevity of the thermal disturbances that resulted from these impacts, and the inferred water-rich nature of the surrounding crust, it appears likely that the impacts triggered an extended period of hydrothermal activity that may have eventually led to the formation of an interior lake or sea. This conclusion is consistent with the presence of interior layered deposits (ranging from hundreds of meters to as much as several kilometers thick and varying widely in apparent age) in both basins (Moore and Edgett 1993, Tanaka and Leonard 1995, Parker 1996, Tanaka 2000). However, when the basin lakes eventually froze, and the exposed ice sublimed away, the low porosity and permeability of the surrounding igneous rock may have greatly restricted any further communication with the

global aquifer, minimizing the potential for any later episode of reflooding.

Although we have discussed only the four most distinct impact basins, there is evidence that other impacts, of comparable size and age, occurred planet-wide (Schultz *et al*. 1982, Schultz and Frey 1990). The potential significance of these events cannot be overstated for, beyond their influence on the Noachian topography, the seismic and long-lived thermal disturbances they created would have had a profound effect on the evolution of the early hydrosphere and climate (Carr 1984, Clifford 1997).

10.3. Valles Marineris

The last major influences on the topography of Mars were the formation of Tharsis (by volcanic construction and possible uplift) and Valles Marineris (by rifting, mass wasting, and hydraulic disruption) (Lucchitta *et al*. 1992). These concurrent and potentially related developments began in the Late Noachian and have apparently continued through the Amazonian (Scott and Tanaka 1986, Tanaka *et al*. 1992, Lucchitta *et al*. 1992). Analysis of the topography and gravity field of Tharsis (Smith *et al*. 1999, Zuber *et al*. 2000), and MOC high-resolution images of the interior walls of Valles Marineris (McEwen *et al*. 1999), have provided evidence of extensive construction by massive regional volcanism. Evidence of a high rate of early resurfacing is particularly evident at the east end of Valles Marineris, where the canyon truncates a number of valley networks in the Late Noachian plateau material to the south. This relationship indicates that the underlying ∼3 km of exposed stratigraphy must predate the end of heavy bombardment. The rapid and complex evolution of this region during the Noachian raises the possibility that the very earliest lucustrine environments on Mars may now lie buried beneath many kilometers of volcanic rock.

The extent to which the topographic relationships that currently exist within Valles Marineris have evolved with time is unclear. At its eastern end, the lowest interior elevations are approximately −4 km. However, in the central part of the canyon, and in neighboring Candor and Ophir Chasmas, the interior elevations are as much as a kilometer lower (Smith *et al*. 1999). If these elevations characterized the system at the time of the canyon's formation, then much of its interior must have been flooded by its hydraulic connection with the primordial ocean in the northern plains and by the associated disruption of the global aquifer. This expectation is consistent with the presence of thick finely bedded layered deposits, interpreted to be of lucustrine origin (McCauley 1978, Nedel *et al*. 1987, Malin and Edgett 2000), within the interiors of Ophir, Candor, Melas, and Hebes Chasmata. If these deposits are sediments that accumulated in ice-covered lakes, their tremendous thickness (up to 8-km) implies that the lakes were extremely long-lived (Lucchitta *et al*. 1994, Carr 1996). Given the instability of ice at low latitudes, this prolonged existence requires that the lakes were frequently or continuously replenished. Under current climatic conditions, the only plausible source of water for this replenishment would have been an aquifer of equal or greater height (Carr 1996). The similarity in age and hydraulic conditions required to explain the existence of the canyon lakes, and the elevated source regions of the circum-Chryse outflow channels, provides additional support for the belief that the water for both originated from the presence of an elevated water table in the southern highlands (Fig. 12, T3).

Although massive ice deposits may still survive at depth, the apparent absence of ice in the interior of Valles Marineris is not a surprising result. Given the equatorial location of Valles Marineris, high rates of sublimation could have removed any frozen and nonreplenished interior lake (even one several kilometers deep) in a geologically short period of time ($\sim 10^5$–10^9 years). But what caused the sudden (and geologically recent) disappearance of the lakes after their apparent stable existence in the canyon for billions of years? One possibility, suggested by the present analysis, is that, following the peak in outflow channel activity that occurred in the Late Hesperian, the progressive assimilation of the groundwater inventory by the thickening cryosphere caused the global water table to fall below the level required for the canyon lakes replenishment—after which any remaining ice simply sublimed away.

11. QUALIFICATIONS AND POTENTIAL TESTS

Although primarily intended as a theoretical analysis of the evolution of the Martian hydrosphere, our findings appear remarkably consistent with the geomorphic and topographic evidence that Mars once possessed a primordial ocean and that a substantial relic of that body continues to survive as massive ice deposits beneath the northern plains. However, while this study appears to provide a consistent description of first-order behavior, the actual hydrologic evolution of Mars was undoubtedly more complex. In this section, we consider the sensitivity of our findings to several of our initial assumptions, attempt to address the most obvious uncertainties, and discuss what observations can be made to test our principal conclusions.

11.1. Early Crustal Heat Flow and the Depth of Hydraulic Communication

Based on the assumptions and arguments discussed earlier in this paper, the cryosphere's ability to confine an elevated water table appears to have evolved sometime during Hesperian and may, even then, have been a precarious balance (e.g., Section 8.2). However, a recent study (Zuber *et al*. 2000) suggests that the planet's early crustal heat flow was initially higher, and declined more quickly, than assumed in this study—an evolution that would have contributed to a more rapid development of the cryosphere and a shallower depth of hydraulic communication beneath the northern plains.

Estimates of the thickness of the elastic lithosphere, calculated from an analysis of the Martian global topography and gravity fields obtained by MOLA, have been used to assess regional variations in lithospheric thermal gradients and heat

flow at the time of crustal loading (Zuber *et al*. 2000). These results indicate that the early heat flow through the southern highlands was smaller than previously thought, suggesting that the Martian interior cooled at a faster rate than illustrated in Fig. 2. If so, how did this heat loss occur? An important clue is provided by the hemispheric asymmetry in present crustal thickness, which averages ∼55–65 km throughout most of the southern highlands and ∼35–40 km in the northern plains (Zuber *et al*. 2000). This disparity suggests that much of the planet's early heat loss occurred in the north, delaying crustal development.

This revised picture of the early thermal history of Mars has at least two important consequences for the evolution of the hydrosphere. First, it suggests that the early growth of the cryosphere was more rapid than assumed in this study. If true, this means that the cryosphere's ability to support an elevated water table developed at an earlier time. Exactly how much earlier is difficult to say, because no complete thermal history model has yet been published based on the MGS results. Any quantitative estimate is further complicated by the regional differences between the highlands and the plains. Although these details may affect the relative timing of events between the northern and southern hemispheres, their impact on the general evolutionary scenario outlined in this paper appears to be small. For this reason, and because a slower rate of geothermal cooling offers the greatest challenge for hydraulic confinement, we chose to stick with the qualitatively similar, and more widely recognized, pre-MGS thermal history as the basis for our discussion.

But the possibility of a higher early heat flow in the northern plains raises another issue whose impact on the hydraulic evolution of Mars may have been considerably greater, resulting in both a steeper geothermal gradient, and shallower depth of the brittle/ductile transition zone, compared with the highlands. From a hydrologic perspective, this implies a more rapid decline in crustal permeability with depth beneath the plains. Unfortunately, without knowledge of the actual subsurface thermal conditions, or the subsequent geologic evolution of the crust, it is virtually impossible to estimate the actual depth to which hydraulic communication persists. Nonetheless, Carr (2000) has noted that, if this depth were reduced to as little as 3–5 km, it would have had profound effect on the evolution of the hydrosphere, once the northern ocean had frozen throughout. The early downward propagation of the cryosphere into such a shallow, low-permeability region would have eventually trapped any surviving groundwater into localized pockets, effectively cut off from communication with any other reservoirs that might have existed within the crust. The continued growth of the cryosphere would have placed these pockets of groundwater under increasing compressive stress—eventually triggering a rupture of the frozen confining layer and the discharge of groundwater under significant hydraulic head. Carr (1979, 2000) argues that such an evolutionary scenario might well explain the origin of many of the outflow channels.

The depth of hydraulic communication beneath the northern plains is unknown, but a shallow zone would help to resolve several of the low elevation stability issues discussed in Section 8. Specifically, the hydraulic isolation of the northern plains from the southern highlands would eliminate the potential development of destabilizing hydraulic pressures associated with the rise of the highlands' water table during the Hesperian, greatly diminishing the potential for massive reflooding. The extent to which regional variations in geothermal evolution affected the development and hydraulic properties of the northern plains is an issue that will likely only be resolved following an extensive program of geophysical sounding and deep-drilling.

11.2. The Efficiency of Sublimation

Carr (1996) initially questioned the ocean hypothesis based, in part, on the enormous volume of ice that must be sublimed away to explain the elevation of the shorelines identified by Parker *et al*. (1989, 1993). This objection arises from the relative stability of ice at high latitudes, particularly when covered by a thin mantle of debris (Carr 1990).

The efficiency of sublimation, both at low and high latitudes, is a valid concern. The stability of ice on or beneath the Martian surface is essentially dependent on four things: the relative humidity of the atmosphere, the local surface temperature, and the thickness and diffusive characteristics of any overlying mantle of debris. At low latitudes, the combination of high mean annual temperatures, large diurnal temperature fluctuations, and low relative humidity can yield sublimation rates from a bare ice surface that readily exceed 0.1 m yr^{-1}. However, the presence of a debris mantle (or lag deposit) only 10–20-cm thick provides enough thermal insulation to attenuate the diurnal temperature wave to its mean value, reducing the sublimation rate by more than an order of magnitude. This insulating effect becomes even more important at latitudes $\geq 40^{\circ}$, where the mean annual temperature is at or below the ∼196 K H_2O frost point of the atmosphere (Farmer and Doms 1979). At these high latitudes, early stability calculations indicated that ice could survive beneath a thin (1–2 m-thick) mantle of debris for billions of years (Clifford and Hillel 1983, Fanale *et al*. 1986, Zent *et al*. 1986, Carr 1990). Such mantles might originate from the deposition of fluvial sediments, volcanic ash deposits, lavas emplaced over the ice, or, most probably, by the accumulation of dust resulting from eolian deposition.

The accumulation of dust mantles is expected at high latitudes because atmospheric dust, raised by local and global dust storms, is thought to act as nucleation centers for the condensation and precipitation of H_2O and CO_2 during the formation of the seasonal polar cap (Pollack *et al*. 1979). Such mantles retard sublimation by both their thermal insulating effect (which limits the exposure of the underlying ice to the high diurnal and seasonal temperature extremes) and by the diffusive barrier created by their limited gaseous permeability.

At low latitudes it appears unlikely that any reasonable accumulation of atmospheric dust could impede the sublimation of $\sim 10^3$ m of ocean ice over geologic time. This conclusion is based on: (1) recent calculations of stability of equatorial ground

ice which demonstrate that sublimation can deplete the equatorial regolith of similar amounts of ice (Clifford 1998), and (2) the visibility of submeter-scale rocks at the Pathfinder and Viking landing sites, which appears to place an upper limit on the depth to which mantles of dust normally accumulate. This last observation is important, because it implies that the geographic sources and sinks of atmospheric dust generally vary with sufficient frequency to prevent the widespread accumulation of thick, long-lived depositional mantles, at least at low- to mid-latitudes. Such variations in local erosion and deposition may originate from interactions between the topography and insolation-induced changes in local and global wind patterns caused by variations in season, precession, and obliquity (Greeley *et al*. 1992, Kahn *et al*. 1992).

Under current obliquity conditions, ice at high latitudes is generally stable except during the spring and summer, when high diurnal temperature excursions can lead to short periods of high sublimation. The thermal insulation provided by a ~0.1–1 m-thick dust mantle can virtually eliminate this seasonal mass loss, reducing the present day sublimation rate to values $\leq$0.1 m in 10^9 years (Carr 1990).

But the obliquity of Mars is not static—oscillating with a period of $\sim 1.2 \times 10^5$ years about its present mean value ($i \sim 25^\circ$) with an amplitude of oscillation that varies with a period of $\sim 1.3 \times 10^6$ years. At the time Carr performed his original stability analysis, the obliquity was thought to vary between ~15°–35°. During the low obliquity portion of this cycle, Carr found that high-latitude ice was stable. However, when the obliquity rose to its highest values, he found that sufficient ice was lost to increase the average sublimation rate by a factor of 10 over its present (25°) value. This rate is still many orders of magnitude smaller than that required to sublime away the several kilometers of ice associated with a former ocean—a result that led Carr (1996) to doubt that such an ocean had ever existed.

However, shortly after the publication of Carr's (1990) analysis, Touma and Wisdom (1993) and Laskar and Robutel (1993) demonstrated that the Martian obliquity is chaotic on a time scale of $\sim 10^7$ years, reaching peak values of as much as 60°. At obliquities above ~54° the mean annual insolation at the poles actually exceeds that at the equator (Ward 1992). Even at lower obliquities, maximum daytime temperatures at the poles can still exceed 273 K throughout much of the spring and summer (Toon *et al*. 1980, Pathare and Paige 1998). Under these conditions, high latitude sublimation rates for exposed ice may reach ~0.1 m yr^{-1} averaged over a single obliquity cycle (Jakosky *et al*. 1995). Although burial beneath several meters of dust (resulting from either eolian deposition or the development of a lag deposit in response to sublimation) could reduce this rate significantly, it still yields potential loss rates sufficient to sublime away as much as several kilometers of ice in 10^9 years.

Clearly, there remain enormous uncertainties associated with these calculations. Factors such as the optical depth of the atmosphere, the potential development of a water vapor greenhouse, and the stability of dust mantles at high obliquity, are just some of the unknowns. Nonetheless, the potential for significant mass loss at high obliquity could well resolve the last dynamical obstacle to identifying a self-consistent theoretical explanation for the origin and fate of a primordial ocean on Mars.

11.3. Observational Tests

Although the geomorphic, topographic, and theoretical arguments for the existence of a primordial ocean appear persuasive, it is necessarily a case built on inference and interpretation. However, over the next decade, geophysical investigations conducted from orbit and the Martian surface will provide opportunities to verify several key aspects of this analysis.

The first opportunity will occur in 2003, when the European Space Agnecy (ESA) launches a sophisticated and ambitious mission called Mars Express, consisting of both a polar orbiter and a lander called *Beagle 2*. Among the instruments that will be carried by the orbiter is the Mars Advanced Radar for Subsurface and Ionosphere Sounding (MARSIS), whose primary purpose is to map the distribution of water and ice in the top ~1–5 km of the crust (Plaut 1999). MARSIS is a multifrequency, coherent pulse, synthetic aperture radar sounder that operates by detecting reflections from the interface between two materials of differing dielectric properties. For this reason, the instrument is particularly sensitive to the large dielectric contrast between ground ice and groundwater. Under favorable conditions of surface roughness and rock composition, MARSIS may also be capable of detecting the much smaller contrast between frozen soil and massive segregated lenses of ground ice.

In 2007, the results from MARSIS will be supplemented by the seismic and ground penetrating radar (GPR) investigations of another ambitious mission called NetLander. NetLander, which is being developed by a European consortium led by the Centre National d'Etudes Spatiales (CNES), consists of four separate (and independently targetable) landers whose identical instrument payloads can be networked together to conduct coordinated investigations of the Martian atmosphere and interior (http://www-projet.cst.cnes.fr:8060/NETLANDER/). As with MARSIS, one of the primary goals of the NetLander mission is the detection of ground ice and groundwater.

From the perspective of the present study, the two most important observations that the Mars Express and NetLander missions could make are confirmation that: (1) a frozen relic of a former ocean survives beneath the surface of the northern plains, and (2) that Mars possesses a groundwater system of global extent. Of these, the presence of massive ice deposits may be the easiest to verify. Although the geophysical characteristics of segregated ice and ice-saturated rock are similar, the expected shallow depth of the deposits, combined with the low relief and small-scale smoothness of the northern plains, should improve the chances for detection.

If massive ice deposits are not present, it will provide a persuasive argument against the evolutionary model described in this paper. The expected "leakiness" of the proposed global aquifer,

and the considerable potential for the long term preservation of ice beneath the plains, are simply too great to be consistent with a null result. Even the detection of modest volumes of massive ice, located in the interiors of local basins, would have ambiguous implications—being consistent with both the formation of terminal lakes by the discharge of the outflow channels and with the survival of a highly depleted/sublimed remnant of a former ocean. On the other hand, the detection of thick ($\sim 10^2$–10^3 m), massive ice deposits over a substantial fraction of the northern plains would essentially confirm the ocean hypothesis.

Confirmation of the presence of a global groundwater system is likely to be considerably more difficult, with a negative result providing no clear insight as to its actual cause. For example, while a null result might suggest that Mars never had a substantial inventory of groundwater, it could just as easily imply that a once large inventory has since been assimilated into the thickening cryosphere (Section 8.2), or that the combination of geothermal heat flow and crustal thermal conductivity has simply resulted in a thickness of frozen ground that exceeds the sounding depth of MARSIS and NetLander.

On the other hand, the successful detection of groundwater at multiple locations across the planet's surface (at sites far removed of any obvious source of transient production, such as volcanoes) would provide persuasive evidence that Mars is water-rich and that it must have possessed an even larger reservoir of groundwater in the past (Clifford 1993, 1996). Such a discovery, combined with identification of widespread massive ice deposits in the northern plains, would be difficult to reconcile with any evolutionary model of the hydrosphere that differed substantially from the one presented here.

Given the ~5 km maximum sounding depth of MARSIS, the locations that provide the best opportunity for detecting groundwater are those that combine low latitude (minimizing the thickness of frozen ground) and low elevation (minimizing the depth to a water table in hydrostatic equilibrium) (Clifford 1996). Those locations that appear to offer the best combination of these criteria are the interior of Valles Marineris, southern Amazonis Planitia, Isidis Planitia, a region to the southeast of Elyisum, and the northern interior of Hellas (Table VI).

TABLE VI
Optimal Locations for the Geophysical Detection of Subpermafrost Groundwater[a]

Location	Latitude range	Longitude range	Elevation[b] (km)
Interior of Valles Marineris	Varies between ~5–10°S	~30–80°W	<−4 km
Southern Amazonis Planitia	~5°S–20°N	~150–170°W	<−3 km
Southeast of Elysium	~0–10°N	~180–200°W	<−3 km
Isidis Planitia	~5–20°N	~265–280°W	<−2 km
Northern interior of Hellas	30–40°S	~280–305°W	<−6 km

[a] All latitude and longitude ranges represent approximate maximum extensions.

[b] Smith *et al*. (1999).

12. CONCLUSIONS

This analysis suggests that the existence of a primordial ocean on Mars, covering as much as a third of the planet, was an inevitable consequence of the hydraulic and thermal conditions that existed during the Early Noachian. It further suggests that the assimilation of the resulting frozen ocean, the rise of the global water table, the episodic reflooding of the northern plains, and the decline in the level of outflow channel activity during the Amazonian were a natural consequence of the evolution of the post-Noachian climate and geothermal heat flow. This conclusion is consistent with the growing geomorphic and topographic evidence for a former ocean and with the belief that a substantial relic of that body continues to survive as massive ice deposits within the northern plains.

Confirmation of the presence of such deposits, combined with the potential detection of a global-scale groundwater system, would provide persuasive support for the validity of this analysis. Orbiter and lander-based geophysical investigations of the subsurface, that are potentially capable of identifying such reservoirs, are major elements of several spacecraft missions that will be flown to Mars during the next decade.

Whether the early martian climate was warm or cold, the presence of a long-lived ocean in the northern plains (and possible additional standing bodies of water elsewhere) has profound implications for both the potential development of life and the planet's subsequent hydrologic evolution. If a frozen remnant of this early ocean still survives, then there is no better target for future exobiological investigations, for studies of the planet's hydrologic history, or for accessing and developing *in situ* resources to support future human exploration.

APPENDIX A

Physical, Thermal, and Hydraulic Properties of the Martian Crust

Plausible values of the large-scale physical, thermal, and hydraulic properties of the martian crust have been discussed by Clifford (1993). Here we briefly review and revise several aspects of that earlier analysis in an effort to more accurately describe the potential range of these properties and the effects of crustal heterogeneity. We also discuss several new insights provided by observations of the Mars Global Surveyor (MGS) spacecraft.

A.1. Crustal Structure, Porosity, and Permeability

Impacts, volcanism, weathering, and various erosional and sedimentary processes have all clearly contributed to the evolution of the martian crust (Fanale 1976, Carr 1979, Clifford 1993). However, the structure and cumulative thickness of the resulting stratigraphy, as well as the relative volumetric contributions of its various components, are all unknown.

The structure and lithology of the subsurface is best exposed in Valles Marineris, where high-resolution images obtained by the Mars Orbiter Camera (MOC) have revealed layered sequences up to 8 km-thick in the canyon walls. The strata possess individual thicknesses that range from ~50 m down to the limit of resolution (~1.4 m) (McEwen *et al*. 1999). Although an unambiguous identification of any geologic unit is difficult to make on the basis of orbital

imagery alone (e.g., see Parker and Saunders 1988), McEwen *et al.* (1999) argue that the layers visible in the canyon walls are likely volcanic. Whatever the actual nature of these layers, the Late Noachian age (~4 Ga) of the surface units capping the stratigraphy at the east end of the canyon suggests that a minimum of several kilometers of construction occurred in this region prior to the end of heavy bombardment. This fact, combined with the extensive geomorphic evidence for abundant water (Carr 1986), suggests that the crustal evolution of early Mars may have closely resembled that of the Earth. This conclusion is reinforced by the recent discovery of residual magnetic lineations within the southern highland crust (Acuña *et al.* 1999, Connerny *et al.* 1999), the potential signature of an early period of incipient plate tectonics (e.g., Sleep 1994).

From a hydrologic perspective, the two most important properties of crustal rocks are their porosity and permeability, properties whose values decline with increasing compressive stress. For dry rock considered *in situ*, the compressive stress is simply equal to the lithostatic pressure exerted by the local overburden. However, if the pores of the rock are saturated with water, then the resulting hydrostatic pressure will partially offset the lithostatic component, allowing crustal porosity and permeability to persist to greater depths (Hubert and Rubey 1959).

The variation of Martian crustal porosity as a function of depth has been modeled by Clifford (1993) based on a relationship previously applied to both the Earth (Athy 1930, Schmoker and Gautier 1988) and Moon (Binder and Lange 1980). The model predicts an exponential decline in porosity with increasing depth, falling to less than 1% at an effective pressure of $\sim 10^8$ Pa (=1 kbar). By this relationship, the porosity at a depth z is given by

$$\Phi(z) = \Phi(0)\exp(-z/K), \tag{1}$$

where $\Phi(0)$ is the surface porosity and K is the gravitationally scaled porosity decay constant (≈2.82 km for Mars; Clifford 1993).

On the Moon, a surface porosity of 20% is consistent with the measured value of lunar breccias (Warren and Rasmussen 1987) and the seismic propagation characteristics of the near-surface crust (Binder and Lange 1980). However, on Mars, the effect of weathering, the abundance of eolian and fluvial sediments, and the potential for large-scale ice segregation (e.g., see Section 9) have likely contributed to a substantial increase in the effective porosity and storage capacity of the near-surface crust. These considerations led Clifford (1993) to conclude that the globally averaged surface porosity of Mars will likely fall in the range of ~0.35 (±0.15) (Fig. A1).

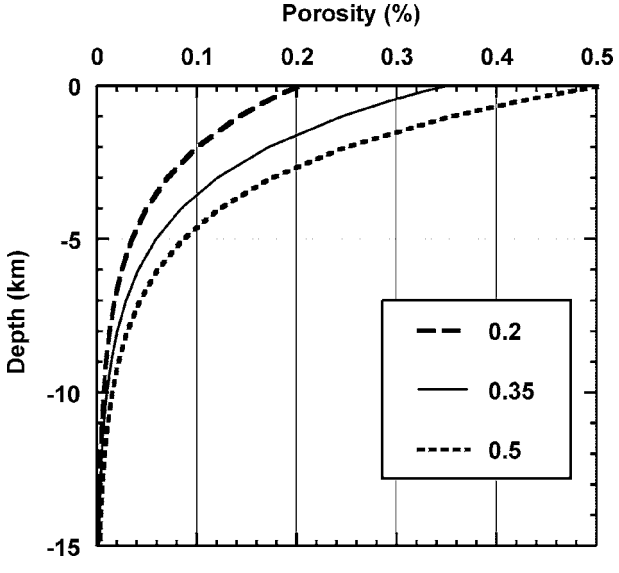

FIG. A1. Theoretical porosity profile of the Martian crust based on Eq. (1) and an assumed value of surface porosity of 0.35 (±0.15). Note that a surface porosity of 50% is only plausible if the regolith has undergone extensive weathering (resulting in the production of large amounts of high-porosity clays) or includes a substantial volume of segregated ice (e.g., see Section 9).

Of course, at any specific location, the local porosity profile of the crust is likely to exhibit significant departures from that predicted on the basis of Eq. (1). In this respect, its structure and physical properties are expected to display all of the range, complexity, and heterogeneity found on Earth.

Estimates of the permeability of the uppermost several kilometers of the martian crust (based primarily on hydraulic arguments associated with the inferred discharges of the large outflow channels) have covered a wide range, with km-scale values estimated to be as high as 10^{-9} m^2 (=10^3 darcies) (e.g., Carr 1979, Mackinnon and Tanaka 1989). Although local permeabilities as high as 10^{-9} m^2 undoubtedly occur on Mars, it appears unlikely that the absolute range and frequency of near-surface permeabilities differs appreciably from that of Earth—when evaluated at similar size scales and under equivalent conditions of effective stress.

The depth to which porosity and hydraulic continuity persist on Mars is unknown. Terrestrial laboratory and lunar seismic data both suggest that the fracture porosity of crustal rocks is significantly reduced at effective lithostatic pressures $\geq 10^8$ Pa (Clifford 1993). If true, this implies that the extent of hydraulic continuity on Mars is limited to a maximum depth of ~10–13 km, depending on local differences in geologic evolution and crustal saturation.

However, investigations of the large-scale permeability of the Earth's crust suggest that the actual extent of hydraulic continuity may substantially exceed the depth implied by a $\sim 10^8$ Pa fracture closure pressure—a conclusion supported by the observation that, in crystalline rock, fluid pressures are typically near hydrostatic values down to depths of ~10 km (Huenges *et al.* 1997, Zoback and Zoback 1997). Gravitationally scaling these results to Mars suggests that hydraulic communication may persist to depths of ~26 km. Although this result appears at odds with the extremely low porosities predicted at depth by Eq. (1), the hydraulic characteristics of fractured rock are inherently more efficient at conducting a fluid per unit porosity than those of an intergrannular pore network (Freeze and Cherry 1979, Fetter 1980).

Early studies of the large-scale permeability of terrestrial rocks suggested that, on a kilometer size-scale, the average permeability of the top 10 km of the Earth's crust was $\sim 10^{-14}$ m^2 (Brace 1980, 1984). However, more recent studies (based on a substantially larger suite of measurements) indicate that crustal permeability, like crustal porosity, is sensitive to confining pressure, falling by as much as three to four orders of magnitude over the effective stress interval of 100–300 MPa (Ingebritsen and Sanford 1998, Manning and Ingebritsen 1999).

At any given depth, the measured permeability of terrestrial rocks can vary by as much as four orders of magnitude (Manning and Ingebritsen 1999). Although the stochastic nature of these variations prohibits any attempt to accurately predict the permeability of the crust at a particular location, when the global data is considered together, it appears to follow a general trend. Manning and Ingebritsen (1999) have found that the best fit to this data is given by the relation

$$\log(k) = -14 - 3.2\log(z) \quad \text{(for Earth)}, \tag{2a}$$

where k is the permeability in m^2 and z is the depth in kilometers. In the absence of any comparable field data for Mars, it seems reasonable to assume that the permeability of martian crustal rocks will be similar under equivalent conditions of effective stress. If so, the corresponding gravitationally scaled expression for Mars is

$$\begin{aligned}\log(k) &= -14 - 3.2\log(z/(g_{\text{Earth}}/g_{\text{Mars}})) \\ &= -12.65 - 3.2\log(z) \quad \text{(for Mars)},\end{aligned} \tag{2b}$$

which predicts that the permeability of the crust will decline from $\sim 10^{-13}$ m^2 at a depth of 1 km, to $\sim 10^{-17}$ m^2 at a depth of 25 km (Fig. A2)—with local permeabilities expected to vary by as much as several orders of magnitude about the predicted mean.

The potential for hydraulic communication to depths ≳10 km suggests that, on a km-size scale, the extent of hydraulic continuity within the crust is essentially global, when considered over sufficiently long (i.e., $\geq 10^8$ yr) time

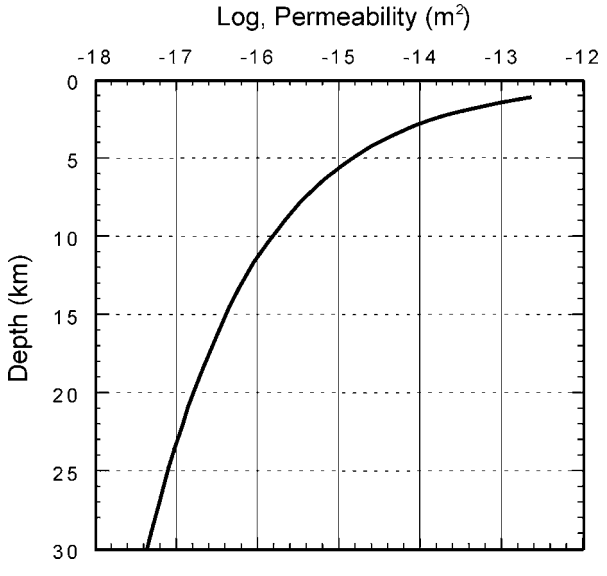

FIG. A2. Permeability of crustal rocks as a function of depth, based on the terrestrial data of Ingebritsen and Manning and Ingebritsen (1999), gravitationally scaled to Mars (Eq. (2b)). Units of permeability are m^2 (where 1 darcy = 10^{-12} m^2).

spans (Clifford 1993). However, a substantially shallower depth of hydraulic communication cannot be ruled out. As cautioned by Carr (2000), the higher geothermal heat flow during the Noachian may have accelerated the annealing of crustal porosity at depths >3–5 km (Section 11.1). This potential appears particularly great beneath the northern plains, whose several-km lower elevation (vs. the southern two-thirds of the planet) has been attributed to crustal thinning associated with mantle convection (Wise *et al*. 1979, McGill and Dimitriou 1990)—a process that would have contributed to a substantially higher regional heat flow.

A.2. Thermal Properties and Structure

Current mean annual surface temperatures on Mars range from ∼154 K at the poles to ∼218 K at the equator (±5 K), with radiogenic heating expected to result in increasingly warmer temperatures at depth. The region of frozen ground defined by this thermal structure is known as the cryosphere (Fig. 1), whose depth z, at any location, is given by

$$z = \kappa_{ave} \frac{(T_{mp} - T_{ms})}{Q_g}, \tag{3}$$

where T_{ms} is the mean annual surface temperature, T_{mp} is the melting temperature of ice at the base of the cryosphere, Q_g is the geothermal heat flux, and κ_{ave} is the column-averaged thermal conductivity (Fanale 1976, Rossbacher and Judson 1981, Kuzmin 1983, Clifford 1993).

T_{mp} can be depressed below 273 K by both pressure and the presence of dissolved salts. However, for the depths under consideration here, the effect of pressure is minimal, while the effect of salt can be quite large. The evolution of Martian groundwater into a highly mineralized brine is an expected consequence of three processes: (1) the geochemical reactions that occur when groundwater is isolated in crustal rocks for billions of years, (2) the influx of salts and other minerals leached from the unsaturated region between the water table and base of the cryosphere by low-temperature hydrothermal convection (Clifford 1991, 1993), and (3) the concentration of dissolved minerals by the steady depletion of groundwater in response to the progressive growth of the cryosphere over geologic time (Section 8.2). As a result, at those locations where the cryosphere is in contact with the water table (e.g., Fig. 1), the presence of dissolved salts may significantly reduce the thickness of frozen ground. On Mars, thermodynamic and chemical stability considerations suggest that NaCl-rich brines (which have a freezing point of 252 K at their eutectic) are the most likely to be found within the crust (Clark and Van Hart 1981). Conversely, where the cryosphere and groundwater are not in direct contact, low-temperature hydrothermal convection is likely to have depleted the intervening unsaturated zone of any easily dissolved substances, resulting in a local basal melting temperature of ∼273 K.

Although no direct measurements of Q_g have yet been made, estimates based on a variety of theoretical, compositional, and geophysical arguments, generally cluster around a present-day value of ∼30 mW m^{-2} (±15 mW m^{-2}; Clifford 1993). Surveys of continental heat flow on Earth (Sclater *et al*. 1980, Pollack *et al*. 1993) indicate that there is an additional ±50% variation in regional-scale heat flow (about the global mean) because of local differences in crustal age; thickness; volcanic and tectonic history; and elemental content of U, Th, and K. Given the first-order similarities in geologic diversity and crustal development between the Earth and Mars (e.g., Mouginis–Mark *et al*. 1992, Banerdt *et al*. 1992), it seems reasonable to expect that Martian crustal heat flow will exhibit a comparable range of regional variability.

Various lines of evidence suggest that the thermal properties of the martian crust are best approximated by those of frozen soil and basalt (Clifford 1993). At the centimeter-scale, the thermal conductivity of these materials covers a wide range (0.08–5.40 W m^{-1} K^{-1}); but this variability is significantly reduced when averaged over larger (∼1–10^2 m^3) volumes. Based on this reasoning, and a review of the measured thermal conductivities of 144 samples of frozen soil and 301 samples of basalt, Clifford (1993) argued that the column-averaged thermal conductivity of the cryosphere is likely to vary between ∼1.0–3.0 W m^{-1} K^{-1}, with a probable mean value of ∼2.0 W m^{-1} K^{-1}. However, systematic departures from this mean are likely at both low and high latitudes. At latitudes $\lesssim 40°$, ground ice is generally unstable with respect to the water vapor content of the atmosphere, leading to the progressive desiccation of the near-surface crust (Clifford and Hillel 1983, Fanale *et al*. 1986, Mellon and Jakosky 1993). The rate and ultimate extent of local desiccation is dependent on the mean annual surface temperature, as well as the local thermal and diffusive properties of the crust. Depending on the nature of these properties, their variation with depth, and the potential for replenishment from any deeper reservoir of subpermafrost groundwater, these factors may result in local depths of desiccation that range from centimeters to as much as a kilometer, with the potential for significant and complex variations in saturation state beneath the sublimation front (Clifford 1998). This loss of near-surface ice at low latitudes could lower the meter-scale thermal conductivity of the host rock to values well below 0.1 W m^{-1} K^{-1}, depending on the rock's lithology and residual volatile content. In contrast, at high latitudes ($>40°$), ground ice is generally stable—although some loss may occur even at polar latitudes at times of high obliquity (Section 10.2). Consideration of this latitudinal variation in ice stability, combined with the observed temperature dependence of the thermal conductivities of ice and rock (which increase with decreasing temperature; e.g., Fig. A3), suggests that, near the poles, the column-averaged value of κ will be closer to ∼3.0 W m^{-1} K^{-1}.

In this analysis, we also consider the thermal properties of ice alone, whose temperature-dependent thermal conductivity can be calculated from the empirically derived expression of Ratcliffe (1962), where

$$\kappa_{ice}(T) = 12.52 - 6.902 \times 10^{-2} T + 1.15 \times 10^{-4}\ T^2. \tag{4}$$

This relationship is illustrated in Fig. A3, where κ_{ice} is seen to vary from a low of 2.25 W m^{-1} K^{-1} at 273 K, to a high of 4.62 W m^{-1} K^{-1} at 154 K. Integrating Eq. (4) over the temperature interval from T_{ms} to T_{mp} and substituting the resulting expression for $\kappa(T_{mp} - T_{ms})$ in Eq. (3) yields

$$z = [12.52(T_{mp} - T_{ms}) - 3.45 \times 10^{-2}(T_{mp} - T_{ms})^2 + 3.83 \times 10^{-5}(T_{mp} - T_{ms})^3]/Q_g, \tag{5}$$

which gives the equilibrium thickness of an ocean ice cover as a function of T_{ms}, T_{mp}, and Q_g.

Equation (5) also places an effective upper limit on the maximum depth of the cryosphere, assuming that it is both ice-rich and that the ice component is composed of H_2O alone. The validity of this last assumption appears questionable

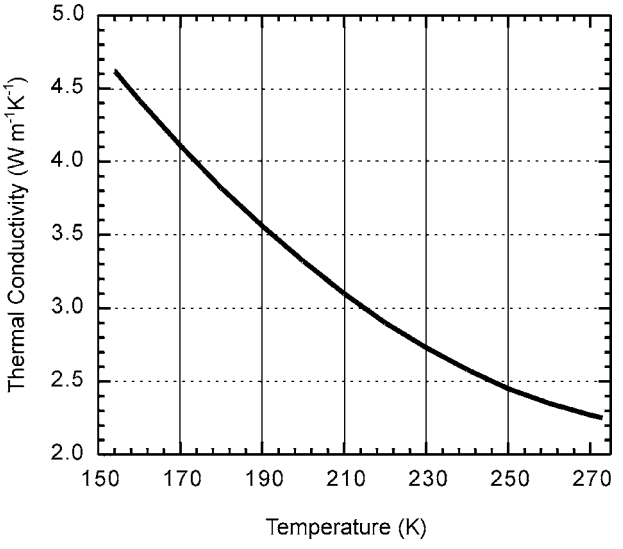

FIG. A3. Thermal conductivity of ice as a function of temperature, as given by Eq. (4) (Ratcliffe 1962).

because, below a depth of ~15 m, the subsurface pressure and temperature regime is also conducive to the formation of gas hydrates—substances that form when molecules of CO_2, CH_4, and other gases, become trapped within the cubic crystalline lattice of water ice (Kargel and Lunine 1998, Fisk and Giovannoni 1999, Max and Clifford 2000; see also Section 4.2). In their pure state, the thermal conductivity of gas hydrates is approximately one-fifth of that of water ice (Davidson 1983, Sloan 1997, deMartin 1999). Therefore, depending on their abundance and distribution within the cryosphere, gas hydrates may contribute to a substantial reduction in the local thickness of frozen ground.

APPENDIX B: NOMENCLATURE

a	radius of basal melting/recharge area, m.
g	acceleration of gravity, 3.71 m s^{-2}.
h	height of water table (for polar cap in Fig. 18) above local datum, m.
h_i	initial height of water table above local datum, m.
h_m	central height of groundwater mound above local datum, m.
Δh	difference in elevation between global water table and base of polar cap, m.
$\bar{h}$	$=.5(h + h_i)$, weighted mean depth of saturation, m.
k	crustal permeability, m^2.
K	porosity decay constant, =2820 m for Mars.
Q_f	frictional heat due to glacial sliding, W m^{-2}.
Q_g	geothermal heat flux, W m^{-2}.
Q_r	$=\pi a^2 w$, aquifer recharge volume, m^3 s^{-1}.
r	radius, m.
t	time, s.
T	temperature, K.
T_{mp}	melting/freezing temperature, K.
T_{ms}	mean annual surface temperature, K.
u_o	$=a^2 v\varepsilon/4kg\bar{h}t$.
V_b	basal sliding velocity, m s^{-1}
w	aquifer recharge rate, m s^{-1}.
$W(u_o)$	well function for a nonleaky aquifer.
z	depth, m.
Δz	thickness, m.
Z	$=h^2 - h_i^2$, m^2.
ε	effective porosity.
κ_{ave}	column-averaged thermal conductivity of crust, W m^{-1} K^{-1}.
κ_{ice}	temperature-dependent thermal conductivity of ice, W m^{-1} K^{-1}.
$\Phi(z)$	crustal porosity at a depth z, 1.00 = 100%.
v	kinematic viscosity, m^2 s^{-1}.
ρ	density, kg m^{-3}.

ACKNOWLEDGMENTS

The authors thank Mike Carr and an anonymous reviewer for their thoughtful and constructive reviews, and Pat McGovern who helped with the presentation of the MOLA data in Fig. 10. The work by S. Clifford was supported by the Lunar and Planetary Institute and a grant from NASA's Planetary Geology and Geophysics Program. The work by T. Parker was conducted at the Jet Propulsion Laboratory, California Institute of Technology, under contract with the NASA Planetary Geology and Geophysics Program. This is LPI Contribution #992.

REFERENCES

Acuña, M. H., J. E. P. Connerney, N. F. Ness, R. P. Lin, D. Mitchell, C. W. Carlson, J. McFadden, K. A. Anderson, H. Rème, C. Mazelle, D. Vignes, P. Wasilewski, and P. Cloutier 1999. Global Distribution of crustal magnetization discovered by the Mars Global Surveyor MAG/ER experiment. *Science* **284,** 790–793.

Aharonson, O., M. T. Zuber, and G. A. Neumann 1998. Mars: Northern hemisphere slopes and slope distributions. *Geophys. Res. Lett.* **25**, 4413–4416.

Allen, C. C. 1979. Volcano-ice interactions. *J. Geophys. Res.* **84**, 8048–8059.

Anderson, D. M., and A. R. Tice 1973. The unfrozen interfacial phase in frozen soil water systems. In *Ecological Studies. Analysis and Synthesis* **4** (A. Hadas, D. Swartzendruber, P. E. Rijtema, M. Fuchs, and B. Yaron, Eds.), pp. 107–124. Springer-Verlag, New York.

Athy, L. F. 1930. Density, porosity, and compaction of sedimentary rocks. *Bull. Am. Assoc. Petrol. Geol.* **14**, 1–24.

Baker, V. R. 1982. *The Channels of Mars*. University of Texas Press, Austin.

Baker, V. R., and R. C. Kochel 1979. Martian channel morphology: Maja and Kasei Valles. *J. Geophys. Res.* **84**, 7961–7993.

Baker, V. R., R. G. Strom, V. C. Gulick, J. S. Kargel, G. Komatsu and V. S. Kale 1991. Ancient oceans, ice sheets and the hydrologic cycle on Mars. *Nature* **352**, 589–594.

Baker, V. R., M. H. Carr, V. C. Gulick, C. R. Williams, and M. S. Marley 1992. Channels and valley networks. In *Mars* (H. H. Kieffer, B. M. Jakosky, C. W. Snyder, and M. S. Matthews, Eds.), pp. 493–522. University of Arizona Press, Tucson.

Banerdt, W. B., M. P. Golombek, and K. L. Tanaka 1992. Stress and tectonics on Mars. In *Mars* (H. H. Kieffer, B. M. Jakosky, C. W. Snyder, and M. S. Matthews, Eds.), pp. 249–297, Univ. of Arizona Press, Tucson.

Banerdt, W. B., and T. J. Parker 1998. *Testing the Plausibility of Martian Shorelines Using MOLA Data*, Fall GSA, A402.

Banin, A., and D. M. Anderson 1974. Effects of salt concentration changes during freezing on the unfrozen water content of porous materials. *Water Resour. Res.* **10**, 124–128.

Binder, A. B., and M. A. Lange 1980. On the thermal history, thermal state, and related tectonism of a moon of fission origin. *J. Geophys. Res.* **85**, 3194–3208.

Birch, F. 1961. The velocity of compressional waves in rocks to 10 kilobars, part 2. *J. Geophys. Res.* **66**, 2199–2224.

Brace, W. F. 1980. Permeability of crystalline and argillaceous rocks. *Int. J. Rock Mech. Min. Sci. & Geomech. Abstr.* **17**, 241–251.

Brace, W. F. 1984. Permeability of crystalline rocks: New in situ measurements. *J. Geophys. Res.* **89**, 4327–4330.

Brandstrom, G. W. 1986. *A Morphologic Analysis of Granicus Valles, Mars*, M.Sc. thesis, Texas A & M University.

Brass, G. W. 1980. Stability of brines on Mars. *Icarus* **42**, 20–28.

Cabrol, N. A., E. A. Grin, and G. Dawidowicz 1997. A model of outflow generation by hydrothermal underpressure drainage in volcano-tectonic environment, Shalbatana Vallis (Mars). *Icarus* **125**, 455–464.

Cabrol, N. A., E. A. Grin, and L. Ragnhild 1998. Ma'adim Vallis evolution: Geometry and models of discharge rate. *Icarus* **132**, 362–377.

Carr, M. H. 1979. Formation of Martian flood features by release of water from confined aquifers. *J. Geophys. Res.* **84**, 2995–3007.

Carr, M. H. 1984. Formation of martian valley networks as a consequence of large impacts. *Lunar Planet. Sci. Conf.* **15**, 131–132.

Carr, M. H. 1986. Mars: A water-rich planet? *Icarus* **68**, 187–216.

Carr, M. H. 1987. Water on Mars. *Nature* **326**, 30–35.

Carr, M. H. 1990. D/H on Mars: The effect of floods, volcanism, impacts and polar processes. *Icarus* **87**, 210–227.

Carr, M. H. 1996. *Water on Mars*. Oxford University Press, New York.

Carr, M. H. 1999. Retention of an atmosphere on early Mars. *J. Geophys. Res.* **104**, 21897–21909.

Carr, M. H. 2000. Martian oceans, valleys, and climate: New insights from Mars Global Surveyor. *Astron. Geophys.* **41**, 3.20–3.26.

Carr, M. H., and F. C. Chuang 1997. Martian drainage densities. *J. Geophys. Res.* **102**, 9145–9152.

Carr, M. H., and G. D. Clow 1981. Martian channels and valleys: Their characteristics, distribution and ages. *Icarus* **48**, 91–117.

Carr, M. H., and G. G. Schaber 1977. Martian permafrost features. *J. Geophys. Res.* **82**, 4039–4055.

Chapman, M. G. 1994. Evidence, age, thickness of a frozen paleolake in Utopia Planitia, Mars. *Icarus* **109**, 393–406.

Chapman, M. B., and K. L. Tanaka 1990. Small valleys and hydrologic history of the lower Mangala Valles region, Mars. *Proc. Lunar Planet. Sci. Conf.* **20**, Lunar and Planetary Institute, 531–539.

Chapman, M. B., and K. L. Tanaka 1993. Geologic maps of the MTM-05152 and -10152 quadrangles, Mangal Valles region of Mars, U.S. Geol. Surv. Misc. Invest. Series Map I-2294.

Chapman, M. B., and K. L. Tanaka 1996. Geologic maps of the MTM-25062 quadrangle (digital compilation) and the MTM-25067 quadrangel (manual compilation), Kasei Valles region of Mars, U.S. Geol. Surv. Misc. Invest. Series Map I-2398.

Clark, B. C., and D. C. Van Hart 1981. The salts of Mars. *Icarus* **45**, 370–378.

Clifford, S. M. 1987. Polar basal melting on Mars. *J. Geophys. Res.* **92**, 9135–9152.

Clifford, S. M. 1991. The role of thermal vapor diffusion in the subsurface hydrologic evolution of Mars. *Geophys. Res. Lett.* **18**, 2055–2058.

Clifford, S. M. 1993. A model for the hydrologic and climatic behavior of water on Mars. *J. Geophys. Res.* **98**, 10,973–11,016.

Clifford, S. M. 1996. Is Mars water rich? Optimal landing site locations for the detection of subpermafrost groundwater. *Lunar Planet. Sci. Conf. XXVII*, 233–234.

Clifford, S. M. 1997. The origin of the martian intercrater plains: The role of liquefaction from impact and tectonic-induced seismicity, *Lunar Planet. Sci. Conf.* **27**, 241.

Clifford, S. M. 1998. Mars: The effect of stratigraphic variations in regolith diffusive properties on the evolution and vertical distribution of equatorial ground ice. *Lunar Planet. Sci. Conf.* **28**.

Clifford, S. M., and D. Hillel 1983. The stability of ground ice in the equatorial region of Mars. *J. Geophys. Res.* **88**, 2456–2474.

Clifford, S. M., and T. J. Parker 1999. Hydraulic and thermal arguments regarding the existence and fate of a primordial martian ocean. *Lunar Planet. Sci. Conf.* [CD-ROM] **30**, 1619.

Connerney, J. E. P., M. H. Acuña, P. J. Wasilewski, N. F. Ness, H. Rème, C. Mazelle, D. Vignes, R. P. Lin, D. L. Mitchell, and P. Cloutier 1999. Magnetic lineations in the ancient crust of Mars. *Science* **284**, 794–798.

Costard, F. M., and J. S. Kargel 1995. Outwash plains and thermokarst on Mars. *Icarus* **114**, 93–112.

Craddock, R. A., and R. Greeley 1994. Geologic map of the MTM-20147 quadrangle, Mangal Valles region of Mars, U.S. Geol. Surv. Misc. Invest. Series Map I-2310.

Craddock, R. A., and T. Maxwell 1993. Geomorphic evolution of the martian highlands through ancient fluvial processes. *J. Geophys. Res.* **98**, 3453–3468.

Crown, D. A., and R. Greeley 1993. Volcanic geology of Hadriaca Patera and eastern Hellas region of Mars. *J. Geophys. Res.* **98**, 3431–3451.

Crown, D. A., and S. C. Mest 1997. Dao, Harmakhis, and Reull Valles-The role of outflow channels in the degradation of the circum-Hellas highlands of Mars. *Lunar Planet. Sci. Conf.* **23**, 269–270.

Crown, D. A., K. H. Price, and R. Greeley 1992. Geologic Evolution of the East Rim of the Hellas Basin, Mars. *Icarus* **100**, 1–25.

Davidson, D. 1983. Gas hydrates as clathrate ices. In *Natural Hydrates—Properties, Occurrence and Recovery*, Butterworth, Woburn, MA, pp. 1–16.

De Hon, R. A. 1991. Polygenetic origin of Hrad Vallis region of Mars. *Proc. Lunar Planet. Sci. Conf.* **22**, 45–51.

De Hon, R. A., and E. A. Pani 1993. Duration and rates of discharge: Maja Valles, Mars. *J. Geophys. Res.* **98**, 9129–9138.

De Hon, R. A., and P. A. Washington 1999. Bahram Vallis, Mars: A brief history of a long term discharge. *Lunar Planet. Sci. Conf.* [CD-ROM] **30**, 1928.

deMartin, B. 1999. Laboratory thermal conductivity measurements of methane hydrate and hydrate-sediment mixtures under simulated in situ conditions. *EOS, Trans. Amer. Geophys. Union* **80**, S337.

Edgett, K. S., and T. J. Parker 1997. Water on early Mars: Possible subaqueous sedimentary deposits covering ancient cratered terrain in western Arabia and Sinus Meridiani. *Geophys. Res. Lett.* **24**, 2897–2900.

Fanale, F. P. 1976. Martian volatiles: Their degassing history and geochemical fate. *Icarus* **28**, 170–202.

Fanale, F. P., J. R. Salvail, A. P. Zent, and S. E. Postawko 1986. Global distribution and migration of subsurface ice on Mars, *Icarus* **67**, 1–18.

Farmer, C. B., and P. E. Doms 1979. Global and seasonal variation of water vapor on Mars and the implications for permafrost. *J. Geophys. Res.* **84**, 2881–2888.

Fetter, C. W., Jr. 1980. *Applied Hydrogeology*. Merrill Columbus, Ohio.

Fishbaugh, K., and J. W. Head III 1999. The geometry of Chasma Boreale, Mars using Mars Orbiter Laters Altimeter (MOLA) data: A test of the catastrophic outflow hypothesis of formation. *5th Int. Conf. Mars*, Lunar and Planetary Institute. [CD-ROM. 6817]

Fisk, M. R., and S. J. Giovannoni 1999. Sources of nutrients and energy for a deep biosphere on Mars. *J. Geophys. Res.* **104**, 11805–11815.

Franklin, B. J., and T. J. Parker 1999, Geologic maps of east Acidalia Planitia, Mars. *Lunar Planet. Sci. Conf.* [CD-ROM] **30**, 1785.

Freeze, R. A. and J. A. Cherry 1979. *Groundwater*. Prentice-Hall, Englewood Cliffs, New Jersey, 604 pp.

Frey, H. V., and J. H. Roark 1997. Lowlying ancient terrain (LAT) on Mars—The Western Arabian Shelf (WAS). *Lunar Planet. Sci. Conf.* **28**, 383–384.

Frey, H. V., and R. A. Schultz 1988. Large impact basins and the mega-impact origin for the crustal dichotomy of Mars. *Geophys. Res. Lett.* **15**, 229–232.

Frey, H. V., and R. A. Schultz 1990. Speculations on the origin and evolution of the Utopia-Elysium lowlands of Mars. *J. Geophys. Res.* **95**, 14203–14213.

Frey, H., S. Sakimoto, and J. Roark 1999. MOLA topographic structure of the Isids and Utopia impact basins, *Lunar Planet. Sci. Conf.* **30**, 1500 (abstract).

Gold, T., B. T. O'Leary, and M. Campbell 1971. Some physical properties of Apollo 12 lunar samples. *Proc. 2nd Lunar Sci. Conf.* **3**, 2173–2181.

Grant, J. A. 1987. The geomorphic evolution of Eastern Margaritifer Sinus, Mars in: *Advances in Planetary Geology*, NASA-TM-89871, 1-268.

Greeley, R. 1987. Release of juvenile water on Mars: Estimated amounts and timing associated with volcanism. *Science* **236**, 1653–1654.

Greeley, R., and J. E. Guest 1987. Geologic Map of the Eastern Equatorial Region of Mars. U.S. Geol. Surv. Map I-1802-B, Atlas of Mars. 1:15,000,000 Geologic Series.

Greeley, R., and B. Schneid 1991. Magma generation on Mars: Amounts, rates, and comparisons with the Earth, Moon, and Venus. *Science* **254**, 996–998.

Greeley, R., N. Lancaster, S. Lee, and P. Thomas 1992. Martian aeolian processes, sediments, and features. In *Mars* (H. H. Kieffer, B. M. Jakosky, C. W. Snyder, and M. S. Matthews, Eds.), pp. 730–766. University of Arizona Press, Tuscon.

Grieve, R. A. F., and M. J. Cintala 1992. An analysis of diferrential impact melt-crater scaling and implications for the terrestrial impact record. *Meteoritics* **27**, 526–538.

Grizzaffi, P., and P. H. Schultz 1989. Isidis basin-Site of ancient volatile-rich debris layer. *Icarus* **77**, 358–381.

Haberle, R. M. 1998. Early Mars climate models. *J. Geophys. Res.* **103**, 28467–28480.

Haberle, R. M., D. Tyler, C. P. McKay, and W. L. Davis 1994. A model for the evolution of CO_2 on Mars. *Icarus* **109**, 102–120.

Hantush, M. S. 1967. Growth and decay of groundwater-mounds in response to uniform percolation. *Water Resour. Res.* **3**, 227–234.

Head, J. W. III 2000. Channels surrounding candidate ancient south polar deposits on Mars: Evidence for drainage of meltwater, *Lunar Planet. Sci. Conf.* [CD-ROM] **31**, 1121 (abstract).

Head, J. W. III, and K. Fishbaugh 2000. Evidence for an extensive south polar ice cap in middle Mars history. In *Second International Conference on Mars Polar Science and Exploration*, LPI Contribution No. 1057, Lunar and Planetary Institute, Houston, pp. 68–69.

Head, J. W. and S. Pratt 2001. Extensive Hesperian-aged south polar ice sheet on Mars: Evidence for massive melting and retreat, and lateral flow and ponding. *J. Geophys. Res.* **106**, 12275–12299.

Head, J. W. III, H. Hiesinger, M. A. Ivanov, M. A. Kreslavsky, S. Pratt, and B. J. Thomson 1999. Possible ancient oceans on Mars: Evidence from Mars Orbiter Laser Altimeter Data. *Science* **286**, 2134–2137.

Head, J. W. III, M Kreslavsky, H. Hiesinger, M. Ivanov, S. Pratt, N. Seibert, D. E. Smith, and M. T. Zuber 1998. Oceans in the past history of Mars: Tests for their presence using Mars Orbiter Laser Altimeter (MOLA) data. *Geophys. Res. Lett.* **25**, 4401–4404.

Hiesinger, H., and J. W. Head III 1999. Shorelines on Mars: Testing for their presence Using Mars Orbiter Laser Altimeter (MOLA) Data. *30th Lunar Planet. Sci. Conf.* [CD-ROM] 1370 (abstract).

Hiesinger, H., and J. W. Head III 2000. Characteristics and origin of polygonal terrain in southern Utopia Planitia, Mars: Results from Mars Orbiter Laser Altimeter and Mars Orbiter Camera data. *J. Geophys. Res.* **105**, 11999–12022.

Howard, A. D. 1981. Etched plains and braided ridges of the south polar region of Mars: Features produced by basal melting of ground ice? *NASA Tech. Memo. TM 84211*, 286–288.

Huenges, E., J. Erzinger, J. Kuck, B. Engeser, and W. Kessels 1997. The permeable crust: Geohydraulic properties down to 9101 m depth. *J. Geophys. Res.* **102**, 18255–18265.

Hubert, M. K., and W. W. Rubey 1959. Role of fluid pressure in mechanics of overthrust faulting. *Bull. Geol. Soc. Am.* **70**, 115.

Ingebritsen, S. E., and W. I. Sanford 1998. *Groundwater in Geologic Processes*. Cambridge Univ. Press, New York.

Jakosky, B. M., B. G. Henderson, and M. T. Mellon 1995. Chaotic obliquity and the nature of the martian climate. *J. Geophys. Res.* **100**, 1579–1584.

Johnson, C. L., S. C. Solomon, J. W. Head, R. J. Philips, D. E. Smith, and M. T. Zuber 2000. Lithospheric loading by the north polar cap of Mars. *Icarus* **144**, 313–328.

Kahn, R. A., T. Z. Martin, R. W. Zurek, and S. W. Lee 1992. The martian dust cycle. In *Mars* (H. H Kieffer, B. M. Jakosky, C. W. Snyder, and M. S. Matthews, Eds.), pp. 1017–1053. University of Arizona Press, Tuscon.

Kargel, J. S., and R. G. Strom 1992. Ancient glaciation on Mars. *Geology* **20**, 3–7.

Kargel, J. S., and J. I. Lunine 1998. Clatherate hydrates on Earth and in the Solar System. In *Solar System Ices* (B. Schmidt *et al.*, Eds.)., pp. 97–117. Kluwer Academic, Dordrecht, Norwell, MA.

Kargel, J. S., V. R. Baker, J. E. Beget, J. F. Lockwood, T. L. Pewe, J. S. Shaw, and R. G. Strom 1995. Evidence of ancient continental glaciation in the martian northern plains. *J. Geophys. Res.* **100**, 5351–5368.

Kasting, J. F. 1991. CO_2 condensation and the climate of early Mars. *Icarus* **94**, 1–13.

Kiefer, W. S. 1999. Time-dependent mantle convection on Mars: Implications for episodic tectonism and volcanism on Mars. *Fifth International Conference on Mars* [CD-ROM] 6154.

Kiefer, W. S., and L. H. Kellog 1998. Geoid anomalies and dynamic topography from time-dependent, spherical axisymmetric mantle convection. *Phys. Earth Plent. Inter.* **106**, 237–256.

Komatsu, G., and V. R. Baker 1997. Paleohydrology and flood geomorphology of Ares Vallis. *J. Geophys. Res.* **102**, 4151–4160.

Kuzmin, R. O. 1983. *Cryolithosphere of Mars*. Izdatel'stvo Nauka, Moscow.

Kvenvolden, K. A. 1993. A primer on gas hydrate. In *The Future of Energy Gases*. (D. G. Howell, *et al.*, Eds.), pp. 279–291. US Geological Survey Professional Paper 1570.

Laskar, J., and P. Robutel 1993. The chaotic obliquity of the planets. *Nature* **361**, 608–612.

Leyva, I. A., and S. M. Clifford 1993. The seismic response of an aquifer to the propagation of an impact generated shock wave: A possible trigger of the martian outflow channels? *Lunar Planet. Sci.* **24**, 875–876.

Lucchitta, B. K. 1981. Mars and Earth: Comparison of cold-climate features. *Icarus* **45**, 264–303.

Lucchitta, B. K. 1984. Ice and debris in the fretted terrain, Mars. *J. Geophys. Res.* **89**, *Lunar Planet. Sci. Conf., 14th Proceedings, pt. 2, Supplement*, B407–B418.

Lucchitta, B. K. 1993. Ice in the northern plains: Relic of a frozen ocean? In *MSATT Workshop on the Martian Northern Plains*. Lunar Planet. Sci. Inst. Tech. Rept. 93-04, Part 1, 9–10.

Lucchitta, B. K., and M. G. Chapman 1988. Ground ice along the northern highland scarp. MEVTV Workshop, Oct. 1988, Lunar and Planetary Institute, Houston, Texas, 34–36.

Lucchitta, B. K., and H. M., Ferguson 1983. Chryse basin channels: low gradients and ponded flow. *J. Geophys. Res.* **88**, *Supplement 13th Proc. Lunar Planet. Sci. Conf., pt. 2*, A553–A568.

Lucchitta, B. K., H. M. Ferguson, and C. A. Summers 1986. Sedimentary deposits in the northern lowland plains, Mars. *J. Geophys. Res.* **91**, *Supplement 17th Proc. Lunar Planet. Sci. Conf.*, E166–E174.

Lucchitta, B. K., N. K. Isbell, and Howington-Kraus 1994. Topography of Valles Marineris: Implications for erosional and structural history. *J. Geophys. Res.* **99**, 3783–3798.

Lucchitta, B. K., A. S. McEwen, G. D. Clow, P. E. Geissler, R. B. Singer, R. A. Schultz, and S. W. Squyres 1992. The canyon system on Mars. In *Mars* (H. H. Kieffer, B. M. Jakosky, C. W. Snyder, and M. S. Matthews, Eds.), pp. 453–492. Univ. of Arizona Press, Tuscon.

MacKinnon, D. J., and K. L. Tanaka 1989. The impacted martian crust: Structure, hydrology, and some geologic implications. *J. Geophys. Res.* **94**, 17359–17370.

Malin, M. C., and K. S. Edgett 1999. Oceans or seas in the martian northern lowlands: High resolution imaging tests of proposed coastlines. *Geophys. Res. Lett.* **26**, 3049–3052.

Malin, M. C., and K. S. Edgett 2000. Sedimentary rocks of early Mars. *Science* **290**, 1927–1937.

Manning, C. E., and S. E. Ingebritsen 1999. Permeability of the continental crust: Implications of geothermal data and metamorphic systems. *Rev. Geophys.* **37**, 127–150.

Mars Channel Working Group 1983. Channels and valleys on Mars. *Geol. Soc. Am. Bull.* **94**, 1035–1054.

Masursky, H., J. M. Boyce, A. L. Dial, G. G. Schaber, and M. E. Strobell 1977. Classification and time of formation of martian channels based on Viking data. *J. Geophys. Res.* **82**, 4016–4038.

Max, M. D., and S. M. Clifford 2000. The state, potential distribution, and biological implications of methane in the martian crust. *J. Geophys. Res.* **105**, 4165–4171.

Max, M. D., and S. M. Clifford 2001. Initiation of martian outflow channels: Related to the dissociation of gas hydrate? *Geophys. Res. Lett.* **28**, 1787–1790.

McBride, K. M. 1991. *An Analysis of Possible Pyroclastic Activity Near Elysium Mons*, *Mars*. M.Sc. thesis, University of Houston—Clear Lake.

McCauley, J. F. 1978. Geologic map of the Coprates quadrangle of Mars, U.S. Geol. Surv. Misc. Invest. Ser. Map, I–897.

McCoy, W. D. 1987. Quaternary aminostratigraphy of the Bonneville basin, western United States. *Geol. Soc. Am. Bull.* **98**, 99–112.

McEwen, A. S., M. C. Malin, M. H. Carr, and W. K. Hartmann 1999. Voluminous volcanism on early Mars revealed in Valles Marineris. *Nature* **397**, 584–586.

McGill, G. E. 1986. The giant polygons of Utopia, northern martian plains. *Geophys. Res. Lett.* **13**, 705–708.

McGill, G. E. 1989. Buried topography of Utopia, Mars: Persistence of a giant impact depression. *J. Geophys. Res.* **94**, 2753–2759.

McGill, G. E. 1992. Origin of giant martian polygons. *J. Geophys. Res.* **97**, 2633–2647.

McGill, G. E., and A. M. Dimitriou 1990. Origin of the martian global dichotomy by crustal thinning in the Late Noachian or Early Hesperian. *J. Geophys. Res.* **95**, 12595–12605.

McGill, G. E., and S. W. Squyres 1991. Origin of the martian crustal dichotomy: Evaluating hypotheses. *Icarus* **93**, 386–393.

McKay, C. P., and W. L. Davis 1991. Duration of liquid water habitats on early Mars. *Icarus* **90**, 214–221.

McKay, C. P., G. D. Clow, R. A. Wharton, Jr., and S. W. Squyres 1985. Thickness of ice on perenially frozen lakes. *Nature* **313**, 561–562.

McKenzei, D., and F. Nimmo 1999. The generation of martian floods by the melting of ground ice above dykes. *Nature* **397**, 231–233.

Mellon, M. T., and B. M. Jakosky 1993. Geographic variations in the thermal and diffusive stability of ground ice on Mars. *J. Geophys. Res.* **98**, 3345–3364.

Metzger, S. M. 1992. The eskers of New York state: Formation process implications and esker-like features on the planet Mars. *Lunar Planet. Sci. Conf.* **23**, 901.

Miller, S. M., and W. D. Smythe 1970. Carbon dioxide clathrate in the martian ice cap. *Science* **170**, 531–533.

Milton, D. J. 1974. Carbon dioxide hydrate and floods on Mars. *Science* **183**, 654–656.

Moore, J. F., and K. S. Edgett 1993. Hellas Planitia, Mars: Site of net dust erosion and implications for the nature of the basin floor deposits. *Geophys. Res. Lett.* **20**, 1599–1602.

Moore, J. M., G. D. Clow, W. L. Davis, V. C. Gulick, D. R. Janke, C. P. McKay, C. R. Stoker, and A. P. Zent 1995. The circum-Chryse region as a possible example of a hydrologic cycle on Mars: Geologic observations and theoretical evaluation. *J. Geophys. Res.* **100**, 5433–5447.

MOLA Science Team 1999. 1x1 degree gridded topographic map of Mars, Experimental Gridded Data Record.

Mouginis-Mark, P. J. 1990. Recent water release in the Tharsis region of Mars. *Icarus* **84**, 362–373.

Mouginis-Mark, P. J., L. Wilson, Lionel, and M. T. Zuber 1992. The physical volcanology of Mars. In *Mars* (H. H. Kieffer, B. M. Jakosky, C. W. Snyder, and M. S. Matthews, Eds.), pp. 424–452, Univ. of Arizona Press, Tucson.

Mouginis-Mark, P. J., L. Wilson, J. W. Head, S. H. Brown, J. L. Hall, and K. D. Sullivan 1984. Elysium Planitia, Mars: Regional geology, volcanology, and evidence for volcano-ground ice interactions. *Earth, Moon, Planets* **30**, 149–173.

Nedell, S. S., S. W. Squyres, and D. W., Anderson 1987. Origin and evolution of the layered deposits in the Valles Marineris. *Icarus* **70**, 409–441.

Nelson, D. M., and R. Greeley 1999. Geology of Xanthe Terra outflow channels and the Mars Pathfinder landing site. *J. Geophys. Res.* **104**, 8653–8669.

Nummendal, D., and D. B. Pryor 1981. Generation of martian chaos and channels by debris flows. *Icarus* **45**, 77–86.

Oviatt, C. G. 1989. Quaternary geology of part of the Sevier Desert, Millard County, Utah. *Utah Geol. and Mineral Surv. Spec. Studies* **70**.

Parker, T. J. 1985. *Geomorphology and Geology of the Southwestern Margaritifer Sinus—Northern Argyre Region of Mars*, Master's thesis, Geology Dept., California State University, Los Angeles.

Parker, T. J. 1989. Channels and valley networks associated with Argyre Planitia, Mars. *Lunar Planet. Sci. Conf.* **20**, 826–827.

Parker, T. J. 1994. *Martian Paleolakes and Oceans*. Ph.D. Dissertation, Dept. of Geological Sciences, University of Southern California, Los Angeles.

Parker, T. J. 1996. Fluvial and lucustrine degradation of large martian basins during the Noachian. In *Conference on Early Mars: Geologic and Hydrologic Evolution, Physical and Chemical Environments, and the Implications for Life* (S. M. Clifford, A. H. Treiman, H. E. Newsom, and J. D. Farmer, Eds.), pp. 65–66. Lunar and Planetary Insititute, Houston.

Parker, T. J. 1998. Mapping of possible "Oceanus Borealis" shorelines on Mars: A status report. *Lunar Planet. Sci. Conf.* **29**.

Parker, T. J., and R. S. Saunders 1988. Origin of martian plains. *Lunar Planet. Sci. Conf.* **19**, 905–906.

Parker, T. J., and R. S. Saunders 1987. Origin of the lowland plains: Constraints on boundary morphology, In *Mars: Evolution of Volcanism, Tectonism, and Volatiles, Workshop on the Nature and Composition of Surface Units on Mars*, LPI Tech. Rep., 88–05, 100–102. Lunar and Planet. Inst., Houston.

Parker, T. J., and P. M. Schenk 1995. Viking stereo of the martian crustal dichotomy in southern Elysium: Evidence for extensive fluvial and coastal erosion? *Lunar Planet. Sci. Conf.* **26**, 1105–1106.

Parker, T. J., D. S. Gorsline, R. S. Saunders, D. C. Pieri, and D. M Schneeberger, 1993. Coastal geomorphology of the martian northern plains. *J. Geophys. Res.* **98**, 11061–11078.

Parker, T. J., R. S. Saunders, and D. M. Schneeberger 1989. Transitional morphology in West Deutronilus Mensae, Mars: Implications for modification of the lowland/upland boundary. *Icarus* **82**, 111–145.

Parker, T. J., S. M. Clifford, and W. B. Banerdt 2000. Argyre Planitia and the Mars global hydrologic cycle. *Lunar Planet. Sci. Conf.* [CD-ROM] **31**, 2033.

Parthare, A. V., and D. A. Paige, Recent liquid water in the polar regions of Mars. In *First International Conference on Mars Polar Science and Exploration*, p. 31. LPI Contribution No. 953, Lunar and Planetary Institute, Houston.

Peale, S. J., G. Schubert, and R. E. Lingfelter 1975. Origin of martian channels: Clathrates and water. *Science* **187**, 273–274.

Pieri, D. 1979. *Geomorphology of Martian Valleys*, Ph.D. thesis, Cornell University, Ithaca, New York.

Plaut, J. J. 1999. Probing the crust of Mars with orbital sounding radar: The MARSIS experiment on Mars Express. *Lunar Planet. Sci. Conf.* [CD-ROM] **30**, 1136.

Pollack, H. N., S. J. Hurter, and J. R. Johnson 1993. Heat flow from the Earth's interior—Analysis of the global data set. *Rev. Geophys.* **31**, 267–280.

Pollack, J. B., D. Colburn, F. M. Flasar, R. Kahn, C. E. Carlston, and D. Pidek 1979. Properties and effects of dust particles suspended in the martian atmosphere. *J. Geophys. Res.* **84**, 2929–2945.

Pollack, J. B., J. F. Kasting, S. M. Richardson, and K. Poliakoff 1987. The case for a wet, warm climate on early Mars. *Icarus* **71**, 203–224.

Ratcliffe, E. H. 1962. The thermal conductivity of ice: New data on the temperature coefficient. *Phi. Mag.* **1**, 1197–1203.

Rice, J. R. Jr., and R. A. De Hon 1996. Geologic map of the Darvel Quadrangle (MTM 20052), Maja Valles region of Mars. U.S. Geol. Surv. Misc. Inv. Series Map I-2432.

Rossbacher, L. A. 1985. Ground ice models for the distribution and evolution of curvilinear landforms on Mars. In *Models in Geomorphology* (M. J. Woldenberg Ed.), pp. 343–372. Allen and Unwin, Winchester, MA.

Rossbacher, L. A., and S. Judson 1981. Ground ice on Mars: Inventory, distribution, and resulting landforms. *Icarus* **45**, 39–59.

Rotto, S., and K. L. Tanaka 1995. Geologic/geomorphologic map of the Chryse Planitia region of Mars. U.S. Geol. Surv. Misc. Inv. Series Map I-2441.

Ruff, S. W. 1994. Comparison of Mars sinuous ridges with terrestrial linear dunes: Observations from the field. *Lunar Planet. Sci. Conf.* **15**, 1171.

Saunders, R. S. 1979. Geologic map of the Margaritifer Sinus Quadrangle of Mars. USGS Map I-1134 (MC-19), U.S. Geological Survey.

Schmoker, J. W., and D. L. Gautier 1988. Sandstone porosity as a function of thermal maturity. *Geology* **16**, 1007–1010.

Schubert, G., S. C. Solomon, D. L. Turcotte, M. J. Drake, and N. H. Sleep 1992. Origin and thermal evolution of Mars. In *Mars* (H. H. Kieffer, B. M. Jakosky, C. W. Snyder, and M. S. Matthews, Eds.), pp. 147–183. Univ. of Arizona Press, Tuscon.

Schultz, R. A., and H. V. Frey 1990. A new survey of multiring impact basins on Mars. *J. Geophys. Res.* **95**, 14175–14189.

Schultz, P. H., and H. Glicken 1979. Impact crater and basin control of igneous processes on Mars. *J. Geophys. Res.* **84**, 8033–8047.

Schultz, P. H., R. A. Schultz, and J. Rogers 1982. The structure and evolution of ancient impact basins on Mars. *J. Geophys. Res.* **87**, 9803–9820.

Sclater, J. G., C. Jaupart, and D. Galson 1980. The heat flow through oceanic and continental crust and the heat loss of the Earth. *Rev. Geophys* **18**, 269–311.

Scott, D. H., and M. G. Chapman 1994. Geologic and topographic maps of the Elysium Paleolake Basin, Mars. U.S. Geological Survey Misc. Inv. Series Map I-2397.

Scott, D. H., and K. L. Tanaka 1986. Geologic Map of the Western Equatorial Region of Mars, scale 1:15,000,000, USGS Misc. Inv. Series Map I-1802-A.

Scott, D. H., M. G. Chapman, J. W. Rice Jr., and J. M. Dohm 1992. New evidence of lucustrine basins on Mars: Amazonis and Utopia Planitiae. *Proc. Lunar Planet Sci. Conf.* **22**, 53–62.

Siegfried, R. W., R. G. McQueen, and G. Simmons 1981. Shock-induced microfractures in six terrestrial igneous rocks characterized with differential strain analysis. *J. Geophys. Res.* **86**, 6205–6218.

Siegfried, R. W., G. Simmons, D. Richter, and F. Horz 1977. Microfractures produced by a laboratory scale hypervelocity impact into granite. In *Proc. Lunar Sci. Conf. 8th*, 1249–1270.

Sleep, N. H. 1994. Martian plate tectonics. *J. Geophys. Res.* **99**, 5639–5655.

Sloan, E. D., Jr. 1997. *Clathrate Hydrates of Natural Gases.* Marcel Dekker, Inc., New York and Basel.

Smith, D. E., M. T. Zuber, S. C. Solomon, R. J. Phillips, J. W. Head, J. B. Garvin, W. B. Banerdt, D. O. Muhleman, G. H. Pettengill, G. A. Neumann, F. G. Lemoine, J. B. Abshire, O. Aharonson, C. D. Brown, S. A. Hauck, A. B. Ivanov, P. J. McGovern, H. J. Zwally, and T. C. Duxbury 1999. The global topography of Mars and implications for surface evolution. *Science* **284**, 1495–1503.

Snow, D. T. 1968. Rock fracture spacing, openings, and porosities. *J. Soil Mech. Found. Div., ASCE* **94**, 73–91.

Squyres, S. W. 1989. Urey prize lecture: Water on Mars. *Icarus* **79**, 229–288.

Squyres, S. W., and M. H. Carr 1986. Geomorphic evidence for the distribution of ground ice on Mars. *Science* **231**, 249–252.

Squyres, S. W., S. M. Clifford, R. O. Kuzmin, J. R. Zimbelman, and F. M. Costard 1992. Ice in the martian regolith. In *Mars* (H. H. Kieffer, B. M. Jakosky, C. W. Snyder, and M. S. Matthews, Eds.), pp. 523–554, Univ. of Arizona Press, Tuscon.

Squyres, S. W., D. E. Wilhelms, and A. C. Moosman 1987. Large-scale volcano-ground ice interactions on Mars. *Icarus* **70**, 385–408.

Stevenson, D. J., T. Sphon, and G. Schubert 1983. Magnetism and the thermal evolution of the terrestrial planets. *Icarus* **54**, 466–489.

Tanaka, K. L. 1986. The stratigraphy of Mars. *Proc. Lunar Planet. Sci. Conf. 17th., J. Geophys. Res.* **91**, 139–158.

Tanaka, K. L. 1999. Debris-flow origin for the Simud/Tiu deposits on Mars. *J. Geophys. Res.* **104**, 8637–8652.

Tanaka, K. L. 2000. Dust and ice deposition in the martian geologic record. *Icarus* **144**, 254–266.

Tanaka, K. L., and M. G. Chapman 1990. The relation of catastrophic flooding of Mangala Valles, Mars, to faulting of Memnonia Fossae and Tharsis volcanism. *J. Geophys. Res.* **95**, 14315–14323.

Tanaka, K. L., and S. M. Clifford 1993. Seismic-triggering history of catastrophic outflows in the Chryse region of Mars. In *MSATT Workshop on the Martian Northern Plains*, Lunar Planet. Sci. Inst. Tech. Rept. 93-04, Part 1, 17–18.

Tanaka, K. L., and G. J. Leonard 1995. Geology and landscape evolution of the Hellas region of Mars. *J. Geophys. Res.* **100**, 5407–5432.

Tanaka, K. L., and D. H. Scott 1986. The youngest channel system on Mars. *Lunar Planet. Sci.* **17**, 865–866.

Tanaka, K. L., and D. H. Scott 1987. Geologic map of the polar regions of Mars. U.S. Geological Survey Misc. Inv. Series Map I-1802C.

Tanaka, K. L., M. G. Chapman, and D. H. Scott 1992. Geologic map of the Elysium region of Mars. U.S. Geological Survey Misc. Inv. Series Map I-2147.

Tanaka, K. L., D. H. Scott, and R. Greeley 1992. Global stratigraphy. In *Mars* (H. H. Kieffer, B. M. Jakosky, C. W. Snyder, and M. S. Matthews, Eds.), pp. 345–382. Univ. of Arizona Press, Tuscon.

Thompson, B. J., and J. W. Head III 1999. Utopia Basin, Mars: A new assessment using Mars Orbiter Laser Altimeter (MOLA) data. *Lunar Planet Sci. Conf.* **30**.

Todd, D. K. 1959. *Groundwater Hydrology*. John Wiley, New York.

Todd, T., D. A. Richter, G. Simmons, and H. Wang 1973. Unique characterization of lunar samples by physical properties, *Proc. 4th Lunar Sci. Conf., Geochem. Cosmochim. Acta, Suppl. 4, 3*, 2639–2662.

Toksöz, M. N. 1979. Planetary seismology and interiors. *Rev. Geophys. Space Phys.* **17**, 1641–1655.

Toksöz, M. N., A. M. Dainty, S. C. Solomom, and K. R. Anderson 1974. Structure of the Moon. *Rev. Geophys. Space Phys.* **12**, 539–567.

Toksöz, M. N., F. Press, A. Dainty, K. Anderson, G. Latham, E. Ewing, J. Dorman, D. Lammlein, G. Sutton, and F. Duennebier 1972. Structure, composition, and properties of lunar crust. *Proc. 3rd Lunar Sci. Conf., Geochem. Cosmochim. Acta, Suppl.* **3**, 2527–2544.

Toon, O. B., J. B. Pollack, W. Ward, J. A. Burns, and K. Bilski 1980. The astronomical theory of climatic change on Mars. *Icarus* **44**, 552–607.

Touma, J., and J. Wisdom 1993. The chaotic obliquity of Mars. *Science* **259**, 1294–1296.

Tribe, S., and S. M. Clifford 1993. Temporal Changes in the geographic distribution, elevation, and potential origin of the martian outflow channels. In *Mars: Past, Present, and Future—Results from the MSATT Program* (R. M. Haberle, Ed.), LPI Tech. Rpt. 93-006, Part 1, 51–52, Lunar and Planetary Institute, Houston.

Ward, W. R. 1992. Long-term orbital and spin dynamics of Mars. In *Mars* (H. H. Kieffer, B. M. Jakosky, C. W. Snyder, and M. S. Matthews, Eds.), 298–320. Univ. of Arizona Press, Tuscon.

Warren, P. H., and K. L. Rasmussen 1987. Megaregolith, insulation, internal temperatures, and bulk uranium content of the Moon. *J. Geophys. Res.* **92**, 3453–3465.

Wichman, R. W., and P. H. Schultz 1989. Sequence and mechanisms of deformation around Hellas and Isidis impact basins on Mars. *J. Geophys. Res.* **94**, 17333–17357.

Wilhelms, D. E., and S. W. Squyres 1984. The martian hemispheric dichotomy may be due to a giant impact. *Nature* **309**, 138–140.

Wise, D. U., M. P. Golombek, and G. E. McGill 1979. Tectonic evolution of Mars. *J. Geophys. Res.* **84**, 7934–7939.

Witbeck, N. E., K. L. Tanaka, and D. H. Scott 1991. Geologic map of the Valles Marineris region, Mars. U.S. Geol. Surv. Misc. Invest. Series Map I-2010.

Zent, A. P., F. P. Fanale, J. R. Salvail, and S. E. Postawko 1986. Distribution and state of H_2O in the high-latitude shallow sub-surface of Mars. *Icarus* **67**, 19–36.

Zimbelman, J. R., R. A. Craddock, and R. Greeley 1994. Geologic map of the MTM-15147 quadrangle, Mangala Valles region of Mars, U.S. Geol. Surv. Misc. Invest. Series Map I-2402.

Zoback, M. L., and M. D. Zoback 1997. Crustal stress and intraplate deformation. *Geowissenschaften* **15**, 116–123.

Zuber, M. T., S. C. Solomon, R. J. Phillips, D. E. Smith, G. L. Tyler, O. Aharonson, G. Balmino, W. B. Banerdt, J. W. Head, F. G. Lemoine, P. J. McGovern, G. A. Neumann, D. D. Rowlands, and S. Zhong 2000. Internal structure and early thermal evolution of Mars from Mars Global Surveyor topography and gravity. *Science* **287**, 1788–1793.

Zuber, M. T., D. E. Smith, S. C. Solomon, J. B. Abshire, R. S. Afzal, O. Aharonson, K. Fishbaugh, P. G. Ford, H. V. Frey, J. B. Garvin, J. W. Head, A. B. Ivanov, C. L. Johnson, D. O. Muhleman, G. A. Neumann, G. H. Pettengill, R. J. Phillips, X. Xiaoli, H. J. Zwally, W. B. Banerdt, and T. C. Duxbury 1998a. Observations of the north polar region of Mars from the Mars Orbiter Laser Altimeter. *Science* **282**, 2053–2060.

Zuber, M. T., D. E. Smith, R. J. Phillips, S. C. Solomon, W. B. Banerdt, G. A. Neumann, and O. Aharonson, and J. B. Abshire 1998b. Shape of the northern hemisphere of Mars from the Mars Orbiter Laser Altimeter. *Geophys. Res. Lett.* **25**, 4393–4396.